Dynamic Characteristics and Stability Analysis of Rotors Mounted on Fluid Film Bearings

by

Madhumita Kalita

Thesis Submitted in Fulfilment of the Requirements

For the Award of the Degree

Of

Doctor of Philosophy

Under the Guidance of

Dr. S.K. Kakoty

Department of Mechanical Engineering

Indian Institute of Technology Guwahati, India

May, 2005

Dedicated to my late father,

Soneswar Kalita

CERTIFICATE

It is certified that the work contained in the thesis entitled **Dynamic Characteristics and Stability Analysis of Rotors Mounted on Fluid Film Bearings**, by **Madhumita Kalita**, a student in the Department of Mechanical Engineering, Indian Institute of Technology Guwahati, India, for the award of the degree of the Doctor of Philosophy has been carried out under my supervision and that this work has not been submitted elsewhere for a degree.

Dr. S.K. Kakoty
Associate Professor
Department of Mechanical Engineering
Indian Institute of Technology Guwahati
May 2005

Acknowledgements

First of all, I would like to express my sincere gratitude to my honourable supervisor, Dr. S.K. Kakoty, for his invaluable support and help at each and every step of my work. In the past few years I worked under his guidance to achieve this state of my work. He always provided me his invaluable inspiration, encouragement and knowledge to lead me to keep the research work moving smoothly.

I would like to express my sincere thanks to all my doctoral committee members, namely, Dr. S. Talukdar, Dr. U.S. Dixit and Dr. S.K. Dwivedy for their valuable advice and encouragement during the course of my work.

I am grateful to Prof. A.D. Sahashrabudhe, Deputy Director, IITG Guwahati, for extending cooperation and help from the very beginning of my Ph.D. work. I would also like to sincerely acknowledge Dr. R. Tiwari, Dr. A.K. Dass, Dr. P. Mahanta and Dr. Chandan Mahanta for their help and advice in these years.

I would like to express thanks to all my family members for providing continuous support from the beginning to the end of my work.

And last but not the least, I extend recognition to Karuna Kalita, Manabendra Pathak, Amal Kalita and Tapashi K. Das for their invaluable help and encouragement during the course of this work.

Madhumita Kalita

IIT Guwahati

May 2005

Preface

This dissertation records the work performed in the Department of mechanical Engineering, Indian Institute of Technology Guwahati, India. The objective is to study the dynamic characteristics and stability of rotors supported on fluid film bearings. Dynamic coefficients using both short bearing and finite bearing theory are used. Stability characteristics at different spin speeds are studied by estimating the logarithmic decrements. Simplified models like bearings supporting rigid rotor and flexible rotors are studied to ascertain the threshold frequency of oil whirl for different bearing configurations. The present work is theoretical in nature. It is hoped that this work will lead to a better understanding of stability study of rotors mounted on fluid film bearing and estimation of threshold speed of oil whirl.

After formulation the computer code have been developed in MATLAB. When most of the work is done in a Windows platform, a few programme have been carried out in UNIX.

The thesis is broadly divided into seven chapters. A brief review of the relevant literature has been made in **Chapter 1** besides analysing the state of the art and the scope of the present work. Finite element formulation of rotor-bearing system has been presented in **Chapter 2**. Bearing geometry of different bearings and method of estimation of dynamic coefficiesnts are also outlined in the chapter. Whirling of rotors using different beam models has been presented in **Chapter 3**. **Chapter 4** is devoted to the study of whirling of rotors mounted on fluid film bearings. Study of whirling of rotors mounted on multilobe bearings has been carried out in **Chapter 5**. **Chapter 6** includes the stability analyses of both rigid and flexible rotors. A general discussion of the results, conclusions made thereupon including scope of the future work is incorporated in the concluding chapter (**Chapter 7**).

References and Appendices used in the present study are included in the end of the dissertation.

Madhumita Kalita

Contents

List of Figures

List of Tables

Notations

l	Length of the shaft element (m)
Ω	Rotating speed (spin speed) of the shaft (rad/s)
x	Axial position in the shaft element in local coordinate system
(V, W)	Translation displacement in Y and Z directions, respectively
(B, Γ)	Rotational displacement in Y and Z directions, respectively
X-Y-Z	Fixed frame of reference of the rotor-bearing system
U^e	Potential energy of the shaft element
T^e	Kinetic energy of the shaft element
E	Young's modulus of the shaft material (N/m^2)
I	Second moment of inertia of the shaft (m^4)
ρ	Mass density of the shaft material (kg/m^3)
A	Cross-sectional area of the shaft (m^2)
$[N]$	Shape function matrix
$\{q\}$	Nodal displacement vector
$[M]^e$	Elemental mass matrix
$[K]^e$	Elemental stiffness matrix
I_d	Diametral mass moment of inertia of the shaft per unit length ($kg\text{-}m^2$)
I_p	Polar mass moment of inertia of the shaft per unit length ($kg\text{-}m^2$)
N_i	One dimensional shape function
$[N_t]$	Translational shape function matrix
$[N_b]$	Rotational shape function matrix
$[M_T]^e$	Elemental translational mass matrix
$[M_R]^e$	Elemental rotational mass matrix
$[G]^e$	Elemental gyroscopic matrix
$[M^d]$	Disk mass matrix
$[G^d]$	Disk gyroscopic matrix
κ	Shear coefficient
G	Shear modulus (N/m^2)

$(V's, W's)$	Shear strain
$[K_b]^e$	Elemental stiffness matrix due to bending
$[K_s]^e$	Elemental stiffness matrix due to shear
m	Poisson's ratio
$[\eta]$	Internal damping matrix
η_H	Hysteretic damping coefficient of the shaft material
η_v	Viscous damping coefficient of the shaft material (s ˙)
$[K_C]^e$	Circulation matrix
$c_{VV}, c_{VW}, c_{WV}, c_{WW}$	Elements of bearing damping matrix (N/m/s)
$k_{VV}, k_{VW}, k_{WV}, k_{WW}$	Elements of bearing stiffness matrix (N/m)
$[c^b]$	Bearing damping matrix
$[k^b]$	Bearing stiffness matrix
$\{F^b\}$	Vector of bearing forces
$[M^s]$	System mass matrix
$[G^s]$	System gyroscopic matrix
$[K^s]$	System stiffness matrix
v	Complex eigen value
t	Time (s)
α	Real part of the complex eigen value
ω	Natural whirl speed (rad/s)
δ	Logarithmic decrement, Bearing ellipticity ratio
F	Forward whirl
B	Backward whirl
SS	Sub-synchronous whirl
d	Distance of the lobe centre from bearing geometric centre (m)
e	Bearing eccentricity (m)
ε	Bearing eccentricity ratio
ϕ	Attitude angle of bearing (rad)
S	Sommerfeld number
μ	Viscosity of bearing lubricant (Ns/m^2)

L	Length of the bearing (m)
D	Diameter of the rotor or bearing (m)
L/D	Aspect ratio
N	Journal Speed (rpm)
W	Bearing load (N)
C	Radial clearance of the bearing (m)
R	Radius of the journal (m)
r	Radius of the shaft (m)
$s\boldsymbol{r}$	Slenderness ratio of the shaft (= $r/2L$)
ϖ_n	Natural frequency parameter (non-dimensional)
Φ	Shear deformation parameter
X	Vertical direction
Z	Horizontal direction
U	Speed of the journal (rpm)
θ	Angular coordinate
λ	Whirl ratio=Ω/ω
M	Mass of the rotor per bearing (kg)
$\overline{K}_{XX}$, $\overline{K}_{XZ}$, $\overline{K}_{ZX}$, $\overline{K}_{ZZ}$	Dimensional stiffness coefficients = $\frac{kijC}{W}$ where i=X, Z and j=X, Z
$\overline{C}_{XX}$, $\overline{C}_{XZ}$, $\overline{C}_{ZX}$, $\overline{C}_{ZZ}$	Dimensional damping coefficients= $\frac{cijC\Omega}{W}$ where i=X, Z and j=X, Z
$\overline{M}$	Non-dimensional mass parameter = $\frac{MC\Omega^2}{W}$
F_X	Vertical component of hydrodynamic force (N)
F_Z	Horizontal component of hydrodynamic force (N)
$F\varepsilon$, F_ϕ	Hydrodynamic forces in ε-ϕ coordinate (N)
χ	Rigid rotor non-dimensional parameter
χ_f	Flexible rotor non-dimensional parameter

Abstract

Stability analysis of high-speed machinery based on rigid rotor model mounted on rigid supports was found to be inadequate for stability predictions. Critical speeds of a rotor are frequently computed assuming the bearing to act as rigid supports whereas in actual practise, bearings have some flexibility, resulting lower critical speeds. Fluid film bearings, commonly used in heavy rotating machines, play a significant role in the dynamic behaviour of rotors as the stiffness and damping properties of the oil film significantly alter the critical speeds of a rotor. Dynamic coefficients of fluid film bearing are speed dependent and these coefficients also change with the geometry of the bearing and other operating conditions. Hydrodynamic bearings are regarded as the best sources of damping. Generally plain circular bearings do not suit the stability requirements of high-speed machines and precision machine tools and new bearing designs are sought to meet the new requirements. These bearings are usually characterized by their noncircular cross sections, which will enhance shaft stability and also reduce power losses and increase oil flow, thus reducing temperatures under proper conditions. The instability of rotor-hydrodynamic bearing systems has been a major concern in high-speed rotating machine design and this has been observed that very little information is available on the behaviour of rotor-bearing systems mounted on fluid film bearings and more particularly mounted on non-circular bearings. In this context a fresh study of stability behaviour of rotors supported on hydrodynamic bearings is a necessity.

In this work the behaviour including dynamic characteristics and stability of rotor-bearing system supported on circular as well as non-circular hydrodynamic bearings has been studied. Finite element formulation is carried out for Timoshenko beam by incorporating translational inertia, rotary inertia, bending deformation, shear deformation, gyroscopic effect and internal damping.

Both short bearing and finite bearing dynamic coefficients are used to estimate dynamic characteristics and it is observed that in addition to the synchronous natural whirl frequencies for every spin speed, another whirling frequency appears in the solution. When short bearing theory is used these additional frequencies are of the same order as

that of the regular synchronous whirling frequencies. This has shown the deficiency in the use of short bearing approximation and therefore finite bearing dynamic coefficients are used in the present study.

Synchronous and sub-synchronous whirling speeds are plotted in Campbell diagrams and critical frequencies are estimated for different bearings; namely, two grooved circular, two-lobe, three lobe and four-lobe bearings. Mode shapes for first four modes and mode shapes corresponding to half frequency whirling are also plotted.

Stability characteristics at different spin speeds are studied by estimating the logarithmic decrements. It is observed from the estimated results that except for few forward synchronous frequencies, logarithmic decrements are found to be positive in all other cases for all types of bearing considered in this work. It is important to note that when rotor instability is studied by estimating synchronous whirling frequency, stability due to sub-synchronous whirling also should be checked.

Many researchers consider the rotors to be rigid while studying stability of bearings, when some consider simplified flexible rotor in such study. To demonstrate that the present study is worth it is proposed to take up simplified models like bearings supporting rigid rotor and simplified flexible rotors for different bearing configurations. Stability margins are estimated for these bearings by using existing methods. It has been observed that as slenderness ratio vis-à-vis first critical frequency increases threshold speed of flexible rotor also increases. Therefore rotors with different slenderness ratios are considered to estimate threshold speeds and it is observed that at a particular value of slenderness ratio, threshold speed of flexible rotor approaches rigid rotor threshold speed. Therefore, from this observation it is clear that the estimation of threshold speed for rotors with relatively low first critical frequency should be made by using FEM model and plotting Campbell diagram as has been done in the present study.

This study appears to provide a better understanding of the performance of rotors supported on fluid film bearing. The present results should be utmost importance to rotor-bearing system designers and analysts.

Chapter 1

Introduction

1.1 State of the Art

1.1.1 Rotor-bearing System

Rotor-bearing systems are widely used assemblies in diverse engineering applications such as power stations, marine propulsion systems, aircraft engines, machine tools, automobiles etc. Power machinery, such as compressors and turbo machines, usually transmits power by means of rotor-bearing systems. With the increase in performance requirements of high-speed rotating machineries in various fields, the engineer is faced with the problem of designing a unit capable of smooth operation under various conditions of speed and load. In many of these applications the design operating speed is well beyond the first critical speed. The design trend of such systems in modern engineering is towards lower weight and operating at super critical speeds. Under these circumstances, for different machineries, it is difficult to perform with stable low-level amplitude of vibration. The accurate prediction of dynamic characteristics of such system is important in the design of any type of rotating machinery.

The study of rotor dynamics has in recent years become of increasing importance in engineering design. There have been many studies relating to the field of rotor dynamic systems during the past years. Out of the published works, the most extensive portion of literature on rotor dynamics is concerned with determination of critical speeds, natural whirl frequencies, instability thresholds and unbalance response. Determination of natural frequencies and mode shapes is thus important from design point of view. Several numerical approximations have been successfully developed to analyse the dynamic behaviour of rotor systems. However, the most popular approach well suited for modelling large-scale and complicated rotor systems is the Finite Element Method.

1.1.2 Instability of Rotor-bearing System

The problem associated with stability of high-speed rotor-bearing system was not well understood, or, predictable until the late sixties and early seventies. Stability analysis of high-speed machinery based on rigid rotor model with bearings on rigid supports was found to be inadequate for stability predictions. Critical speeds of a rotor are frequently computed assuming the bearing to act as rigid supports. Calculation of critical speeds of a simple shaft in rigid support is somewhat an easy task. But it is, however, well known that in actual practice, bearings have some flexibility, resulting lower critical speeds.

In recent years, due to design trend towards high spin rates to raise the operating efficiency, the resulting instability problems of such systems have become aggravated. Such instabilities may originate from fluid film bearings, shaft stiffness asymmetry, internal friction between mating components and aerodynamic forces.

Fluid film bearings, commonly used in heavy rotating machines, play a significant role in the dynamic behaviour of rotors. The stiffness and damping properties of the oil film significantly alter the critical speeds of a rotor. But in high-speed applications, the bearing load carrying capacity is secondary in comparison to the rotor stability. This is an important factor to be considered in the rotor design. Dynamic coefficients i.e., stiffness and damping coefficients of fluid film bearing are speed dependent. Again these coefficients also change with the geometry of the bearing e.g., plain cylindrical, axial grooved, multi lobes etc. and other operating conditions. Operating condition of rotor-bearing system includes not only the speed but also viscosity of oil, length to diameter ratio of bearing. Critical speeds of rotor evaluated at different operating conditions using appropriate dynamic coefficients are found to have some errors due to simplified theoretical models.

1.2 Literature Review

1.2.1 Hydrodynamic Bearing Instability

The hydrodynamic bearings which are self acting and capable of carrying heavy loads are of particular interest in studying rotor-bearing stability. Because the thin film that

separates the moving surfaces supports the rotor load, these bearings act like a spring and provide damping due to squeeze film effect. There are two fluid film instability phenomena in these systems. The first is manifested with a sub harmonic component having a frequency equal to half the synchronous component arising in the motion of the journal; the second is manifested with the onset of a sub harmonic having a frequency roughly equal to half the rotor speed. Several authors have described the above forms of instability. The first of these is typical of unbalanced rotors and is referred to as "half frequency whirl". It is sometimes also called "parametric excitation instability" as, according to one interpretation, it can be attributed to the presence of a parametric excitation resulting from the variation of the stiffness and damping coefficients of the fluid film along the orbit described by the journals due to unbalance [1]. The second form of instability also concerns balanced rotors and, as said above, is manifested with the onset of about half that corresponding to the rotor angular velocity. This form of instability has been studied many times and is defined as "fractional frequency whirl", "oil whirl" or "resonant whip" [2]. The large number of experiments carried out, both numerically and on test equipment, has pointed out that as the spin speed increases, first "parametric excitation" instability sets in followed by the other form of instability [3]. For high-speed rotor these phenomena are very important. However, sub-synchronous whirling is not reported in most of the analyses of flexible rotor systems mounted on hydrodynamic bearing. It is mostly due to use of simplified (short-bearing approximation) bearing models.

Hydrodynamic bearings are regarded as the best sources of damping. A lot of interest has been paid to the rotor dynamic characteristics of hydrodynamic bearings. Newkirk and Taylor [4] reported the first experimental evidence of violent whipping of a flexible shaft due to action of the lubricating oil film. The whip started at a speed equal to twice the first critical speed of the shaft and persisted at higher speeds. Stadola [5] showed that the oil film behaved like a non-linear spring. Hummel [6] extending the work of Stadola [5] considered the forces due to a momentary infinitesimal displacement of the rigid shaft from an equilibrium position to some arbitrary new position. Squeeze film terms in the Reynold's equation were neglected in calculating the resultant oil film forces. Newkirk [7] reported whirling of a very short and stiff shaft at low speeds with whirl frequencies

approximately equal to one half of the running speed of the shaft. Hagg [8] studied the influence of fluid film journal bearing on the stability of rotating machine and considered the continuity condition of lubricant flow for a whirling journal. The upper limit of the whirling frequency was one-half the rotating speed. Ono and Tamuri [9] did the analysis of vibration of horizontal shaft supported in oil-lubricated bearings.

Akers *et al.* [10] had solved the equations of motion for a finite journal bearing for various *L/D* ratios in a time transient analysis. The effect of out of balance load was not found to be uniform. Lund [11,12] studied the stability and damped critical speeds and modal response of a flexible rotor in fluid film bearings. The bearings are represented by their linearized dynamic properties, also known as the stiffness and damping coefficients of the bearing. These can be used to represent the forces developed in the bearing due to small amplitude motion of journal about its equilibrium position and used to calculate the stability behaviour of rotors. The calculation includes hysteretic internal damping in the shaft and destabilizing aerodynamic forces. Kirk and Gunter [13,14] performed both linear and non-linear stability studies using short bearing approximation. Non-dimensional plots of stiffness and damping coefficients for the short bearing data were given. Rotor transient response orbits were obtained to show the effect of imbalance, steady loading, and cyclic and rotating loads upon the stability. Muller- Karger *et al.* [15] derived hydrodynamic bearing coefficients using minimum square method.

Rao *et al.* [16] studied the effect of damping on the synchronous whirl of rotor on hydrodynamic bearings. Bhat *et al.* [17] evaluated optimum journal bearing parameter for minimum unbalance in the synchronous whirl of a rotor. Rao [18] was one to study the synchronous whirl of flexible rotor on hydrodynamic bearings. Rao and Sarma [19] analysed simulation of multi-shaft rotors mounted on fluid film bearings to determine unbalance response. Subbiah *et al.* [20] studied about backward whirl of a simple rotor supported on fluid film bearing between two critical speeds. Ken and Mori [21] investigated the effects of variation in cavity pressure and the movement of the cavity boundary on the dynamic oil film coefficients. Rajalingham *et al.* [22] studied the effect of modified inlet boundary conditions on the dynamic characteristics of hydrodynamic journal bearing.

Rao *et al.* [23] presented an analytical approach to evaluate dynamic coefficients and non-linear transient analysis of hydrodynamic journal bearings. Raghunandana *et al.* [24] studied the effect of non-Newtonian lubricant on the stability of oil film journal bearings mounted on flexible support using linear perturbation technique. The dynamic co-coefficients were calculated for different values of power law index and length to diameter ratio. These were then used to find stability margin for different support parameters to study the effect of the non-Newtonian lubricant. Cheng *et al.* [25] studied the non-linear dynamic analysis of a flexible rotor supported by externally pressurized porous gas journal bearings. The analysis revealed how the dynamic behaviour of this type of system varies with changes in rotor mass and bearing number. Zhu and Zhang [26] described a non-linear model and analysis of the axial transient response of the sector-shaped hydrodynamic thrust bearing-rotor system in a turbo-expander under a suddenly applied step load. Matsuda *et al.* [27] optimised a clearance configuration of fluid-film journal bearing. The optimal clearance configuration was computed for various ratios of length to diameter of a bearing. A rigid-rotor system was used and verified that the designed bearing improved the system stability compared with that of a full circular bearing and the optimisation was more effective for shorter bearings.

1.2.2 Non-circular and Other Bearings

Generally plain circular bearings are used in rotating machineries. But it does not suit the stability requirements of high-speed machines and precision machine tools. Hydrodynamic bearings called upon to operate under these conditions are confronted with some new problems, among which instability is one of the most prevalent and the most troublesome. Because of high amplitude of vibration, the instability of the shaft constitutes a serious threat to the bearings and the machine itself. Bearings have failed and the operation of many machines has been impeded because of the excessive vibrations. Also power losses and subsequently bearing temperatures become excessive at high speeds. New bearing designs are sought to meet the new requirements and these bearings are usually characterized by their noncircular cross sections. Almost any noncircular bearing geometry will enhance shaft stability and under proper conditions this will also reduce power losses and increase oil flow, thus reducing temperatures.

Among these noncircular bearings, multi-lobe bearings with two lobes, three lobes, four lobes etc. are most commonly used. Though the advantage of multi-lobe bearings were known since many decades but the complexity of manufacturing of these types of bearings could not make them widely used in industries. However now a day the highly precision machine tools can be used to manufacture multi-lobe bearings and thus the acceptance of these bearings is increasing in industries. Hydrodynamic lubrication theory is employed to find the dynamic characteristics like stiffness and damping parameters.

In plain bearings, eccentricity, the distance between bearing centre and journal centre, mainly controls the bearing performance and only one converging fluid film is developed during the rotation of the journal. It is not much difficult to find the fluid film force components in case of plain bearings. But in multi-lobe bearings, the lobe geometry provides multiple converging fluid films. Fluid film forces developed due to these converging films are to be added carefully, taking the proper direction of forces, to obtain the resultant force component in desired direction. When number of lobe increases, complexities arise in analysis as well as in manufacturing of multi-lobe bearings. Ellipticity, the distance between lobe centre and bearing centre plays a vital role in multi-lobe bearing performance characteristics.

Since the research work by Newkirk and Taylor [4], the problems related with predicting the stability of a rotor-bearing system have gradually become the most important subject in the field of rotor-bearing dynamics. The work of Newkirk and Grobel [28] was mainly concerned with improving a bearing that would resist whipping. Pinkus [29-32] was one to study non-circular multi-lobe bearings. An analysis of elliptical bearings was presented in [29] based on the numerical solution of Reynolds equation for finite bearings. The bearings had two oil grooves at the horizontal split of approximately 30^0 each. The power losses for elliptical and three-lobe bearings, both symmetrical and asymmetrical, were derived as functions of the customary bearing parameters and bearing ellipticity in [30]. Expressions were given for two cases; one assuming a complete oil film, and one taking into account the incompleteness of the oil film that existed in the diverging section of the bearing. The expressions were derived for a concentric shaft position and thus these may be considered as equivalent to those given by Pettroff for cylindrical bearing. Pinkus did the experimental investigation of resonant whip in [31].

The investigation had a threefold purpose: to determine the susceptibility of bearings of various designs; to obtain a characteristic pattern of resonant whip; and to investigate the effect of some of the numerous design and operating variables on whip. Among the variables tested were loading, speed, bearing tightness, viscosity and amount of oil, unbalance, flexibility and external excitations. The test included circular (two and three groove), elliptical, three lobe (symmetrical and asymmetrical), pressure, tilting pad and self-energizing bearings. Pinkus in his work [32] presented an analytical solution of three lobe bearings based on the solution of Reynolds equation. Expressions for eccentricity, lubricant flow, power loss and spring constant were given for a range of *L/D* ratios and ellipticities. The bearing was shown to be superior quality both in its stability characteristics and in its hydrodynamic performance.

Glienicke [33] and Glienicke *et al.* [34] experimentally determined static and dynamic fluid film bearing characteristics (stiffness, damping and equilibrium position) of several two lobe, three lobe and four lobe bearings using a spring mass rotor model. Falkenhagen *et al.* [35] did the analysis of stability characteristics and general transient motion of the finite width vertical three-lobe bearing. In this analysis, a time transient procedure, based on an approximate solution of the Reynolds equation was presented. It was thus possible to rapidly and economically evaluate various rotor bearing design configurations. Schuller [36] experimentally studied the stabilizing characteristics of water-lubricated multi-lobe bearings with zero load. Schuller [37] also tested a rigid rotor in several bearings using water and oil. Three, five and seven lobe bearings were tested and instability threshold were found. Holmes *et al.* [38] theoretically examined the response of a flexible rotor mounted on two-lobe bearing. Lund and Thomson [39] provided data of stiffness and damping coefficients for two axial, elliptical, offset cylindrical and three-lobe bearings for static characteristics and fluid film stiffness and damping coefficients by using a finite difference approach. Akkok and Ettles [40] predicted the rigid rotor stability thresholds for two and three-lobe bearing, both with symmetric and asymmetric pad orientation. Leader *et al.* [41] studied the dynamic response and stability threshold of a flexible rotor mounted in two axial groove, pressure dam and tilting pad bearings.

Flack *et al.* [42] carried out a theoretical and experimental investigation of pressure distribution in four-lobe bearing and compared both the results. Four-lobe bearings in two different orientations were used. Although experimental dynamic coefficients were available for several bearings, the results had not always given good agreement with experimental which might be due to accuracy of pressure distribution of a theoretical solution. Leader *et al.* [43] experimentally tested a pair of preloaded four-lobe bearings with a simple flexible rotor and determined the unbalance response and instability threshold. Ten orientations of the bearing were used. All the bearing parameters were held constant during test except the angle between the load vectors and oil grooves. Kumar *et al.* [44] studied the performance characteristics of two-lobe hydrodynamic journal bearings. Using a variational solution, detailed design data were computed. The data included Sommerfeld number, equilibrium locus, fluid film stiffness and damping coefficients, end flow, friction parameter, and temperature rise parameter. Although a linearized analysis accurately predicts the bearing characteristics for small journal dynamic motions, it does not give any information when large journal motions occur. For this purpose, Li *et al.* [45] investigated the fundamental problem of linear stability and non-linear behaviour of a single mass rotor and determined the stability threshold of four multi-lobe bearing configurations (Elliptical, offset elliptical, three-lobe and four-lobe bearings). A non-linear transient analysis of a single mass rigid rotor in each of these bearings was carried out above and below the threshold speed.

Sinhasan *et al.* [46] and Malik *et al.* [47] analysed both two lobe and three-lobe porous hydrodynamic journal bearing. Soni *et al.* [48] determined static and dynamic performance characteristics of non-circular two-lobe bearing using finite element method for both laminar and turbulent lubrication. The performance characteristics of the bearings had been studied in terms of Sommerfeld number, oil flow, fluid film stiffness and damping coefficients and non-dimensional critical mass for various values of Reynolds number (up to 12000). For the analysis in turbulent regimes, the linearized turbulent lubrication theory of Ng and Pan [49] was used. Malik *et al.* [50] provided design data for three-lobe bearings for both laminar and turbulent regimes. The theoretical analysis of the bearing was based on the solution of usual form of the Reynolds equation for laminar regime and the modified Reynolds equation of Ng and Pan

[49] for turbulent regime. The design data that included bearing load support, frictional power loss, stiffness and damping coefficients, and stability margins in terms of critical non dimensional journal mass had been presented in graphical and tabular form. Flack and Allaire [51] presented a theoretical and experimental comparison of the operating eccentricities for nine three-lobe bearings. Malik [52] did a comparative study of performed characteristics of two-lobe journal bearings with different configurations. The elliptical, offset-halves and two other configurations that were geometrical variations of the first two bearing forms were considered. It had been shown that, unlike elliptical and offset halves bearings, which have only limited range of effective dynamic performance, a two-lobe configuration could provide consistently good dynamic performance over a wide range of load conditions. Taylor *et al.* [53,54] studied the static and dynamic characteristics of highly preloaded three-lobe bearing for different operating speed. Kostrezewsky *et al.* [55] compared the numerically evaluated and experimentally predicted steady state parameters as well as stiffness and damping coefficients for two axial groove bearings. Muller-Karger *et al.* [56] studied the effect of fluid film non-linearity on experimental determination dynamic coefficients of three-lobe journal bearing and found that the fluid film non-linearity produced an uncertainty in the coefficients of up to 20 percent compared to the linearized coefficients obtained from small perturbation solution of the Reynolds equation, which are commonly used in rotating machinery design and analysis. Rao *et al.* [57] developed a methodology for prediction of dynamic coefficients and non-linear simulation of multi lobe bearings. Four multi lobe journal bearings, two axial groove, elliptical, three lobe and offset bearings were studied in terms of non-dimensional stiffness and damping. The journal centre trajectories obtained were compared with numerical results and the effect of stability of rotor-bearing system was studied for both balanced and unbalanced rotor.

1.2.3 Instability of Rotor-bearing System

The instability of rotor-hydrodynamic bearing systems has been a major concern in high-speed rotating machine design. In his early research work, Rankine [58] stated that the stable operation of the rotor above the shaft first critical speed would be impossible which convinced all engineering circles for more than half a century that a rotating

machine operated above the shaft first critical speed could not be manufactured. It was Jeffcott [59] who developed the fundamentals of the dynamic response of the damped single mass unbalanced rotor on a massless elastic shaft mounted on rigid bearing supports and this analysis showed that operating speeds above the first critical speed is possible and that a low level of vibration would be attained once the rotor had exceeded the first critical speed. As various compressor and turbine manufacturers adapted the flexible rotor design concept in which the rotors were designed to operate above the first critical speed, various units developed severe operating difficulties, which could not be explained by the elementary Jeffcott model. Newkirk [60] and Kimball [61] in their early investigations of self-excited instability in compressors due to internal friction were able to determine experimentally that the introduction of a flexible support system could greatly extend the rotor stability threshold speed. Smith [62] was the first to verify Newkirk's finding theoretically by expanding the Jeffcott model with internal damping to include a massless damped flexible support system. Prohl [63] described a general method to calculate undamped critical speeds of flexible rotors supported on fluid film bearing. In that method, the rotor was idealized with lumped masses connected by massless shaft sections. The deflection, slope, moment and shear were calculated from one end of the idealized rotor to the other for a given frequency. Frequencies at which the boundary conditions at each end of the rotor satisfied were the natural frequencies of the rotor. Portisky [64], assuming small shaft displacements and a radial force in the bearing, showed that the rotor became unstable at twice the first critical speed of the shaft.

Hagg and Warner [65] investigated the phenomena of oil whip of flexible rotors through an electric analogue study and determined that the flexibility of the rotor decreased the region of stable operation. Pinkus [31] showed that there does not exist any simple criterion that separates the regions or conditions of rotor stability. Newkirk and Lewis [66] ran tests on horizontal shaft and concluded that short bearings, large clearances and moderate unit bearing load increase the range of stable operation. Boekar and Sternlicht [67] examined translatory fluid whirl in vertical unloaded vertical shafts and did some analytical work on stability criteria. Hori [68] also studied about oil whip and treated the oil whip problem as a problem of dynamic stability of a rotor supported by an elastic shaft rotating in oil film bearings. Dimentberg [69], Tondl [70], Lund [71] and Gunter

[72] had shown that the flexible damped supports might improve the stability characteristics of high-speed rotors. Lund and Sternlicht [73] presented a theoretical analysis for studying the dynamic response of a symmetric rotor supported in two cylindrical journal bearings. Reddi and Trumpler [74] studied the stability of high-speed journal bearing under steady load. Sternlicht [75] analysed the stability and dynamics of rotors supported on fluid film bearing. Alford [76] found that disturbing forces of aerodynamic origin could cause instability in turbo-machinery. Gunter [77] examined the single mass unbalanced symmetric rotor and analysed the effect of support flexibility and damping on stability. Kirk [78] considered the effect of unbalanced external loading in a transient journal bearing analysis. De Choudhury and Gunter [79] analysed the dynamic stability of flexible rotor bearing system using flexibility influence coefficients, but the analysis was limited to five mass stations. Kirk and Gunter [80] studied the effect of support flexibility and damping on the synchronous response of a single mass flexible rotor.

Kirk [81] conducted non linear transient analysis of a flexible rotor including the influence of an external flexible damped support and noticed that there might be the multiple stability regions in flexible rotors with external flexible damped support. Bansal and Kirk [82] also studied stability and damped critical speed of a flexible rotor supported on fluid film bearing. Allaire [83] performed the stability analysis of several types of bearings and gave stability charts and a summary chart indicating advantages and disadvantages of journal bearings. Barret *et al.* [84] showed that the application of unbalance to a journal operating above the stability threshold speed introduces a synchronous component to the half frequency unstable whirl motion. Majumdar *et al.* [85] studied the stability characteristics of finite bearings under steady, periodic and variable rotating loads using non-linear transient method. Ramesh and Kirk [86] extended these works to study the stability and response of rotors supported on active magnetic bearings. Elrod and Vijayaraghavan [87,88] did a linearized stability analysis for liquid lubricated bearings, which included the flow within the cavitated region. Tieu and Qiu [89] studied the stability of finite journal bearings using linear and non-linear bearing forces.

Ramesh *et al.* [90] did non-linear transient analysis of submerged oil journal bearings considering surface roughness and thermal effects. Crandall [91,92] calculated the stability of a Jeffcott rotor supported in cylindrical fluid film bearings that incorporated the effect of rotor damping. A speed-load figure for stability borderlines was given in [92] and it could be seen from that figure for each rotating speed of the rotor that there are two corresponding thresholds respectively representing the loss of stability of either equilibrium configuration or limit cycle. Horattas *et al.* [93] showed from their test rig data that multiple instability threshold speed and multiple hysteresis loops could exist in rotating machinery. Guo [94] also found in his studies of rotor vibration optimum design, that multiple stability regions might be possible under some circumstances and to better understand these fundamental phenomenon, it was beneficial to conduct a further theoretical study. Ramesh *et al.* [95] studied stability characteristics of rough submerged oil elliptical bearings under dynamic load. The non-linear transient simulation was used to predict the threshold of instability. Jang *et al.* [96,97] investigated the performance of herringbone grooved journal bearings considering the effect of a rotating or stationary herringbone groove by both linear and non-linear dynamic analysis. FEM was used to solve the Reynolds equation in order to calculate the pressure distribution in a fluid film. Guo and Kirk [98] studied the instability boundary for both vertical and horizontal configurations of both Jeffcott and extended Jeffcott rotor with external damping supported on hydrodynamic bearing. For Jeffcott rotor, it had been shown by both analytical and numerical that there was one threshold speed in the vertical system at which the rotor would get into an upper stable region from the previous unstable one. For the horizontal system an extended Lund Stability Method was presented which proved that there might be two threshold speeds to evolve a stability pattern as one region of instability sandwiched between two regions of stability. With the introduction of equivalent journal mass, another threshold appeared which formed a top and final boundary to the stable operation of the extended Jeffcott rotor. Guo and Kirk [99] also studied the instability boundary of same rotor-hydrodynamic bearing system with external flexible damped bearing supports, which was more complicated than the previous one. The results showed that there could be up to four threshold speeds in the configuration that form a consecutive regional pattern, taking turns by stable or unstable

regions. The value of external damping had a strong effect on the first several lower threshold speeds. But it had little effect on the last top threshold speed. Ghosh *et al.* [100,101] carried out a small amplitude perturbation analysis to determine the rotor dynamic characteristics of multi lobe hybrid bearings with short axial and circumferential sills. Stiffness and damping coefficients of the bearing were determined from the dynamic load capacity of the bearing. Rao and Sawicki [102,103] studied stability characteristics of both herringbone grooved journal bearings and rough journal bearing considering cavitation effects.

1.2.4 Finite Element Method in Rotor-Bearing Analysis

The need for higher speed, yet reliable operation of rotating machinery continues to increase. A key factor in achieving this objective continues to be the ability to accurately predict the dynamic response and stability of a rotor system. There are two basic numerical procedures in common use for vibration analysis of rotor-bearing systems, namely (1) transfer matrix method, and (2) finite element method.

The bulk of the reported analytical procedures in rotor dynamics were based on transfer matrix techniques, in part because of the success attained by Lund and others [12,104,105] in its application. The finite element approach was sometimes considered as requiring more computer time and storage than the transfer matrix approach, but it was also noteworthy that this approach provided significantly greater accuracy for a given rotor discretization [105]. Some indications of numerical difficulties with the transfer matrix approach had also been observed when problem size increased [106]. The finite element method has had a major impact on the static and dynamic analysis of structures and equipment, and is becoming more common in diverse fields such as acoustics, heat transfer and fluid mechanics. This method is particularly well suited for modelling large scale and complicated rotor system. The utilization of finite element models, introduced by Archer [107], in the area of rotor dynamics has yielded highly successful results.

Ruhl [105] and Ruhl & Booker [108] were the first to utilise the finite element method to study the stability and unbalance response of turbo-rotor systems. In their finite element formulations, only elastic bending energy and translational kinetic energy were included. However, many effects, such as the rotary inertia, gyroscopic moments, shear

deformations, internal and external damping, which could be very important for some configurations, were all neglected in their finite element analysis. After Ruhl's work, many researchers studied similar problem by introducing different effects in the finite element analysis. Thorkildsen [109] developed a finite element model, which was more general than Ruhl's model. It also included rotary inertia and gyroscopic moments. Polk [110] presented the development of a Timoshenko beam finite element in his work but did not present any numerical results. Diana *et al.* [111] published the results of a finite element analysis of a rotating shaft. Their element was similar to Ruhl's element. Dimaragonas [112] studied the stability analysis of a rotating shaft with all effects except shear deformation, axial load and axial torque. Gasch [113] published a paper quite similar to that of Dimaragonas [112], but also included the effect of distributed eccentricity. Nelson and McVaugh [114] generalised Ruhl's work by developing a Rayleigh beam finite element model including the effects of rotary inertia, gyroscopic moments and axial load to simulate a flexible rotor system supported on linear stiffness and viscously damped bearings. In order to facilitate the computations of natural whirl speeds and unbalance response, the element equations were transformed into a rotating frame of reference and results were presented for two sets of bearing parameters; undamped orthotropic and undamped isotropic. A comparison of results was made with an independent lumped mass analysis. To save computational time, the Guyan reduction procedure [115] was adopted to reduce the size of the system matrices. Gunter's [77,116] work included an evaluation of internal viscous damping. This contribution demonstrated the destabilizing effect of internal viscous damping at speeds beyond the first critical speed. Dimentberg [69] studied both viscous and hysteretic forms of internal damping and noted that unlike viscous damping, which was destabilizing at speeds beyond the first critical, hysteretic damping was destabilizing at all speeds. Other works by Lund [11], Tondl [70], Bolotin [117] and Vance *et al.* [118] also demonstrated that internal damping is a primary destabilizing mechanism for high-speed rotors.

The work of Zorzi and Nelson [119] was the generalization of the work of Nelson and McVaugh [114] by including both internal viscous and hysteretic damping in the same finite element model. This study had confirmed that both hysteretic and viscous damping had a destabilizing effect on rotor systems. Viscous damping did not encourage

instability until the first critical speed was reached, whereas the hysteretic form destabilized the forward precessional modes at all speeds. Rouch and Kao [120] and Nelson [121] utilized Timoshenko beam theory for establishing shape functions, and based on these shape functions the system finite element matrices of governing equations were derived. In these system finite element matrices, a shear parameter was included to take into account the effect of transverse shear deformations. The governing equation could be quickly changed into a Rayleigh beam or Euler Bernoulli beam if the shear parameter in the shape functions is set equal to zero. Comparison was made of the finite element analysis with classical closed form Timoshenko beam theory analysis of non-rotating and rotating shafts. Rouch and Kao [120] offered the conclusion that the finite element approach provided a convenient means of modelling a complex rotor bearing system. Ozguven and Ozkan [122] and Edney *et al.* [123] presented the combined effects of shear deformations and internal damping in their finite element formulation to analyse the natural whirl speeds and unbalance response of multi-bearing rotors. Flexibility and damping of bearings were considered by using constant bearing coefficient matrices in [122]. A general computer program for determining whirl speeds, corresponding mode shapes, stability regions and unbalance response of a rotor bearing system was briefly described. Many other works that utilised the finite element technique for rotor dynamics analysis could be found in [124-129]. Chen and Ku [130] developed a three nodal C^0 class Timoshenko beam finite element model and analysed natural whirl speeds of a rotating shaft with different end conditions. The effects of translational and rotary inertia, gyroscopic moments and bending and shear deformations were included in the mathematical model. In order to facilitate the calculations of the natural whirl speeds, a rotating frame of reference was used in the formulation. Ku [131] included internal viscous and hysteretic damping in the same model to study the dynamic characteristics. The combined effect of transverse shear deformations and internal damping on forward and backward whirl speeds and damped stability was presented. Rao [132] provided analysis of dual rotor supported on fluid film bearings and concluded that for an undamped system, the eigen values could be directly obtained for synchronous whirl with either of the shafts of a dual rotor system or a general rotor system. But for damped system, it is necessary to draw the Campbell diagram to obtain the critical speeds.

1.2.5 Timoshenko Beam

The vibrating beams are most frequently modelled using the Euler-Bernoulli model of a beam because it is simple and well established as an accurate approximation to real motion. Rotary inertia effects were included into the Euler-Bernoulli beam model by Lord Rayleigh [133] and subsequently the effects of shear deformation were added to the Rayleigh beam model by Timoshenko [134,135].

Huang [136,137] had made numerical comparisons between several important beam theories, including Euler-Bernoulli beams, Rayleigh beams and Timoshenko beams. The frequency and normal mode equations for six common types of simple and flexible beams were presented. Wang and Guan [138] had modelled a single flexible link using the Euler-Bernoulli model, the Rayleigh model (which they refer to as the Euler-Bernoulli model with rotary inertia) and the Timoshenko model. Through both analytical and experimental means they confirmed that the Timoshenko model is superior to the other models. The Timoshenko beam provides a more complete model than either the Euler-Bernoulli or Rayleigh beams.

There have been a number of works dealing with the vibration of the Timoshenko beam. Stafford and Giurgiurtiu [139] developed the equations for a beam, modelled with the Timoshenko beam theory that was assumed to be rotating at a constant angular velocity in a fixed plane. Abbas [140] presented a finite element investigation into the stability of a rotating Timoshenko beam that included the effects of centripetal acceleration. Datta and Ganguli [141] used a Ritz solution that employed polynomial trial functions, to treat the problem of a rotating Timoshenko beam that had a damaged section. Zu and Han [142] presented a parallel development to Huang's work [136,137] but for a Timoshenko beam which was rotating about its longitudinal axis. Rossi *et al.* [143], Gutierrez *et al.* [144] and Lee and Lin [145] studied about non-uniform Timoshenko beam. Cleghorn and Tabarrrok [146] did finite element formulation of a tapered Timoshenko beam for free lateral vibration. White and Heppler [147-150] studied vibration of a rotating Timoshenko beam. The frequency equation and mode shapes for a Timoshenko beam that had rigid body attached to its ends were reported. Du *et al.* [151] used Timoshenko beam model to formulate the equations of motion of a rotating beam that had a finite hub

and had a mass attached at the free end of the beam. Tong *et al.* [152] presented an analytical solution for free and forced vibrations of stepped Timoshenko beam and used this for the approximate analysis of generally non-uniform Timoshenko beam. White and Heppler [153] used Timoshenko beam theory to model a flexible slewing link with an attached payload using two different frames of rotating reference.

1.3 Scope of the present work

There are two distinct approaches observed in Rotor-Bearing Analysis in general. Most of the study on Bearing Stability is limited to the assumption of rigid rotors. On the other hand Rotor Stability Analysis is limited to the assumption of hypothetical bearings in many studies. Further, this has been observed from the foregoing review that very little information is available on the behaviour of flexible rotor systems mounted on fluid film bearings and more particularly mounted on non-circular fluid film bearings. In view of the above the present investigation is made to find out the behaviour including stability of rotor-bearing system supported on circular as well as non-circular, *i.e.*, multi-lobe hydrodynamic bearings.

Besides it has been observed that in rotor-bearing analysis, approximate solution like short bearing theory is used for estimation of dynamic parameters in general even when numerical solution of finite bearing is available. In view of this finite bearing dynamic coefficients are used in the present work.

In the present work a Timoshenko beam is used as it provides a more complete model than either the Euler-Bernoulli or Rayleigh beam. Therefore, a finite element formulation is carried out for Timoshenko beam by incorporating translational inertia, rotary inertia, bending deformation; shear deformation, gyroscopic effect and internal damping. Synchronous and sub-synchronous whirling speeds are plotted in Campbell diagrams and critical frequencies are estimated for different bearings; namely, two grooved circular, two-lobe, three lobe and four-lobe bearings. Mode shapes for first four modes and mode shapes corresponding to half frequency whirling are also plotted. Stability characteristics at different spin speeds are studied by estimating the logarithmic decrements. Bearings supporting rigid rotor and flexible rotors are studied for different bearing configurations. The stability margins are estimated for these bearings. In the study of flexible rotors

supported on different bearings, a simplified formulation is used [132] to estimate the threshold speed. It has been demonstrated that the threshold speed approaches the rigid rotor threshold speed when the first critical frequency of the rotor is quite high corresponding to high slenderness ratio.

Finally the threshold speed estimated using different approaches are compared. The threshold speed estimated from Campbell type diagram using FEM formulation is found to be different than those estimated using approximate methods. It is recommended that the threshold speed of oil whirl for flexible rotors mounted on hydrodynamic bearings should be estimated theoretically by using FEM model only for better prediction.

Chapter 2

Formulation

2.1 Introduction

In this chapter, finite element formulation of typical rotor-bearing system has been discussed. Three different types, namely, Timoshenko Beam theory, Rayleigh Beam theory and Euler-Bernoulli Beam theory, all considered in the present analysis. Four different types of bearings and their geometries are also discussed. System equations of motion and eigen value problem of the rotor bearing system have been provided

2.2 Finite element formulation of rotors

A rotor-bearing system is composed of a uniform flexible shaft of length l rotating at a constant speed Ω (Fig. 2.1) and supported by two bearings. It is assumed that as compared to the translational motion, the axial motion is small enough to be neglected. Therefore, a typical cross-section of the shaft, in a deformed state, located at a distance x from the left end can be described by the translations $V(x,t), W(x,t)$ in Y and Z directions and small rotations $B(x, t)$, $\Gamma(x, t)$ about Y and Z directions. Fixed reference X-Y-Z is employed to describe the system motion.

The two translations (V, W) consist of a contribution (V_b, W_b) due to bending and a contribution (V_s, W_s) due to shear deformation. The two rotations (B, Γ) are only influenced by bending deformation (V_b, W_b) [122,131,132].

These relationships can be expressed as

$$\begin{aligned} V(x,t) &= V_b(x,t) + V_s(x,t) \\ W(x,t) &= W_b(x,t) + W_s(x,t) \\ B(x,t) &= -\partial W_b(x)/\partial x \\ \Gamma(x,t) &= \partial V_b(x)/\partial x \end{aligned} \qquad (2.1)$$

In the present analysis, different types of beams are considered:

2.2.1 Euler-Bernoulli beam

2.2.2 Rayleigh beam

2.2.3 Timoshenko beam

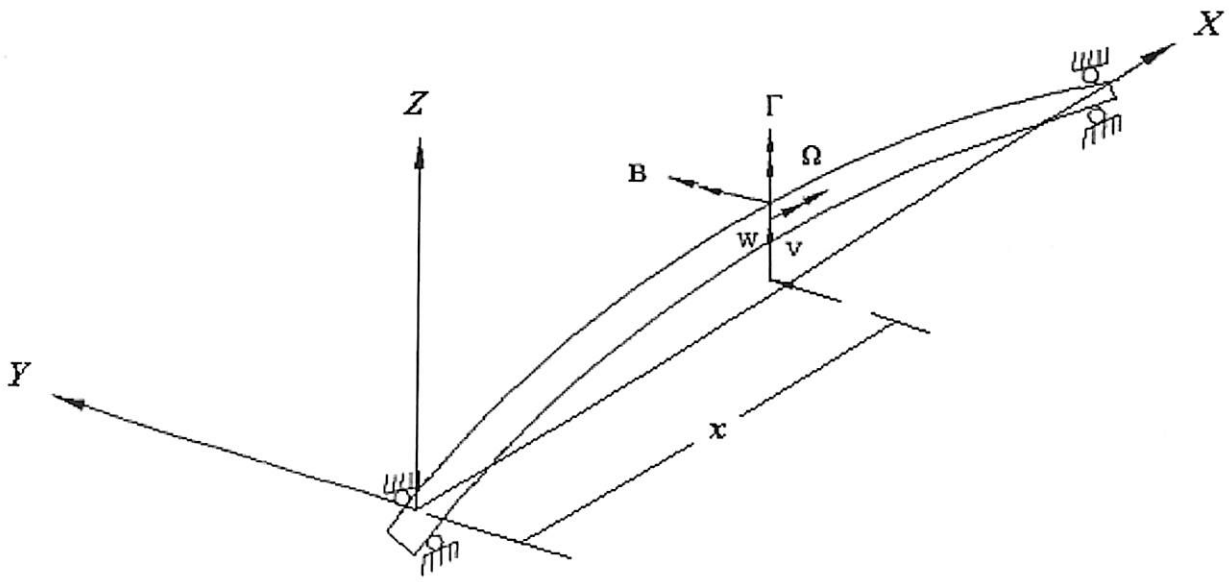

Fig. 2.1: Displacement variables and coordinate system

2.2.1 Euler-Bernoulli beam

For an Euler-Bernoulli beam, the major effect is due to only pure bending. No rotary inertia effect and gyroscopic effect is present. For the present case the whirling motion of the shaft in vertical and horizontal directions are uncoupled, the analysis in the vertical plane is identical to the analysis of horizontal plane. The potential energy U^e and the kinetic energy T^e of a shaft element rotating at a constant speed Ω, are given by

$$U^e = \frac{1}{2}\int_0^l EI\left\{(B')^2\right\}dx \tag{2.2}$$

$$T^e = \frac{1}{2}\int_0^l \rho A\left\{(\dot{V})^2\right\}dx \tag{2.3}$$

In the finite element method, the continuous displacement field can be expressed in terms of the discretized generalized displacements of the element nodes. In the present finite element model each element has two nodes and each node has two generalized displacements. Therefore, by using appropriate shape function or interpolation function, the displacement field internal to an element *e* can be approximated as

$$\{V(x,t), B(x,t)\} = [N]\{q\}^e \tag{2.4}$$

where [*N*] is the shape function matrix and

$$\{q\}^e = \{V_1, B_1, V_2, B_2\}^T \tag{2.5}$$

is the nodal displacement vector.

For shaft element, the element potential energy and element kinetic energy can be rewritten in terms of nodal displacement vector as, respectively,

The element equation of motion is given by

$$[M]^e\{\ddot{q}\}^e + [K]^e\{q\}^e = \{0\} \tag{2.6}$$

where

$$[K]^e = [N'']^T EI[N'']dx$$
$$[M]^e = \int_0^l [N]^T \rho A[N]dx \tag{2.7}$$

are the elemental stiffness and mass matrices respectively.

2.2.2 Rayleigh beam

For Rayleigh beam, deformation is only due to bending. No shear effect is present. But rotary inertia and gyroscopic effect are considered. The energy expressions are given by

$$U^e = \frac{1}{2}\int_0^l EI\left\{(B')^2 + (\Gamma')^2\right\}dx \tag{2.8}$$

$$T^e = \frac{1}{2}\int_0^l \rho A\left\{(\dot{V})^2 + (\dot{W})^2\right\}dx + \frac{1}{2}\int_0^l I_d\left\{(\dot{B})^2 + (\dot{\Gamma})^2\right\}dx - \frac{1}{2}\int_0^l \Omega I_p(\dot{\Gamma})B\,dx + \frac{\Omega^2}{2}\int_0^l I_p dx \tag{2.9}$$

In the present finite element model each element has two nodes and each node has four generalized displacements, therefore the displacement field internal to an element *e* can

be approximated as

$$\{V(x,t), W(x,t), B(x,t), \Gamma(x,t)\} = \sum_{i=1}^{2} N_i(x)\{V_i, W_i, B_i, \Gamma_i\}. \tag{2.10}$$

The displacement field can be expressed in a matrix form as

$$\left\{\frac{V}{W}\right\} = [N_t(x)]\{q\}^e = \left[\frac{N_v(x)}{N_w(x)}\right]\{q\}^e, \tag{2.11}$$

$$\left\{\frac{B}{\Gamma}\right\} = [N_b(x)]\{q\}^e = \left[\frac{N_\beta(x)}{N_\gamma(x)}\right]\{q\}^e. \tag{2.12}$$

where $N_i(x)$ is the one dimensional shape function.

The nodal displacement vector is given by

$$\{q\}^e = \{V_1, W_1, B_1, \Gamma_1, V_2, W_2, B_2, \Gamma_2\}^T, \tag{2.13}$$

and $[N_t(x)]$ and $[N_b(x)]$ are the translational and rotational shape function matrices, respectively.

The element equation of motion is given by

$$\left([M_T]^e + [M_R]^e\right)\{\ddot{q}\}^e - \Omega[G]^e\{\dot{q}\}^e + [K]^e\{q\}^e = \{0\} \tag{2.14}$$

where

$$[K]^e = \int_0^l \left[N_b'\right]^T EI\left[N_b'\right] dx \qquad [M_T]^e = \int_0^l [N_t]^T \rho A [N_t] dx$$

$$[M_R]^e = \int_0^l [N_b]^T I_d [N_b] dx \qquad [H]^e = \int_0^l [N_\gamma]^T I_p [N_\beta] dx \tag{2.15}$$

$$[G]^e = [H]^e - [H]^{eT}$$

The elemental equation of disk is given by

$$[M^d]\{\ddot{q}^d\} - \Omega[G^d]\{\dot{q}^d\} = \{0\} \tag{2.16}$$

where $[M^d]$ and $[G^d]$ are mass and gyroscopic matrices of disk only.

2.2.3 Timoshenko beam

Timoshenko beam includes all the effects i.e., bending deformation, rotary inertia, gyroscopic effect and shear deformation. The potential energy is due to bending and shear. Translational, rotation and gyroscopic effect contribute towards kinetic energy.

The potential energy U^e of a shaft element of length l, including the elastic bending and shear deformation energy, can be expressed as

$$U^e = \frac{1}{2}\int_0^l EI\left\{\left(B'\right)^2 + \left(\Gamma'\right)^2\right\}dx + \frac{1}{2}\int_0^l \kappa GA\left\{\left(V_s'\right)^2 + \left(W_s'\right)^2\right\}dx \tag{2.17}$$

and

$$V_s' = \partial V/\partial x - \Gamma \tag{2.18}$$

$$W_s' = \partial W/\partial x + B \tag{2.19}$$

are the shear strains.

The kinetic energy T^e of a shaft element rotating at a constant speed Ω, including the translational and rotational forms, can be expressed as

$$T^e = \frac{1}{2}\int_0^l \rho A\left\{\left(\dot{V}\right)^2 + \left(\dot{W}\right)^2\right\}dx + \frac{1}{2}\int_0^l I_d\left\{\left(\dot{B}\right)^2 + \left(\dot{\Gamma}\right)^2\right\}dx - \Omega\int_0^l I_p\left(\dot{\Gamma}\right)B\,dx + \frac{\Omega^2}{2}\int_0^l I_p dx \tag{2.20}$$

In the present finite element model the displacement field internal to an element e can be approximated as equation (2.10), (2.11) and (2.12).

From the equation (2.11) and (2.12), equation (2.18) and (2.19) are related by the nodal displacement vector as

$$\begin{Bmatrix} V_s' \\ W_s' \end{Bmatrix} = \begin{bmatrix} \left[N_v'\right] - \left[N_\gamma\right] \\ \left[N_w'\right] + \left[N_\beta\right] \end{bmatrix}\{q\}^e = \left[N_s(x)\right]\{q\}^e \tag{2.21}$$

For shaft element, the element potential energy and element kinetic energy can be rewritten in terms of nodal displacement vector respectively, as

$$U^e = \frac{1}{2}\{q\}^{eT}\left(\left[K_b\right]^e + \left[K_s\right]^e\right)\{q\}^e = \frac{1}{2}\{q\}^{eT}\{K\}^e\{q\}^e \tag{2.22}$$

and

$$T^e = \frac{1}{2}\{\dot{q}\}^{eT}\left(\left[M_T\right]^e + \left[M_R\right]^e\right)\{\dot{q}\}^e - \Omega\{\dot{q}\}^{eT}\left[H\right]^e\{q\}^e + \frac{1}{2}I_p\Omega^2 \tag{2.23}$$

where

$$[K_b]^e = \int_0^l \left[N_b'\right]^T EI \left[N_b'\right] dx \qquad [K_s]^e = \int_0^l [N_s]^T \kappa GA [N_s] dx$$

$$[M_T]^e = \int_0^l [N_t]^T \rho A [N_t] dx \qquad [M_R]^e = \int_0^l [N_b]^T I_d [N_b] dx \tag{2.24}$$

$$[H]^e = \int_0^l [N_\gamma]^T I_p [N_\beta] dx \qquad [G]^e = [H]^e - [H]^{eT} \qquad [K]^e = [K_b]^e + [K_s]^e$$

Shear correction factor κ is given by

$\kappa = \dfrac{6(1+m)}{(7+6m)}$ with m as the Poisson's ratio.

Substituting the element potential energy and the element kinetic energy, respectively given by equation (2.22) and (2.23),

the elemental equation of motion is

$$\left([M_T]^e + [M_R]^e\right)\{\ddot{q}\}^e - \Omega[G]^e\{\dot{q}\}^e + [K]^e\{q\}^e = \{0\} \tag{2.25}$$

Equation (2.25) describes the element motion to the fixed frame coordinate *X-Y-Z* without internal damping and has the property that the *X-Y* and *X-Z* planar motions are coupled due to skew symmetric gyroscopic matrix, $[G]^e$.

To incorporate the effect of internal damping, using the formulations of Zorzi and Nelson [119] and Ozguven and Ozkan [122], the combined effects of both viscous and hysteretic internal damping can be included. $[\eta]$ is the internal damping matrix, which can be defined as

$$[\eta] = \begin{bmatrix} \eta_a & \eta_b \\ -\eta_b & \eta_a \end{bmatrix}$$

$$\eta_a = \frac{1+\eta_H}{\sqrt{1+\eta_H{}^2}} \tag{2.26}$$

$$\eta_b = \frac{\eta_H}{\sqrt{1+\eta_H{}^2}} + \Omega\eta_v$$

Here η_H and η_v denote the viscous damping coefficient and hysteretic loss factor of the shaft material.

Following Lagrangian approach, the elemental equation of motion including internal damping is given by ([122,131]),

$$\left([M_T]^e + [M_R]^e\right)\{\ddot{q}\}^e + \left(\eta_v[K]^e - \Omega\{G\}^e\right)\{\dot{q}\}^e + \left(\eta_a[K]^e + \eta_b[K_C]^e\right)\{q\}^e = \{F\}^e \qquad (2.27)$$

where $[K_C]^e$ is the circulation matrix (Ziegler [154]) in which the instabilities resulting from internal damping are characterized. Both viscous and hysteretic forms of material damping contribute to the circulation term.

The equation of motion for disk is given as

$$[M^d]\{\ddot{q}^d\} + \Omega[G^d]\{\dot{q}^d\} = \{0\} \qquad (2.28)$$

where $[M^d]$ and $[G^d]$ are mass and gyroscopic matrices of disk only.

2.3 Bearing stiffness and damping coefficients

The classical linearized model with eight spring and damping coefficients are employed for the modelling of bearings in the present work. In this model, the forces at each bearing are assumed to obey the governing equations of the following form ([131]),

$$\begin{bmatrix} c_{VV} & c_{VW} \\ c_{WV} & c_{WW} \end{bmatrix}\{\dot{q}^b\} + \begin{bmatrix} k_{VV} & k_{VW} \\ k_{WV} & k_{WW} \end{bmatrix}\{q^b\} = \{F^b\} \qquad (2.29)$$

where

$\{q^b\} = \{v \quad w\}^T$ is the bearing displacement vector and c_{ij} and k_{ij} are the elements of bearing damping and stiffness matrices respectively; $\{F^b\}$ is the vector of bearing forces.

2.4 System equations of motion

For the analysis of natural whirl speeds and instability thresholds of rotor bearing system the force term can be omitted. The resultant system equation of motion thus can be formulated taking into account internal damping, bearing stiffness and damping along with bending and shear stiffness, gyroscopic, translational and rotational mass matrices and to arrive at ([155]),

$$[M^s]\{\ddot{q}\}^e + \left([c^b] - \Omega[G^s]\right)\{\dot{q}\} + \left([K^s] + [k^b]\right)\{q\}^e = \{0\} \qquad (2.30)$$

where $[M^s]$, $[G^s]$ and $[K^s]$ are the assembled mass, gyroscopic and stiffness matrices of the system including the disk mass matrix and $[c^b]$ and $[k^b]$ are the bearing damping and stiffness matrices respectively.

For sake of computational purposes, the equation is written in first-order state vector form as

$$[A]\{\dot{h}\}+[B]\{h\}=\{0\} \tag{2.31}$$

where

$$\{h\}=\begin{Bmatrix}\{\dot{q}\}\\ \{q\}\end{Bmatrix} \tag{2.32}$$

$$[A]=\begin{bmatrix}[0] & [M]\\ [M] & ([c^b]-\Omega[G^s])\end{bmatrix} \tag{2.33}$$

$$[B]=\begin{bmatrix}-[M] & [0]\\ [0] & ([K^s]+[k^b])\end{bmatrix} \tag{2.34}$$

The associated eigen value problem for the equation is sought from an assumed solution as $\{h\}=\{h_0\}e^{vt}$ (2.35)

where $v=\alpha+i\omega$ is the complex eigen value, ω is the natural whirl speed and the parameter of logarithmic decrement, δ, is defined as $\delta=-\frac{2\pi\alpha}{\omega}$. The real part of the eigen value, α, indicates the damping on the system at the given speed. The response of a dynamic system is a decay function that involves the damping term. In order to get stable response the amplitude of vibration should decay as time increases. This will happen if the damping index is negative. In other words, for a stable system, logarithmic decrement, δ, should be greater than zero.

For each of the eigen value, there exists a corresponding eigen vector. This eigen vector represents the mode shape for a given frequency of the system.

2.5 Bearing types

In the present analysis four different types of bearings are used, namely, two-groove bearing, two-lobe bearing, three-lobe bearing and four-lobe bearing. The basics of different types of bearings like geometry, co-ordinate systems etc. are described below.

2.5.1 Two-groove bearing

Geometry and co-ordinate systems for two-groove bearing are shown in Fig. 2.2. In this analysis, two axial grooves of 20^0 circumferential extents each are considered for the provision of oil inlet in the journal bearing clearance area.

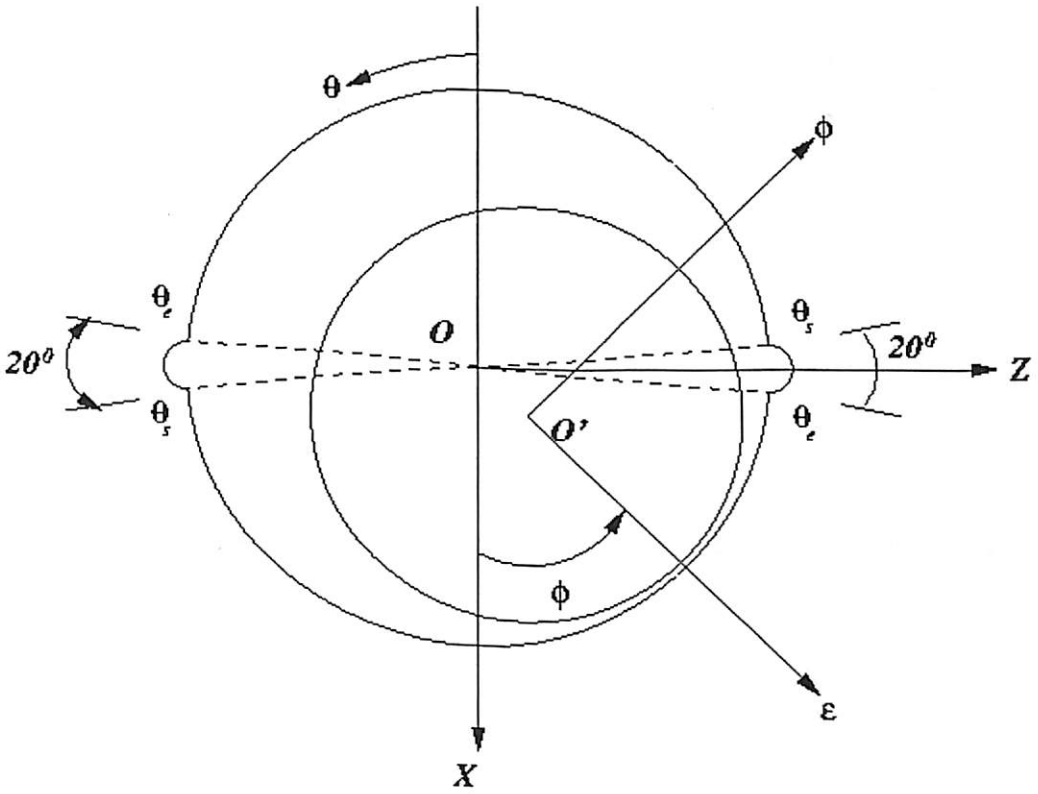

Fig. 2.2: Geometry and Coordinate system of Two-groove bearing

2.5.2 Two-lobe bearing

Geometry and co-ordinate systems for two-lobe bearing are shown in Fig. 2.3 and Fig. 2.4. In this analysis, lobes are separated by axial grooves of 20^0 circumferential extents each for the provision of oil inlet in the journal bearing clearance area.

Two-lobe bearing is made up of two circular arcs each with its own centre of curvature O displaced at a distance 'd' from the geometric centre of the bearing. In the present analysis two lobes of 160^0 arc each are separated by two axial oil grooves of 20^0 circumferential extensions in horizontal direction. In Fig. 2.3, geometry and co-ordinate

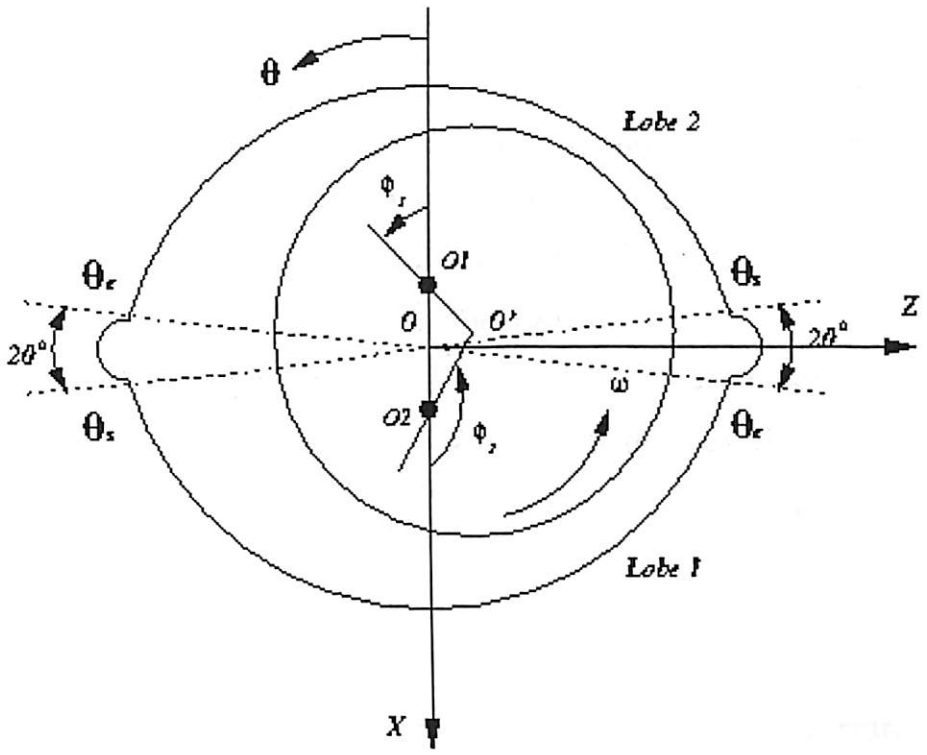

Fig. 2.3: Geometry and Coordinate system of Two-lobe bearing

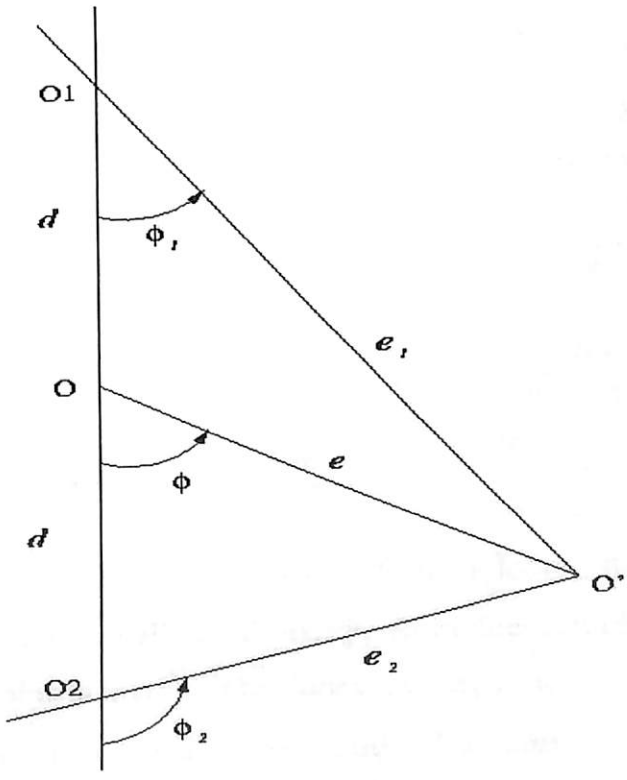

Fig. 2.4: Trigonometry of Two-lobe bearing

systems used for the analysis of two-lobe bearing are shown. For any given shaft position, lobe eccentricity ratios (ε_1, ε_2) and attitude angles (ϕ_1, ϕ_2) can be related with bearing eccentricity ratio (ε), attitude angle (ϕ) and ellipticity ratio (δ) by simple trigonometry relations from Fig. 2.4. In Fig. 2.4, journal centre, bearing geometric centre, centre of lobe 1 and lobe 2 are represented by O', O, O_1 and O_2 respectively. From simple trigonometry, following relations can be obtained.

For lobe 1,

$$e^2{}_1 = e^2 + d^2 - 2ed\cos(\pi - \phi)$$

Dividing both sides by c^2, one gets,

$$\varepsilon^2{}_1 = \varepsilon^2 + \delta^2 + 2\varepsilon\delta\cos\phi$$

Or

$$\varepsilon_1 = \sqrt{\varepsilon^2 + \delta^2 + 2\varepsilon\delta\cos\phi}$$

where $\delta = \frac{d}{c}$ is the bearing ellipticity ratio and $\varepsilon_1 = \frac{e_1}{c}$ is the eccentricity ratio of Lobe 1.

Also

$$\tan\phi_1 = \frac{e\sin\phi}{d + e\cos\phi}$$

$$\phi_1 = \tan^{-1}\frac{\varepsilon\sin\phi}{\delta + \varepsilon\cos\phi}$$

For lobe 2,

$$e^2{}_2 = e^2 + d^2 - 2ed\cos\phi$$

Dividing both sides by c^2, one gets,

$$\varepsilon^2{}_2 = \varepsilon^2 + \delta^2 - 2\varepsilon\delta\cos\phi$$

Or

$$\varepsilon_2 = \sqrt{\varepsilon^2 + \delta^2 - 2\varepsilon\delta\cos\phi}$$

where $\varepsilon_2 = \frac{e_2}{c}$ is the eccentricity ratio of Lobe 2.

$$\tan(\pi - \phi_2) = \frac{e\sin\phi}{d - e\cos\phi}$$

$$\phi_2 = \pi - \tan^{-1}\frac{\varepsilon\sin\phi}{\delta - \varepsilon\cos\phi}$$

2.5.3 Three-lobe bearing

The bearing as shown in Fig. 2.5, consists of three lobes; the centre of each lobe displaced an equal distance, called ellipticity, from the centre of the bearing. The maximum span of a lobe is 120^0. The lobes are separated by 20^0 axial grooves for admitting oil. So the net span of each lobe is 100^0. The individual lobe eccentricities (ε_1, ε_2, ε_3) and attitude angles (ϕ_1, ϕ_2, ϕ_3) can be related with bearing eccentricity and attitude

angle. These relationships are obtained from Fig. 2.6 by following a similar procedure used for two-lobe bearing.

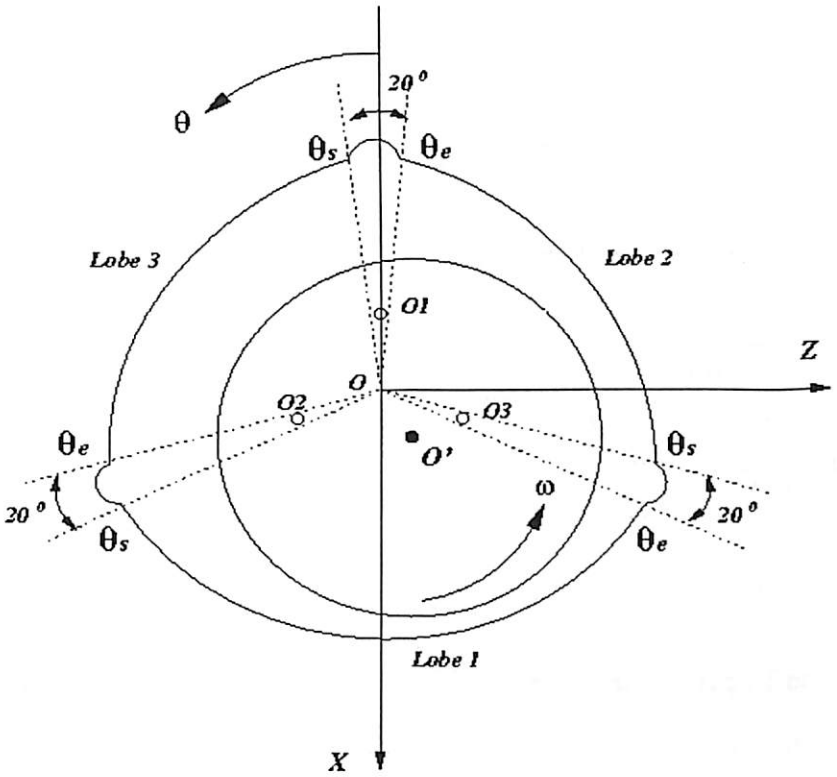

Fig. 2.5: Geometry and Coordinate system of Three-lobe bearing

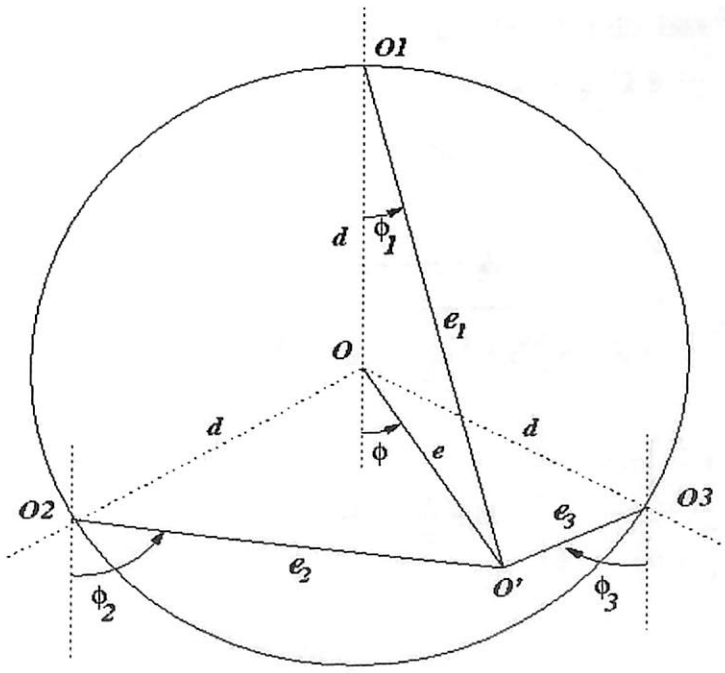

Fig. 2.6: Trigonometry of Three-lobe bearing

For lobe 1,

$$\varepsilon_1 = \sqrt{\varepsilon^2 + \delta^2 + 2\varepsilon\delta\cos\phi}$$

$$\phi_1 = \tan^{-1}\frac{\varepsilon\sin\phi}{\delta + \varepsilon\cos\phi}$$

For lobe 2,

$$\varepsilon_2 = \sqrt{\varepsilon^2 + \delta^2 - 2\varepsilon\delta\cos\left(\frac{\pi}{3} + \phi\right)}$$

$$\phi_2 = \frac{2\pi}{3} - \tan^{-1}\frac{\varepsilon\sin\left(\frac{\pi}{3} + \phi\right)}{\delta - \varepsilon\cos\left(\frac{\pi}{3} + \phi\right)}$$

For lobe 3,

$$\varepsilon_3 = \sqrt{\varepsilon^2 + \delta^2 - 2\varepsilon\delta\cos\left(\frac{\pi}{3} - \phi\right)}$$

$$\phi_3 = \frac{2\pi}{3} - \tan^{-1}\frac{\varepsilon\sin\left(\frac{\pi}{3} - \phi\right)}{\delta - \varepsilon\cos\left(\frac{\pi}{3} - \phi\right)}$$

2.5.4 Four-lobe bearing

The bearing as shown in Fig. 2.7, consists of four lobes; the centre of each lobe displaced by an equal distance, called ellipticity, from the centre of the bearing. The maximum span of a lobe is 90^0. The lobes are separated by 10^0 axial grooves for admitting oil. So the net span of each lobe for each bearing is 80^0. The individual lobe eccentricities (ε_1, ε_2, ε_3, ε_4) and attitude angles (ϕ_1, ϕ_2, ϕ_3, ϕ_4) can be related with bearing eccentricity and attitude angle. These relationships are obtained from Fig. 2.8 by following a similar procedure used for two-lobe and three-lobe bearing.

For lobe 1,

$$\varepsilon_1 = \sqrt{\varepsilon^2 + \delta^2 + 2\varepsilon\delta\cos\phi}$$

$$\phi_1 = \tan^{-1}\frac{\varepsilon\sin\phi}{\delta + \varepsilon\cos\phi}$$

For lobe 2,

$$\varepsilon_2 = \sqrt{\varepsilon^2 + \delta^2 - 2\varepsilon\delta\cos\left(\frac{\pi}{2} + \phi\right)}$$

$$\phi_2 = \frac{\pi}{2} - \tan^{-1}\frac{\varepsilon\sin\left(\frac{\pi}{2} + \phi\right)}{\delta - \varepsilon\cos\left(\frac{\pi}{2} + \phi\right)}$$

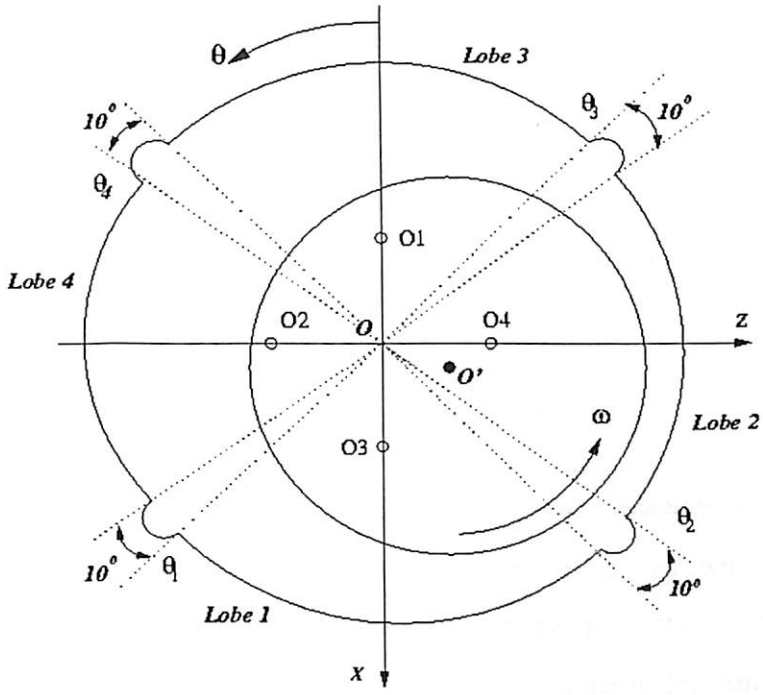

Fig. 2.7: Geometry and Coordinate system of Four-lobe bearing

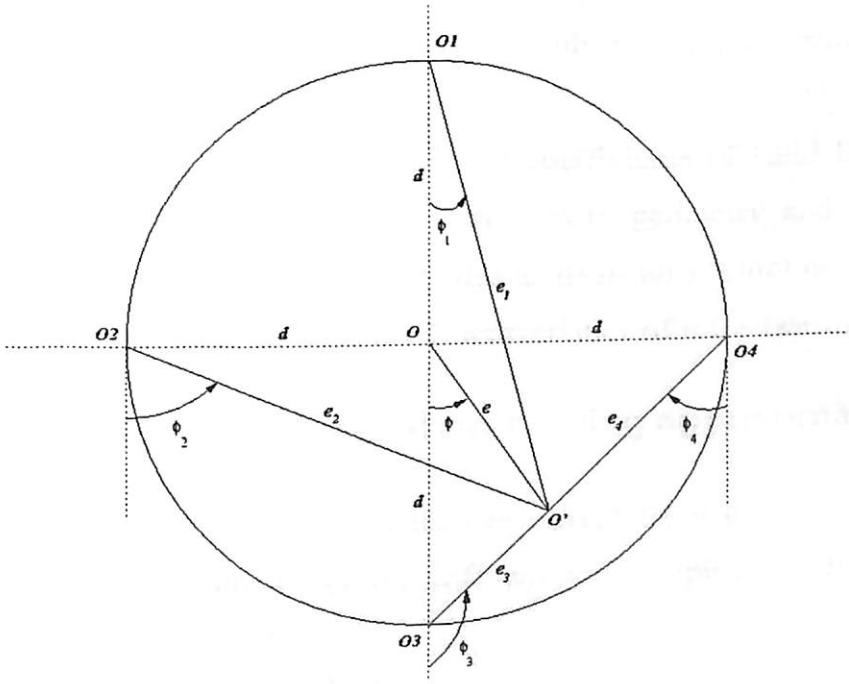

Fig. 2.8: Trigonometry of Four-lobe bearing

For lobe 3,

$$\varepsilon_3 = \sqrt{\varepsilon^2 + \delta^2 - 2\varepsilon\delta\cos\phi}$$

$$\phi_3 = \pi - \tan^{-1}\frac{\varepsilon\sin\phi}{\delta - \varepsilon\cos\phi}$$

For lobe 4,

$$\varepsilon_4 = \sqrt{\varepsilon^2 + \delta^2 - 2\varepsilon\delta\cos\left(\frac{\pi}{2} - \phi\right)}$$

$$\phi_4 = \frac{\pi}{2} - \tan^{-1}\frac{\varepsilon\cos\phi}{\delta - \varepsilon\sin\phi}$$

2.6 Dynamic coefficients of fluid film bearing

Fluid film bearings commonly used in heavy rotating machines and at high-speed applications, play a significant role in the dynamic behaviour of rotors as the stiffness and damping properties of the oil film significantly influence the critical speeds of a rotor. In high-speed applications, rotor stability is an important factor to be considered in the rotor design. The stiffness and damping properties of the oil film also affect the stability of a rotor. The dynamic coefficients, i.e., stiffness and damping coefficients of hydrodynamic bearing are estimated first to utilize these in the study of dynamic behaviour of rotor-bearing system.

Dynamic coefficients i.e., stiffness and damping coefficients of fluid film bearing are speed dependent. These coefficients also change with geometry and other operating conditions like viscosity, bearing load etc. In this analysis an attempt is made to find out effect of viscosity and geometry on stability characteristics of rotor-bearing system.

2.6.1 Dynamic coefficients using short bearing approximation

Short bearing approximation of bearings lead to closed form expressions of dynamic coefficients. The non-dimensional bearing stiffness and damping coefficients are given as,

$$\overline{K}_{XX} = \frac{4\left\{\pi^2 + \left(32 + \pi^2\right)\varepsilon^2 + 2\left(16 - \pi^2\right)\varepsilon^4\right\}Q(\varepsilon)}{\left(1 - \varepsilon^2\right)} \tag{2.36}$$

$$\overline{K}_{XZ} = \frac{4\left\{\pi^2 + \left(32 + \pi^2\right)\varepsilon^2 + 2\left(16 - \pi^2\right)\varepsilon^4\right\}Q(\varepsilon)}{\varepsilon\sqrt{\left(1 - \varepsilon^2\right)}} \tag{2.37}$$

$$\overline{K}_{ZX} = \frac{-\pi^2\left\{\pi^2 - 2\pi^2\varepsilon^2 - \left(16-\pi^2\right)\varepsilon^4\right\}Q(\varepsilon)}{\varepsilon\sqrt{\left(1-\varepsilon^2\right)}} \tag{2.38}$$

$$\overline{K}_{ZZ} = 4\left\{2\pi^2 + (16-\pi^2)\varepsilon^2\right\}Q(\varepsilon) \tag{2.39}$$

and

$$\overline{C}_{XX} = \frac{2\pi\left\{\pi^2 + 2\left(24-\pi^2\right)\varepsilon^2 + \pi^2\varepsilon^4\right\}Q(\varepsilon)}{\varepsilon\sqrt{\left(1-\varepsilon^2\right)}} \tag{2.40}$$

$$\overline{C}_{XZ} = \overline{C}_{ZX} = 8\left\{\pi^2 + 2\left(\pi^2 - 8\right)\varepsilon^2\right\}Q(\varepsilon) \tag{2.41}$$

$$\overline{C}_{ZZ} = \frac{2\pi\sqrt{\left(1-\varepsilon^2\right)}}{\varepsilon}\left\{\pi^2 + 2\left(\pi^2 - 8\right)\varepsilon^2\right\}Q(\varepsilon) \tag{2.42}$$

where

$$Q(\varepsilon) = \frac{1}{\left\{\pi^2\left(1-\varepsilon^2\right)+16\varepsilon^2\right\}^{3/2}} \tag{2.43}$$

To determine the stiffness and damping coefficients of a short bearing, first Sommerfeld number 'S' should be determined which is equal to

$$S = \frac{\mu DLN}{W}(R/C)^2 \tag{2.44}$$

Eccentricity ratio under steady state operating condition can be determined from Sommerfeld number. The relationship is given as,

$$S\left(\frac{L}{D}\right)^2 = \frac{\left(1-\varepsilon^2\right)^2}{\pi\varepsilon\sqrt{\pi^2\left(1-\varepsilon^2\right)+16\varepsilon^2}} \tag{2.45}$$

While determining the eccentricity ratio, an iteration procedure is required as equation (2.45) is transcendental in nature. A plot of Sommerfeld number 'S' as a function of eccentricity ratio 'ε' for short bearing ($L/D=0.5$) according to equation (2.45) is given in Fig. 2.9.

From the given operating conditions and geometric parameters of bearing, 'S' can be obtained. From Fig. 2.9 'ε' can be obtained for a particular value of 'S'. Once the eccentricity ratio is obtained stiffness and damping coefficients are evaluated from equation (2.36) through equation (2.42).

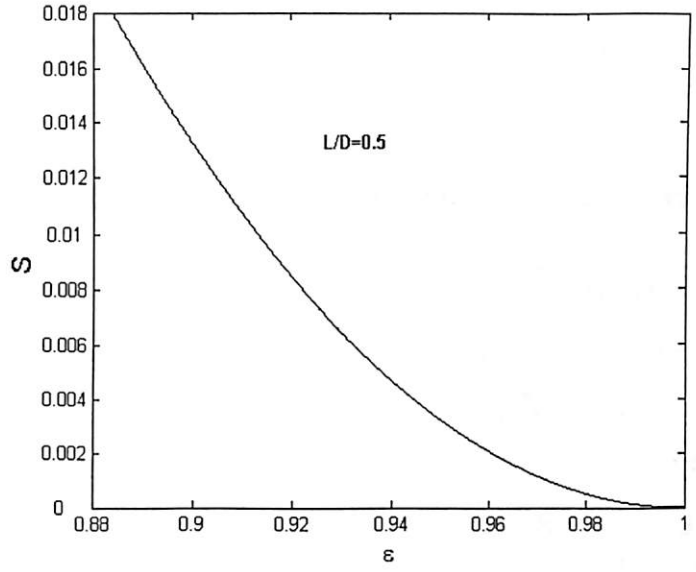

Fig. 2.9: Sommerfeld number for short bearing as a function of eccentricity ratio

2.6.2 Finite bearing dynamic coefficients

Critical speeds of rotor evaluated at different operating conditions using dynamic coefficients of short bearing theory are bound to have some amount of inherent error due to its approximation. Therefore, the dynamic coefficients evaluated for finite bearings using numerical scheme are used in the present model. Results using finite bearing dynamic coefficients are compared with those using short bearing approximation. Operating condition of rotor-bearing system includes not only the speed but also viscosity of oil, length to diameter ratio of bearing.

Initially the dynamic coefficients for different bearings are evaluated using the code based on the numerical scheme of Lund [156]. Sommerfeld numbers are calculated for different operating conditions; then corresponding eccentricity ratios are found from the code. The code facilitates estimation of the stiffness and damping coefficients for particular eccentricity ratio. The same classical linearized model ([131]) as shown in the section 2.3 with eight spring and damping coefficients is employed for the modelling of bearings in the present work.

A few sample dynamic coefficients evaluated for different bearings and used for rotor-bearing analysis are provided in Table 2.1 and Table2.2. These dynamic coefficients of the bearings are used in the FEM model to estimate natural whirl frequencies.

Table 2.1: Sample stiffness coefficients of different bearings

Bearing Type	Sommerfeld Number	Stiffness coefficients			
		k_{XX} (N/m) (10^8)	k_{XZ} (N/m) (10^8)	k_{ZX} (N/m) (10^8)	k_{ZZ} (N/m) (10^8)
Grooved circular	0.03724	6.832	4.056	0.4510	1.507
	0.29790	1.944	3.718	-0.969	1.597
	0.89390	1.711	6.472	-1.796	1.366
Two-lobe	0.03724	2.7269	1.5548	0.1520	0.5528
	0.29790	3.3994	2.1320	-1.8210	0.2206
	0.89390	9.2102	-5.4921	-5.2683	-0.0229
Three-lobe	0.03724	3.8061	1.9410	0.0451	0.0517
	0.29790	2.2103	1.8199	-1.8561	0.7033
	0.89390	3.8886	2.5560	-6.2448	1.2678
Four-lobe	0.03724	4.7671	2.0267	-0.1338	0.5378
	0.29790	1.9838	2.9005	-1.3660	1.7230
	0.89390	2.3573	4.8169	-3.9480	2.7123

Table 2.2: Sample damping coefficients of different bearings

Bearing Type	Sommerfeld Number	Damping coefficients			
		c_{XX} (Ns/m) (10^5)	c_{XZ} (Ns/m) (10^5)	c_{ZX} (Ns/m) (10^5)	c_{ZZ} (Ns/m) (10^5)
Grooved circular	0.03724	8.114	1.783	1.791	1.00
	0.29790	7.592	1.894	1.893	2.494
	0.89390	12.88	1.245	1.244	3.867
Two-lobe	0.03724	60.135	12.062	12.0620	7.5307
	0.29790	16.362	-4.1000	-4.0941	4.3815
	0.89390	15.066	-5.2148	-5.2068	3.5974
Three-lobe	0.03724	81.312	11.9150	11.9660	7.3833
	0.29790	1.1362	-1.4552	-1.4497	7.5159
	0.89390	6.0192	-3.3554	-3.3514	8.7176
Four-lobe	0.03724	91.910	10.1390	10.1830	8.5770
	0.29790	14.059	3.3306	3.3379	7.8337
	0.89390	7.7769	0.8879	0.8919	6.8242

2.7 Conclusions

In the present work, finite element method is used to model the rotor-bearing system for the study of natural whirl frequencies, critical speeds, mode shapes and stability analyses. Three different types of beams, namely, Euler-Bernoulli beam, Rayleigh beam and Timoshenko beam are considered. In this chapter, the finite element formulations for all three types of beams are presented. System equation of motion and eigen value solution are given. The analysis is extended to use fluid film bearing in the same rotor-bearing system. Four different types of bearings (both circular and non circular) are used. Therefore geometry, co-ordinate system, trigonometry involved in those bearings are also provided in this chapter.

Chapter 3

Whirling of rotors using different beam models

3.1 Introduction

In the present chapter initially Euler-Bernoulli beam theory is considered for the whirl analysis of rotor mounted on rigid supports. Then this simple analysis is extended to include gyroscopic effect, rotary inertia effect and shear effect and further extended to rotor mounted on fluid film bearings.

Results for different cases are given either in tabular or in graphical forms. Maple package is used to perform symbolic matrix operations while obtaining shape functions, mass, stiffness and gyroscopic element matrices. A computer code is developed to generate the assembled (system) mass and stiffness matrix and to apply boundary conditions to get the dynamic matrix. From the dynamic matrix the system natural whirl frequencies and corresponding mode shapes are obtained by eigen value and eigen vector extraction module of MATLAB package.

For all types of beams, analysis is done for consistent mass approach. Lumped mass analysis is also done for all types of beams and results are validated with classical solution results, which are not presented here.

3.2 Euler-Bernoulli beam

In the beginning of the analysis Euler-Bernoulli beam theory is considered for the whirl speed analysis of rotor mounted on rigid supports. The mass matrices, stiffness matrices and assembled system equations of motion are obtained [132] and are given in the appendix. Gyroscopic effect is not considered. Therefore the whirling motions of the shaft in vertical and horizontal directions are uncoupled and the analysis in vertical plane is identical with the analysis in horizontal plane.

For Euler-Bernoulli beam the following two cases are analyzed:

3.2.1 Consistent mass analysis without disk

3.2.1.1.1 Simply supported beam

3.2.1.1.2 Overhung beam model

3.2.2 Consistent mass analysis with disk

3.2.1 Consistent mass analysis without disk

3.2.1.1 Simply supported beam

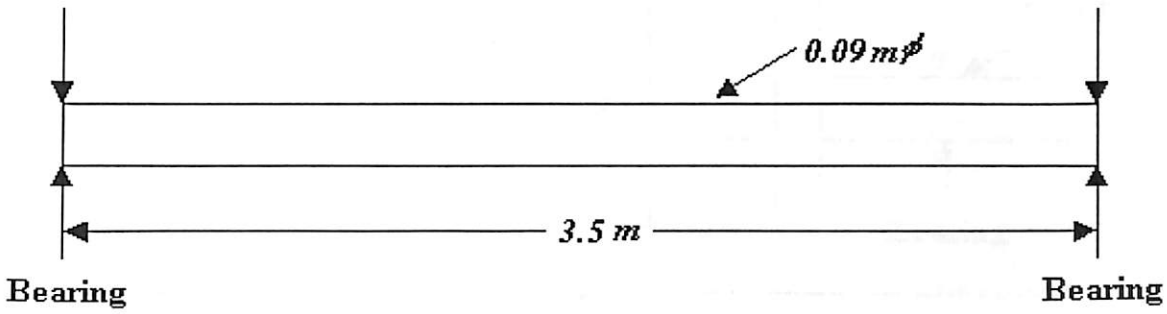

Fig. 3.1: Simply Supported Rotor system on bearings

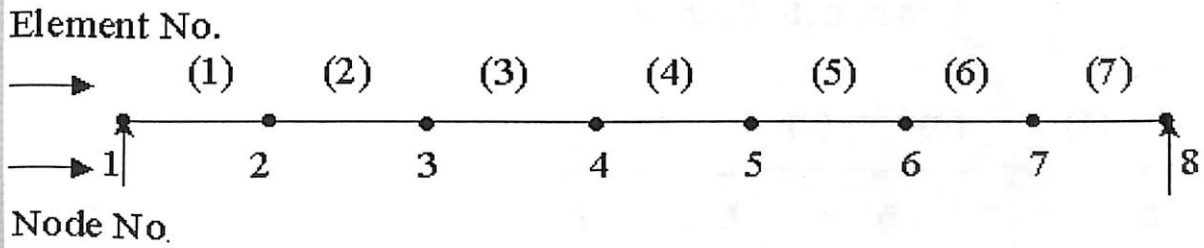

Fig. 3.2: Simply Supported seven-element rotor model (length of each element is 0.5m)

In order to check the present developed code for consistent mass approach a simply supported uniform beam as sown in the Fig. 3.1 is analyzed. The analysis is conducted

with seven-element model as shown in the Fig. 3.2. The physical properties of the shaft are listed in Table 3.1.

Table 3.1: Physical properties of the shaft

Density of the shaft material, ρ	7830 kg/m^3
Elastic Modulus of the shaft material, E	2.07E+11 N/m^2

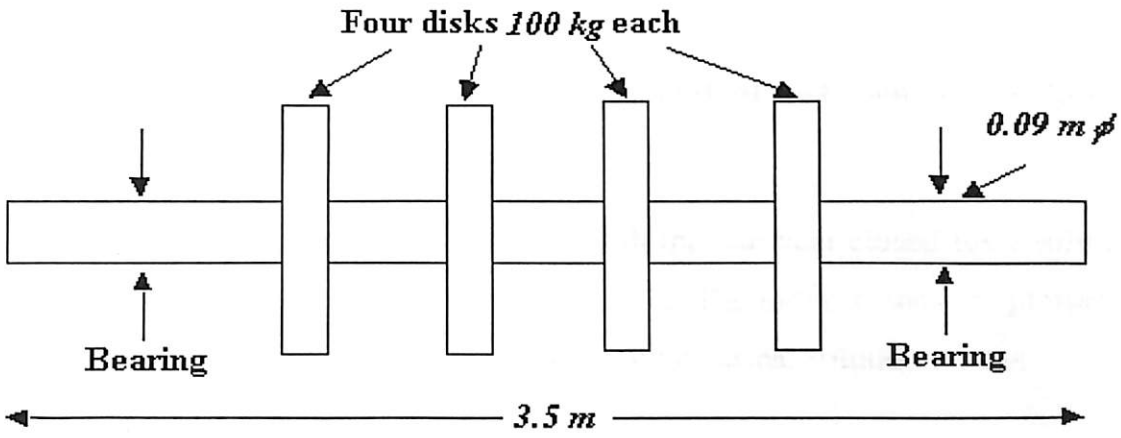

Fig. 3.3: Overhung Rotor system on bearings

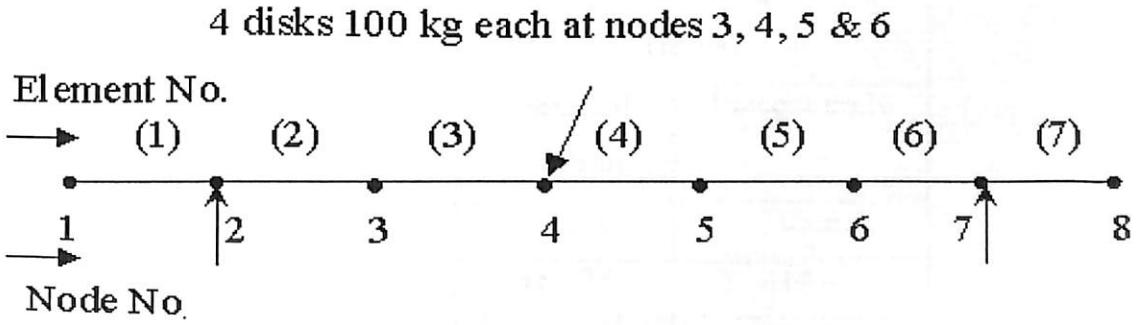

Fig. 3.4: Seven-element rotor model (length of each element is 0.5m)

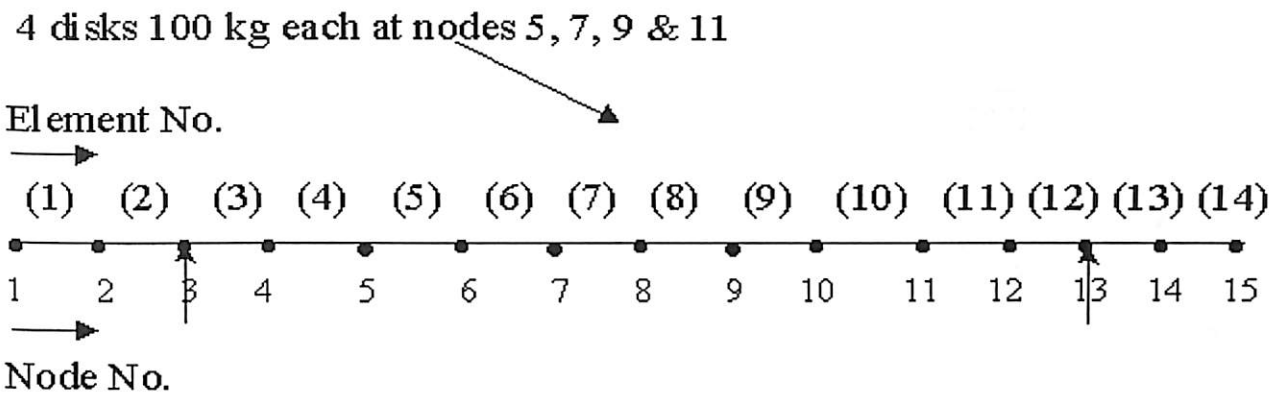

Fig. 3.5: Fourteen-element rotor model (length of each element is 0.25m)

Comparisons of the present results are made with the classical closed form solution and results for first fourth mode are shown in Table 3.2. The mode shapes are plotted in Fig. 3.6. The present results are in good agreement with classical solution results.

Table 3.2: Comparison of Natural whirl frequencies of a Rotor-Bearing System: Simply Supported Euler-Bernoulli beam –Consistent mass analysis without disk

Mode No.	Natural whirl frequencies (rad/s)	
	Classical solution	Present code
1	103.56	103.6
2	414.25	414.4
3	932.07	934.1
4	1657.00	1667.9

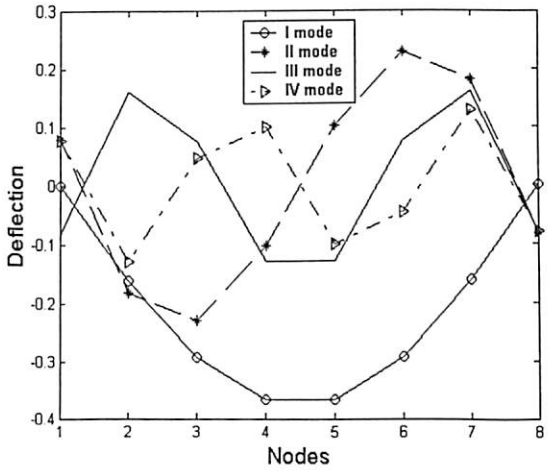

Fig. 3.6: Mode shapes for Euler-Bernoulli beam: Simply Supported beam (Consistent mass analysis without disk)

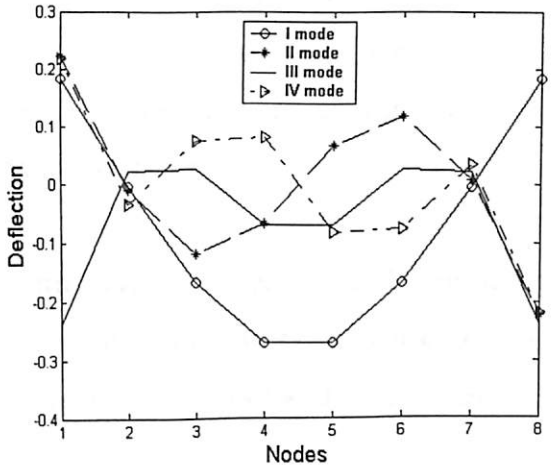

Fig. 3.7: Mode shapes for Euler-Bernoulli beam: Overhung beam model (Consistent mass analysis without disk)

3.2.1.2 Overhung beam model

Having validation of the code, next, an overhung rotor system as shown in Fig. 3.3 (without disk) is considered in order to evaluate the natural whirl frequencies and mode shapes. The analysis is conducted with seven-element model as shown in the Fig. 3.4

Table 3.3: Natural whirl frequencies of a Rotor-Bearing System: Overhung Euler-Bernoulli beam model -Consistent mass matrix analysis without disk

Mode No.	Natural whirl frequencies (rad/s)
1	192.8
2	642.9
3	1036.9
4	1463.5

(without disk). The physical properties of the shaft are listed in Table 3.1. Two identical rigid supports are located at stations two and seven. For the analysis, shaft is considered to be of uniform cross section. The first four natural whirl frequencies are listed in Table 3.3 and mode shapes are plotted in Fig. 3.7. As the results are matching excellently for simply supported beam with consistent mass approach, the results presented in Table 3.3 are expected to be acceptable.

To demonstrate the convergence of the results with seven-element model, the analysis is also done using fourteen-element model (Fig. 3.5) also and the results are found to be identical. In view of this, seven-element model of the rotor is used in the forthcoming analysis.

3.2.2 Consistent mass analysis with disk

In the section 3.2.1, the present computer code is validated for consistent mass approach without disk. Now, it is proposed to extend the work by introducing four identical disks on the rotor as shown in the Fig. 3.3. The undamped natural whirl frequencies of the overhung rotor system with distributed mass of shaft and lumped mass of disks (i.e. mass moment of inertia of the disks are not considered) are computed from seven-element eigen value problem. The first four natural whirl frequencies are listed in Table 3.4 and mode shapes are plotted in Fig. 3.8.

Table 3.4: Natural whirl frequencies of a Rotor-Bearing System: Overhung Euler-Bernoulli beam model -Consistent mass matrix analysis with disk

Mode No.	Natural whirl frequencies (rad/s)
1	115.9
2	437.3
3	859.4
4	1206.5

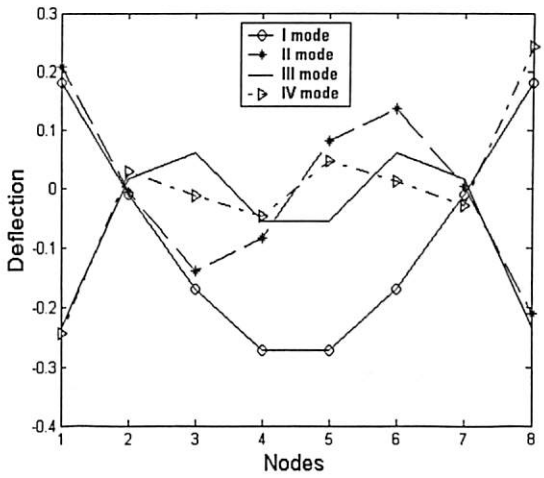

Fig. 3.8: Mode shapes for Euler-Bernoulli beam: Overhung beam model (Consistent mass analysis with disk)

3.3 Rayleigh beam

In this section, the analysis of whirling of simple rotor bearing system is extended to include the gyroscopic effects and rotary inertia effects. A finite element formulation including these effects has been already presented in Chapter 2 and it yields the gyroscopic matrix as a skew symmetric one. The eigen value problem gives the eigen values as pure imaginary conjugate pairs with magnitude equal to the natural whirl frequencies. A positive root indicates that the whirl is in the same direction as the spin speed, and it is called as forward whirl. A negative value of the whirl frequency indicates that the rotor whirls in a direction opposite to that of the spin speed and this is termed as backward whirl. Because of the gyroscopic terms, the natural whirl frequencies are function of spin speed of the shaft. To determine the critical speeds, Campbell diagrams have been drawn. The intersection of the points of natural whirl frequencies with 1 per rev excitation (for synchronous whirl, $\lambda = \omega$) gives the critical speeds.

The following cases are analyzed:

3.3.1 Consistent mass analysis without disk

3.3.1.1 Simply supported beam

3.3.1.2 Overhung beam model

3.3.2 Consistent mass analysis with disk

3.3.2.1 Supported on rigid supports

3.3.2.2 Supported on fluid film (short) bearings

3.3.1 Consistent mass analysis without disk

3.3.1.1 Simply supported beam

In order to validate the present developed code a simply supported beam is analyzed first. The critical speeds for forward and backward whirl are given in Table 3.5. Comparisons of the present results are made with the classical closed form solution of Tondl [70] and are given in the Table 3.5. It shows that present results are in good agreement with the classical solutions particularly for first and second mode.

Table 3.5: Comparison of Critical speeds of a Rotor-Bearing System: Simply Supported Rayleigh beam –Consistent mass analysis without disk

Mode No.	Critical speeds (rad/s)			
	Classical solution		Present code	
	Forward	Backward	Forward	Backward
1	103.92	103.70	103.6	103.5
2	416.94	414.79	414.9	413.2
3	942.91	933.27	936.2	927.8
4	1688.45	1659.16	1648.1	1674.7

3.3.1.2 Overhung beam model

As the results for simply supported case matched well with the classical closed form solutions, therefore the same model is used in this section to evaluate the undamped natural whirl frequencies of an overhung rotor system as shown in Fig. 3.3 (without disk). The results for first four natural whirl frequencies at different spin speeds are evaluated and results are presented in the form of Campbell diagram in Fig. 3.9. Backward and forward critical speeds are given in Table 3.6.

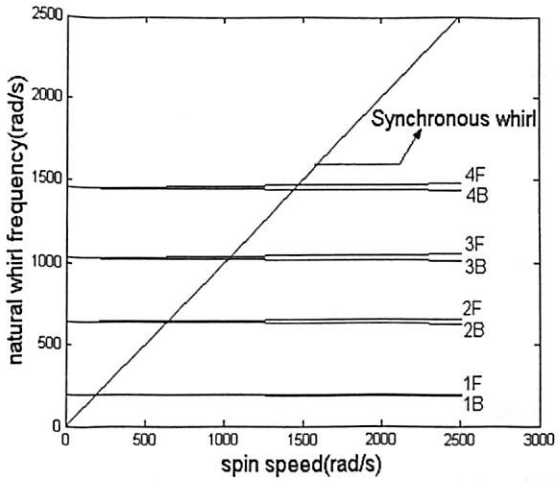

Fig. 3.9: Campbell Diagram for Rayleigh beam: Overhung beam model (Consistent mass analysis without disk)

Table 3.6: Critical speeds of a Rotor-Bearing System: Overhung Rayleigh beam model -Consistent mass matrix analysis without disk

Mode No.	Critical speeds (rad/s)	
	Forward	Backward
1	192.9	192.3
2	644.7	637.4
3	1041.1	1024.6
4	1469.2	1446.7

For both the cases natural frequencies for forward direction increase with increase of spin speed. But it decreases with increase of spin speed in case of backward whirl.

3.3.2 Consistent mass analysis with disk

3.3.2.1 Supported on rigid supports

The undamped natural whirl frequencies of an overhung rotor system as shown in Fig. 3.3 with rigid disks and mounted on rigid supports are computed from eigen value problem of same order equation and results for first four natural whirl frequencies at different spin speeds are evaluated. Campbell diagram is plotted for first four natural whirl frequencies and are given in Fig. 3.10. The first four critical speeds obtained from the Campbell diagram are given in Table 3.7.

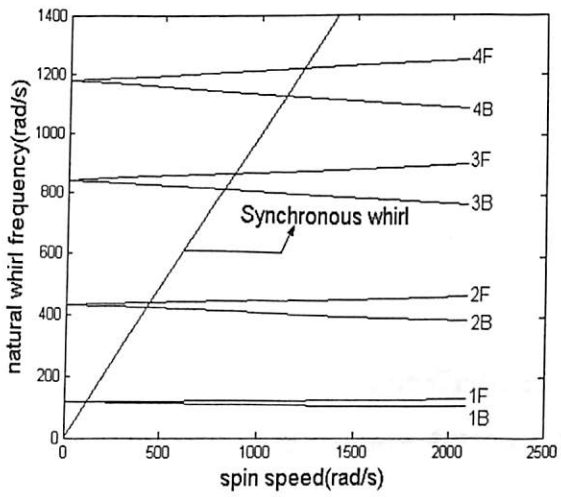

Fig. 3.10: Campbell Diagram for Rayleigh beam: Overhung beam model mounted on rigid supports (Consistent mass analysis with rigid disk)

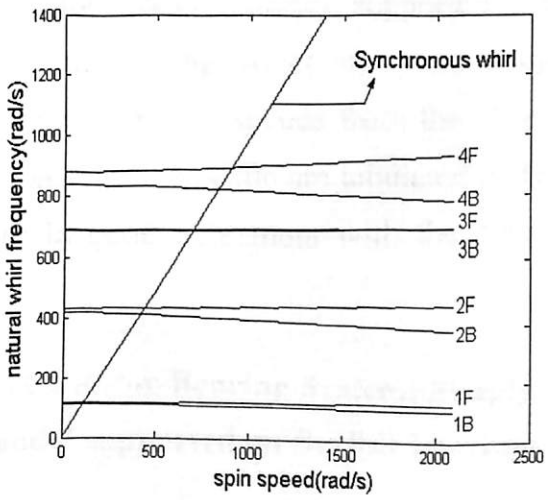

Fig. 3.11: Campbell Diagram for Rayleigh beam: Overhung beam model mounted on fluid film short bearings (Consistent mass analysis with rigid disk)

Table 3.7: Comparison of Critical speeds of a Rotor-Bearing System: Overhung Rayleigh beam model supported on rigid supports

Mode No.	Critical speeds (rad/s)		
	Without gyroscopic effect	With gyroscopic effect	
		Backward	Forward
1	115.5	114.8	116.2
2	431.9	423.3	440.7
3	843.0	816.6	869.8
4	1179.3	1133.0	1223.6

3.3.2.2 Supported on fluid film short bearings

In order to validate the present code a Jeffcott rotor model (simply supported with a central disk) mounted on flexible identical bearings having direct and cross-coupled stiffness coefficients (without damping) is analyzed. Critical speeds from the classical closed form solutions of Rao [132] and from the present FEM code are tabulated in Table 3.8. It shows that the present code results are in good agreement with the classical solution results.

Table 3.8: Comparison of Critical speeds of a Rotor-Bearing System: Simply Supported Rayleigh beam Jeffcott rotor model supported on flexible bearings

First mode	Critical speeds (rad/s)	
	Classical solution	Present code
Forward	143.85	142.4
Backward	140.68	139.3

The undamped natural whirl frequencies of an overhung rotor system as shown in Fig. 3.3 with rigid disks and mounted on fluid film bearings are computed from eigen value problem of same order equation and natural whirl frequencies at different spin speeds are

evaluated. Campbell diagram plotted for first four natural whirl frequencies are given in Fig. 3.11. The physical properties and geometry of the bearings are listed in Table 3.9. The first four critical speeds in forward and backward direction are evaluated. Comparisons of critical speeds of the system supported on rigid supports and fluid film bearings are presented on Table 3.10.

Table 3.9: Physical properties and geometry of the fluid film short bearing considered

Diameter of the bearing, D	0.09 m
Length of the bearing, L	0.045 m
Bearing load, W	1181.88 N
Viscosity of lubricant, μ	0.0242 Ns/m^2
Radial clearance, C	0.00254 cm
$k_{XX}, k_{XZ}, k_{ZX}, k_{ZZ}$	$2.1\text{x}10^9$ N/m, $0.55\text{x}10^9$ N/m, $0.14\text{x}10^9$ N/m, $0.091\text{x}10^9$ N/m
$c_{XX}, c_{XZ}, c_{ZX}, c_{ZZ}$	$1.94\text{x}10^6$ $N/m/s$, $0.33\text{x}10^6$ $N/m/s$, $0.33\text{x}10^6$ $N/m/s$, $0.081\text{x}10^6$ $N/m/s$

Table 3.10: Comparison of Critical speeds of a Rotor-Bearing System: Overhung Rayleigh beam model mounted on rigid supports against fluid film bearings

Mode No.	Critical speeds (rad/s)			
	Rigid support		Fluid film bearing	
	Forward	Backward	Forward	Backward
1	116.2	114.8	115.6	113.1
2	440.7	423.3	436.6	415.1
3	869.8	816.6	691.3	689.3
4	1223.6	1133.0	897.1	826.2

3.4 Timoshenko beam

Rayleigh beam model does not take into account the shear effect. In order to make the model more realistic, the analysis of whirling of simple rotor-bearing system is extended to include shear effect also. Hence the effects of translational inertia, bending deformation, rotary inertia, shear deformation are all considered. A finite element formulation including these effects has been already presented in the Chapter 2.

3.4 1 Non-rotating Timoshenko beam

In order to evaluate the accuracy of the present finite element model, the natural frequencies of a uniform, non-rotating simply supported Timoshenko beam without disk are first evaluated by discretising the beam into numbers of elements. Since the beam is non-rotating, gyroscopic effect is not present. The slenderness parameter *sr (=r/2L)* is varied from *0.02* to *1.0*. Natural frequencies are non-dimensionalised by using natural frequency parameter, ϖ_n ($\varpi_n^4 = \rho AL^4 \omega_n^2 / EI$). The results for first four modes are compared with classical closed form solutions given by Shames and Dym [158] as shown in Table 3.11.

Table 3.11: Natural frequency parameters ϖ_n ($\varpi_n^4 = \rho AL^4 \omega_n^2 / EI$) of a non-rotating Simply Supported Timoshenko beam mounted on rigid supports

sr= (r/2 L)	Natural frequency parameters ϖ_n ($\varpi_n^4 = \rho AL^4 \omega_n^2 / EI$)							
	I mode		II mode		III mode		IV mode	
	Classical	Present	Classical	Present	Classical	Present	Classical	Present
0.02	3.1295	3.1308	6 .1902	6.2056	9.1281	9.2026	11.9108	12.1402
0.04	3.0951	3.0987	5.9584	5.9927	8.4880	8.6418	10.7105	11.1201
0.06	3.0427	3.0492	5.6587	5.7122	7.8143	8.0669	9.6211	10.0962
0.08	2.9777	2.9864	5.3552	5.4089	7.2158	7.4034	8.7397	9.2200
0.10	2.9052	2.9132	5.0699	5.1015	6.7064	6.8473	8.0325	8.4924

It is observed that the present results are found to be in good agreement with those of classical solution. From the results, it is clear that as the diameter of the beam is increased the non-dimensionalised natural frequency decreases.

The natural whirl frequencies of the same overhung rotor bearing system as shown in Fig. 3.3 (with disk) are computed from eigen value problem of equation. The first four natural whirl frequencies are listed in Table 3.12. The natural whirl frequencies of the same rotor bearing system without considering shear and rotary inertia effect are also tabulated. For the present case since '*sr*' is less than *0.02*, the effect of shear is less. But as rotary inertia is also considered, natural whirl frequencies of the rotor bearing system decreases as compared to Euler-Bernoulli case.

Table 3.12: Natural whirl frequencies of a non-rotating Overhung Timoshenko beam with disk

Mode No	Natural whirl frequencies (rad/s)	
	Without considering shear and rotary inertia effect	With shear and rotary inertia effect
1	116.2	116.0
2	438.4	436.2
3	861.5	853.3
4	1209.5	1189.5

3.4.2 Rotating Timoshenko beam

The analysis is extended to whirling of rotating Timoshenko beam, which includes the gyroscopic effect also. Because of the gyroscopic effect two perpendicular transverse motions are coupled and natural frequencies of the systems depends upon angular velocity of the shaft. Forward and backward whirl phenomenon also occurs.

In order to validate the code, a simply supported rotating Timoshenko beam model with gyroscopic effect is discretised into different elements. The critical speeds are non-dimensionalised by using natural frequency parameter; ϖ_n ($\varpi_n^4 = \rho A L^4 \omega_n^2 / EI$) and results are compared to the results published by Eshleman and Eubanks [159]. The

results are listed in Table 3.13. The effect of shear goes on increasing as slenderness parameter *sr* (= *r/2L*, where *r* is the radius of the beam), is changed from *0.02* to *0.10*. The results are in agreement with the values published by Eshleman and Eubanks.

Table 3.13: Non-dimensionalised critical speeds of a rotating Simply Supported Timoshenko beam

sr= (*r/2L*)	I mode				II mode			
	Eshleman & Eubanks [159]		Present work		Eshleman & Eubanks [159]		Present work	
	Backward whirl	Forward whirl	Backward whirl	Forward whirl	Backward whirl	Forward whirl	Backward whirl	Forward whirl
0.02	3.1251	3.1373	3.1294	3.1297	6.1560	6.2489	6.1935	6.1959
0.04	3.0780	3.1245	3.0918	3.0957	5.8387	6.1515	5.9470	5.9707
0.06	3.0067	3.1037	3.0332	3.0439	5.4493	6.0045	5.6335	5.6839
0.08	2.9193	3.0757	2.9614	2.9795	5.0670	5.8250	5.3201	5.3884
0.10	2.8234	3.0416	2.8828	2.9077	4.7231	5.6287	5.0317	5.1089

The same overhung rotor bearing system as shown in Fig. 3.3 is analyzed with seven number of elements. Variation of natural whirl frequencies as a function of spin speed is obtained by solving eigen value problem at different spin speeds. The critical speed map called Campbell diagram is plotted for first four natural whirl frequencies as a function of spin speed.

The following two cases are analyzed:

3.4.2.1 Consistent mass analysis with disk supported on rigid supports

3.4.2.2 Consistent mass analysis with disk supported on fluid film short bearings

3.4 2.1 Consistent mass analysis with disk supported on rigid supports

Natural whirl frequencies of the overhung rotor bearing system (supported on rigid supports) for different spin speeds are plotted for first four modes and are given in Fig. 3.12.

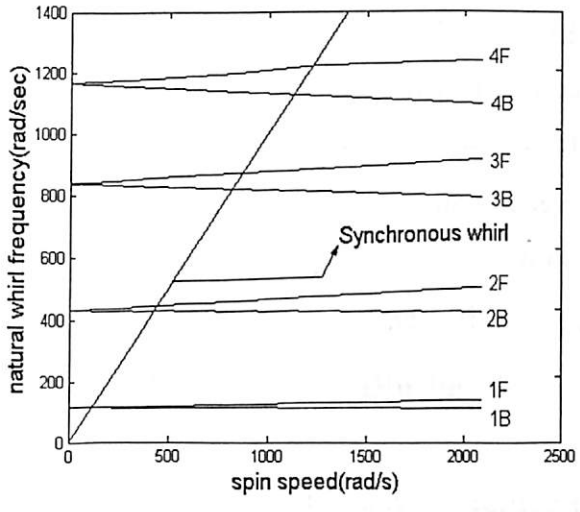

Fig. 3.12: Campbell Diagram for Timoshenko beam: Overhung beam model supported on rigid supports

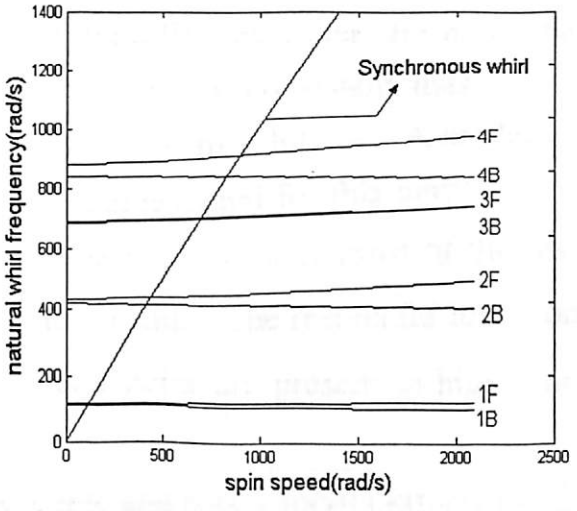

Fig. 3.13: Campbell Diagram for Timoshenko beam: Overhung beam model supported on fluid film short bearings

3.4.2.2 Consistent mass analysis with disk supported on fluid film short bearing

Forward and backward natural whirl frequencies for first four modes of the overhung rotor bearing system (supported on fluid film short bearing) for different spin speeds are evaluated. The physical properties of the bearings are listed in Table 3.9. Campbell diagram plotted for first four modes are given in Fig. 3.13.

From the above results for Timoshenko beam, it is clear that, for lower order mode natural frequencies in case of fluid film bearing are lower than the natural frequencies for rigid supports. But for higher order, natural frequencies for rigid supports are lower than the natural frequencies of fluid film bearing.

3.5 Conclusions

The analysis of rotors mounted on rigid support is done first by Euler- Bernoulli beam theory using FEM. The whirl frequencies are evaluated by consistent mass analysis approaches and the results are compared with the closed form solutions. A model of an overhung rotor with four disks as shown in Fig. 3.3 is considered for this purpose. From the presented results, it has been observed that except for few cases most of the results are in very good agreement with the classical solution results. The results for lower order modes are almost same. But the differences in frequencies are present in higher order modes.

The analysis is then extended to include the gyroscopic and rotary inertia effects by using the same model supported on both rigid support and fluid film bearing. In those cases also most of the results are in very good agreement with the classical solution results.

The analysis is then further extended to include the shear effect by using the same model supported on both rigid support and fluid film bearing. In those cases most of the results are in very good agreement with the classical solution results. Due to shear effect, deflection of the beam increases which reduces the effective stiffness. Therefore, as the diameter of the beam is increased, the non-dimensionalised natural frequency decreases. In the following chapters more detailed study is being carried out for rotors supported on fluid film bearings.

Chapter 4

Whirling of rotors supported on fluid film bearings

4.1 Introduction

In the previous chapter, whirl analysis is done for different types of beam mounted mostly on rigid supports. This has been observed that very little information is available on the behaviour of rotor-bearing systems mounted on fluid film bearings. To characterize such systems, an effort is made to study the effects of different operating conditions on the dynamic behaviour of Timoshenko beam supported on hydrodynamic bearings. Dynamic coefficients of both short bearing and finite bearing are used in the FEM model to estimate natural whirl frequencies. Subsequently internal damping of rotor is also included in the FEM model to study its effects. Jeffcott model gives fairly good results for symmetrical rotors in the fundamental mode region. Therefore along with multi-mass model, rotor-bearing system with Jeffcott model is also used. Grooved circular bearings are used. Synchronous whirling frequencies and additional sub-synchronous whirling frequencies are observed and corresponding mode shapes are plotted. Stability analysis is carried out by estimating logarithmic decrements.

4.2 Models used

Three different models are considered in this study. These models are:

Model 1: A simply supported steel shaft of seven elements having two identical isotropic bearings at both the ends (Fig. 4.1) has been considered as the Model 1. The physical properties of the shaft are given in Table 4.1.

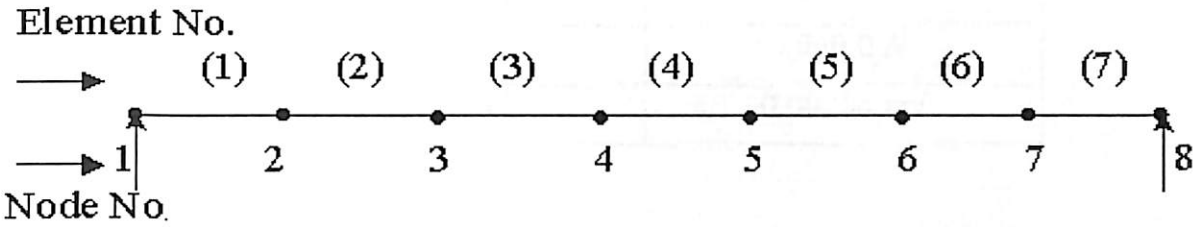

Fig. 4.1: Seven-element Simply Supported rotor model (length of each element is 0.1814 m)

Table 4.1: Physical properties of the shaft

Density of the shaft material, ρ	7833 kg/m^3
Elastic Modulus of the shaft material, E	2.068E+11 N/m^2
Diameter of the shaft, D	10.16 cm
Length of the shaft, L	127 cm

Model 2: A seven-element model, as described in Chapter 3, having four identical disks at nodes three, four, five and six and supported by two identical bearings at stations two and seven has been considered as the Model 2 (Fig. 3.4). The physical properties of the shaft and geometry of the bearings are given in Table 4.2 (a) and Table 4.2 (b).

Table 4.2 (a): Physical property of the shaft

Density of the shaft material, ρ	7830 kg/m^3
Elastic Modulus of the shaft material, E	2.08E+11 N/m^2
Diameter of the shaft, D	0.09 m
Length of the shaft, L	3.5 m

Table 4.2 (b): Geometry of the bearings

Diameter of the bearing, D	0.09 m
Bearing load, W	1960.0 N
Radial clearance, C	0.00254 cm

Model 3: A fourteen-element Jeffcott rotor having two identical bearings located at stations three and thirteen (Fig.4.2) has been studied as the Model 3. The physical properties of the shaft and geometry of the bearings are listed in Table 4.3 (a) and Table 4.3 (b).

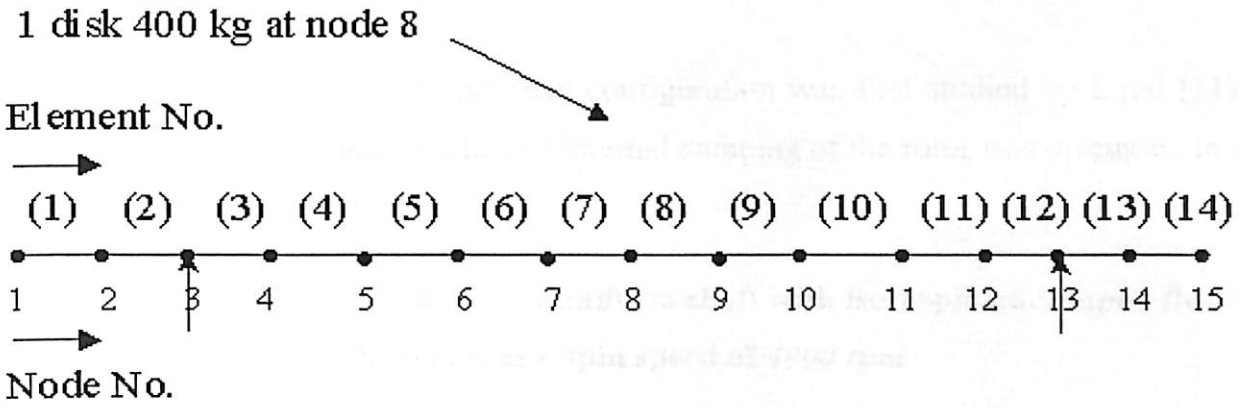

Fig. 4.2: Fourteen-element Jeffcott rotor model (length of each element is 0.25m)

Table 4.3 (a): Physical property of the shaft

Density of the shaft material, ρ	7830 kg/m^3
Elastic Modulus of the shaft material, E	2.08E+11 N/m^2
Diameter of the shaft, D	0.09 m
Length of the shaft, L	3.5 m

Table 4.3 (b): Geometry of the bearings

Diameter of the bearing, D	0.09 m
Bearing load, W	1960.0 N
Radial clearance, C	0.00508 cm

It has also been proposed to include the effect of internal damping in the rotor-bearing set-up considered for analysis as mentioned earlier in this chapter.

4.3 Results and discussion

4.3.1 Validation

For validation, Model 1 whose physical configuration was first studied by Lund [11] is considered. The FEM model including internal damping of the rotor was discussed in the section 2.2.3 of Chapter 2.

Table 4.4: Whirl speeds in rad/s of a uniform shaft with isotropic undamped flexible bearings at a spin speed of *4000 rpm*

	η_v =0.0002 s			η_H =0.0002		
Mode	Present	Reference [131]	Reference [122]	Present	Reference [131]	Reference [122]
1F	519.87	519.75	520.06	519.90	519.78	520.10
1B	521.48	521.48	521.79	519.25	519.23	519.54
2F	1095.50	1095.13	1096.01	1094.70	1094.40	1095.28
2B	1095.20	1094.52	1095.34	1091.50	1090.90	1091.77
3F	2219.30	2216.81	2222.78	2241.40	2238.53	2244.72
3B	2205.20	2201.25	2206.94	2227.60	2223.80	2229.82
4F	4422.20	4413.32	4447.40	4983.50	4968.16	5020.12
4B	4395.42	4378.95	4411.81	4949.90	4935.91	4986.74

Whirl speeds and logarithmic decrements for first four modes are estimated following the solution procedure as described in Chapter 2. The present set of result is compared with those obtained by Ku [131] and Ozguven and Ozkan [122] as shown in Table 4.4 and Table 4.5. It is evident from the comparison that the present results are in good agreement with those in [131] and [122].

Table 4.5: Logarithmic decrements of a uniform shaft with isotropic undamped flexible bearings at a spin speed of *4000 rpm*

η_v =0.0002 *s*				η_H =0.0002		
Mode	Present	Reference [131]	Reference [122]	Present	Reference [131]	Reference [122]
1F	0.0252	0.0252	0.0252	-2.49e-04	-2.85e-04	-2.49e-04
1B	0.2325	0.2325	0.2309	+2.51e-04	+2.87e-04	+2.51e-04
2F	0.0347	0.0347	0.0331	-5.16e-05	-3.66e-05	-5.11e-05
2B	0.0723	0.0723	0.0687	+5.15e-05	+3.63e-05	+5.09e-05
3F	0.7197	0.7187	0.7250	-3.77e-04	-3.88e-04	-3.92e-04
3B	1.0536	1.0528	1.0590	+3.78e-04	+3.90e-04	+3.94e-04
4F	2.9508	2.9409	3.0481	-5.18e-04	-6.27e-04	-5.81e-04
4B	3.5979	3.5634	3.6810	+5.29e-04	+6.31e-04	+5.84e-04

The whirl speed map of simple rotor systems supported on undamped isotropic bearings having stiffness coefficients $k_{XX}=k_{ZZ}=1.7513x10^7$ *N/m* and $k_{XZ}=k_{ZX}=0.0$ are presented in Fig. 4.3 and Fig. 4.4. In Fig. 4.3 hysteretic damping is considered, whereas viscous damping is considered in Fig. 4.4. It has been observed that for the shaft material with viscous internal damping $\eta_v=0.0002$ *s*, critical speeds for the first and second forward modes are found to be 5000 *rpm* and 10,782 *rpm* respectively in the present case, whereas these are reported as 4960 *rpm* and 10,500 *rpm* respectively by Ku [131]. All other results are found to be in good agreement. The damping coefficients $c_{XX}=c_{ZZ}=1.7513x10^3$ *Ns/m*, $c_{XZ}=c_{ZX}=0.0$ are also included along with the stiffness coefficients for the damped isotropic bearings. The whirl speed maps are presented in

Fig. 4.5 and Fig. 4.6. These plots are compared with those obtained by Ku [131] and found to be in good agreement.

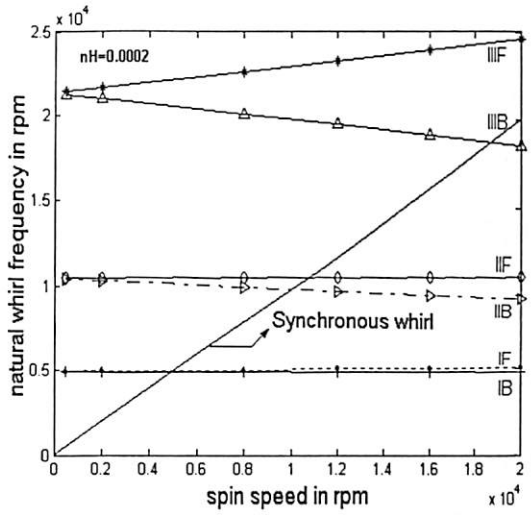

Fig. 4.3: Campbell Diagram for Rotor-Bearing System with undamped isotropic bearing

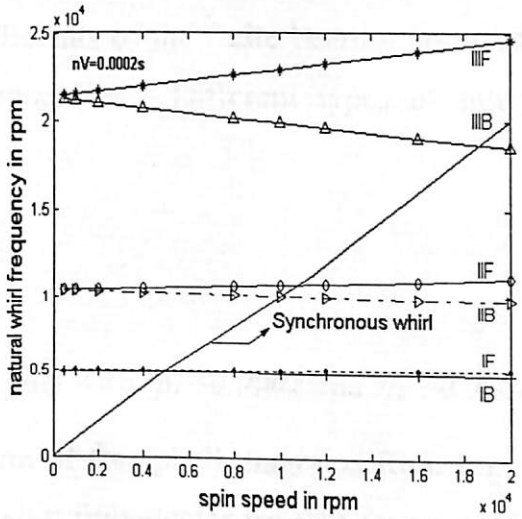

Fig. 4.4: Campbell Diagram for Rotor-Bearing System with undamped isotropic bearing

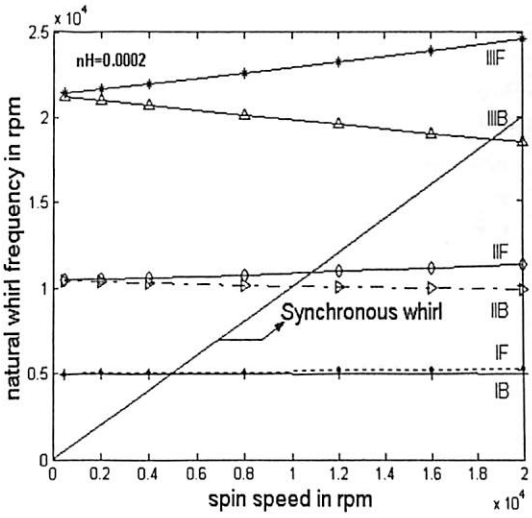

Fig. 4.5: Campbell Diagram for Rotor-Bearing System with damped isotropic bearing

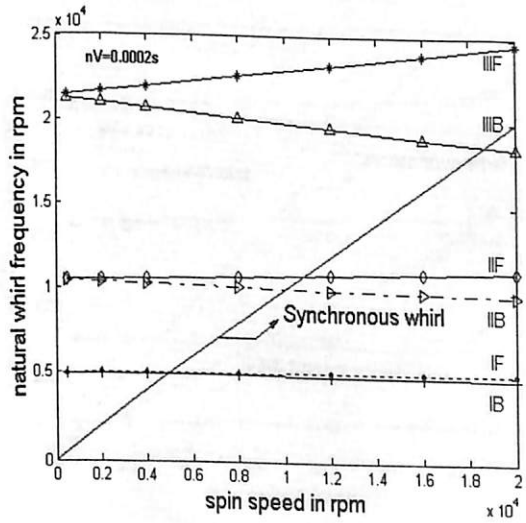

Fig. 4.6: Campbell Diagram for Rotor-Bearing System with damped isotropic bearing

4.3.2 Internal damping

The Model 2 (Fig. 3.4) of Timoshenko beam supported on hydrodynamic bearing is used to incorporate internal damping. Dynamic coefficients of the finite bearing are used in the FEM model to estimate natural whirl frequencies. Different types of internal damping cases are used and these are as follows:

1. Hysteretic damping with $\eta_H = 0.0002$,
2. Viscous damping with $\eta_V = 0.0002s$,
3. Both hysteretic damping and viscous damping with $\eta_H = 0.0002$ and $\eta_V = 0.0002s$.

Results for first four modes are presented in form of Campbell diagrams from Fig. 4.7 through Fig. 4.9. Fig. 4.7 presents synchronous whirl frequencies for first four modes for rotor with hysteretic damping. Synchronous whirl frequencies for rotors with viscous damping are presented in Fig. 4.8. Fig. 4.9 demonstrates the effect of both hysteretic and viscous damping. Not much difference is observed in all the three cases considered

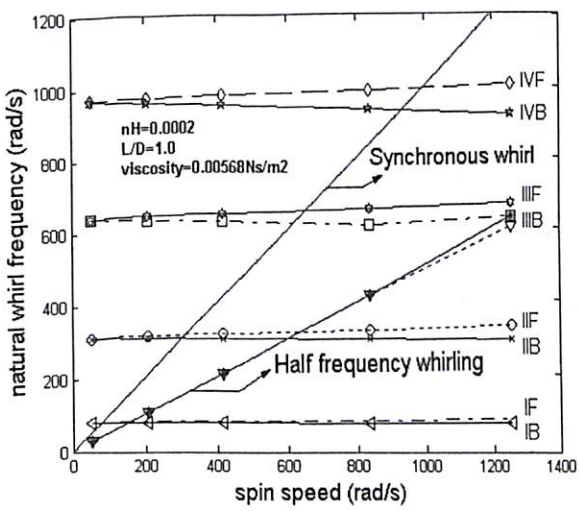

Fig. 4.7: Campbell Diagram for Rotor-Bearing System with hysteretic damping (finite bearing)

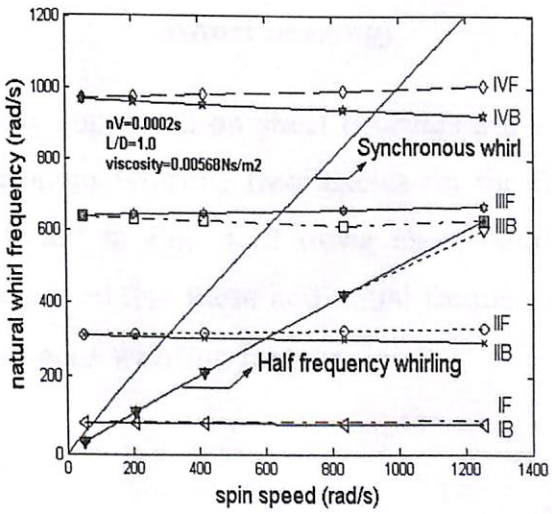

Fig. 4.8: Campbell Diagram for Rotor-Bearing System with viscous damping (finite bearing)

namely hysteretic damping, viscous damping and both hysteretic and viscous damping. An interesting observation of the analysis is that in addition to the synchronous natural whirl frequencies for the first four modes, for every spin speed another whirling

frequency appears in the solution as shown in Fig. 4.7 through 4.9. This particular frequency is around half the spin speed; and therefore this value of frequency is identified as the half-frequency whirling due to the use of fluid film bearings. It may be mentioned that half-frequency whirling is very common in case of fluid film bearings.

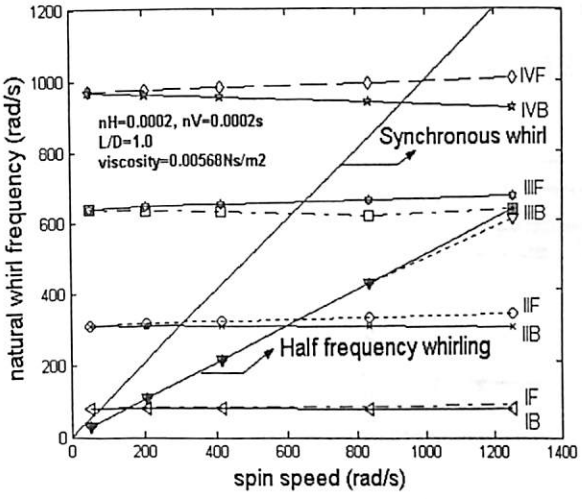

Fig. 4.9: Campbell Diagram for Rotor-Bearing System with both hysteretic and viscous damping (finite bearing)

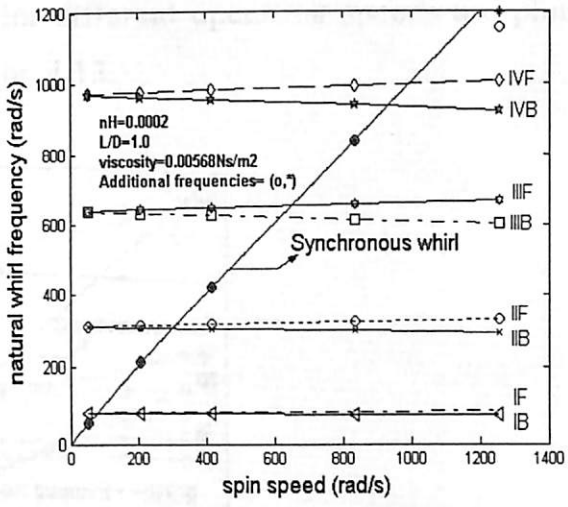

Fig. 4.10: Campbell Diagram for Rotor-bearing System with hysteretic damping (short bearing)

The results of the system with hysteretic damping supported on short bearings are also presented in Fig. 4.10. In addition to the synchronous whirling frequencies for the first four modes, additional frequencies are also plotted in Fig. 4.10 using short bearing stiffness and damping coefficients. It may be observed that these additional frequencies are of the same order as that of the regular synchronous whirling frequencies.

4.3.3 Jeffcott rotor

In order to evaluate the natural whirl frequencies and mode shapes, a Jeffcott rotor bearing system mounted on two identical bearings (Model 3) as illustrated in Fig 4.2 is considered. The analysis is conducted with fourteen-element model. Two identical bearings are located at stations three and thirteen as shown in the figure.

The code is already validated for Timoshenko beam in Chapter 3. Dynamic coefficients of finite grooved bearing are used.

4.3.3.1 Synchronous whirl frequencies

Synchronous whirl frequencies of different modes for the rotor mounted on grooved circular bearings are estimated. Results are presented in form of Campbell diagrams and mode shapes in Fig. 4.11 through Fig. 4.13. Natural whirl frequencies for first four modes are shown in Fig. 4.11. Mode shapes for different operating speeds are plotted and sample results are shown in Fig. 4.12 and Fig. 4.13.

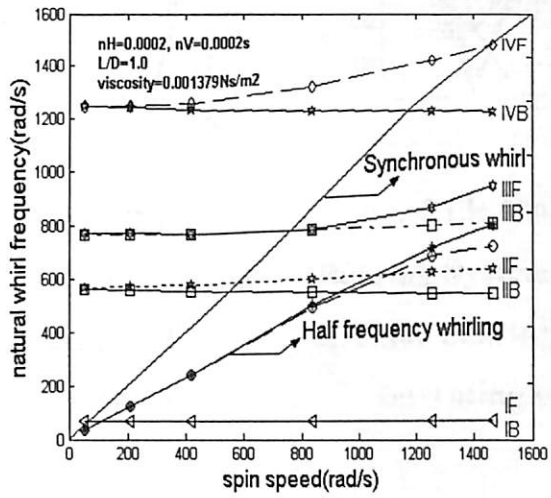

Fig. 4.11: Campbell Diagram for Rotor-Bearing System supported on grooved circular bearings

First four synchronous whirling frequencies in backward and forward directions and logarithmic decrements are shown in Table 4.6. The rotor has the maximum frequency (1173.6 rad/s and 1442.1 rad/s for backward and forward modes) at the fourth mode.

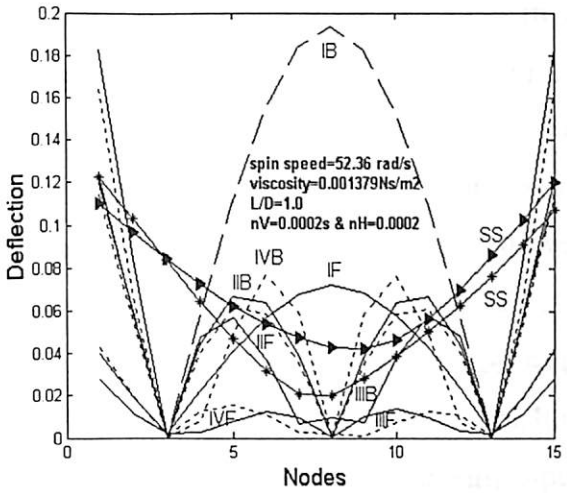

Fig. 4.12: Mode shapes for Rotor-Bearing System supported on grooved circular bearings at station 3 and 13 at operating speed 52.36 rad/s

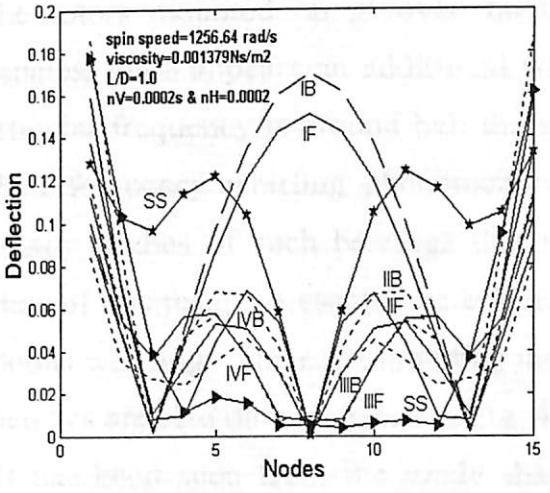

Fig. 4.13: Mode shapes for Rotor-Bearing System supported on grooved circular bearings at station 3 and 13 at operating speed 1256.64 rad/s

Table 4.6: Synchronous frequency and logarithmic decrements of a Rotor-Bearing System supported on grooved circular bearing

Mode	Synchronous frequency (rad/s)	Logarithmic decrements	Sub-synchronous frequency (rad/s)	Logarithmic decrements
1B	65.5	+0.0426	44.1	+9.4478
1F	66.1	-0.0030	44.6	+9.5728
2B	548.3	+0.0033	314.6	+3.2707
2F	582.9	+0.0124	337.2	+3.1706
3B	763.6	+0.0597	440.1	+2.3271
3F	766.6	+0.3563	446.2	+2.3522
4B	1173.6	+0.2884	652.7	+1.5117
4F	1442.1	+1.5454	741.4	+0.3124

4.3.3.2 Sub-synchronous whirl frequencies

From the present study it is clear that for the rotors mounted on grooved circular bearings, in addition to the natural whirl frequencies, there appears an additional whirl frequency as can be seen in Fig. 4.11. This particular frequency is around half the spin speed. This observation is in tune with the half frequency whirling phenomenon of hydrodynamic bearings [4]. It is reported in many studies of such bearings that half frequency whirling causes instability [31]. In view of this results presented here include sub-synchronous whirling in addition to synchronous whirling. The corresponding mode shapes for these sub-synchronous whirling frequencies are also demonstrated in Fig. 4.12 and Fig. 4.13 at different operating speeds. It has been seen from the mode shapes corresponding to the half-frequency whirl for all types of speeds considered that there are deflections of the shaft at the bearing stations.

4.3.3.3 Stability of the rotor-bearing system

As mentioned above the estimated values of logarithmic decrements are shown in Table 4.6. From the estimated results it can be observed that the rotor-bearing system considered in this work is unstable only at the spin speed equal to the first forward synchronous whirl frequency. Logarithmic decrements are found to be positive in all other speeds for bearing considered in this work. Therefore, even for the same spin speed equal to unstable forward synchronous whirl frequency there is no instability due to sub-synchronous whirling.

The eight dynamic coefficients of a fluid film bearing include two direct stiffness coefficients, two cross-coupled stiffness coefficients and four damping coefficients. All these coefficients are speed dependent. It is observed that in many rotor-bearing studies hypothetical bearings are used. In such situations either cross-coupled stiffness coefficients or damping coefficients or both the type of coefficients are ignored. Thus the effects of these coefficients on the behaviour of such systems are discussed next.

4.3.3.4 Effect of cross-coupled stiffness coefficients

To demonstrate the effect of the bearing cross-coupled stiffness, Campbell diagram for first four modes for the rotor bearing system supported on grooved circular bearing without considering cross-coupled stiffness are presented in Fig.4.14. Comparing this figure with Fig. 4.11, it has been observed that in the absence of cross-coupled stiffness the synchronous whirling frequencies in all the four modes are not much different. However, sub synchronous whirl frequency appears to be negligible in absence of cross-coupled stiffness coefficients. Mode shapes for first four modes and sub-synchronous whirling at operating speed 52.36 rad/s are presented in Fig. 4.15. When compared with Fig. 4.12, it may be observed that mode shapes are found to be different only in case of sub synchronous (SS) whirling. It is obvious from this study that the sub-synchronous whirling frequency and corresponding mode shapes are not realistic when cross-coupled stiffness are ignored.

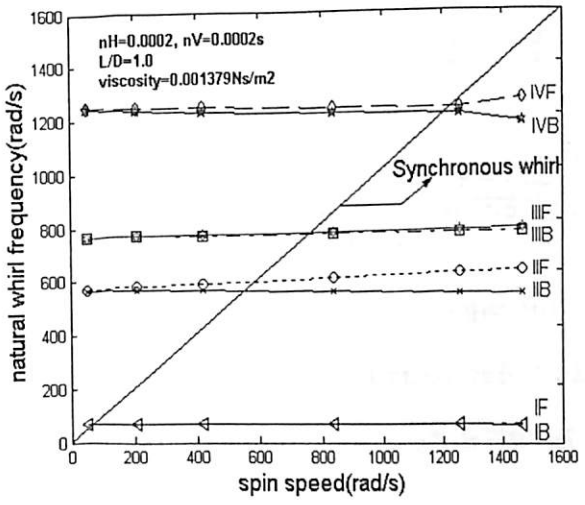

Fig. 4.14: Campbell Diagram for Rotor-Bearing System supported on grooved circular bearings without cross-coupled stiffness

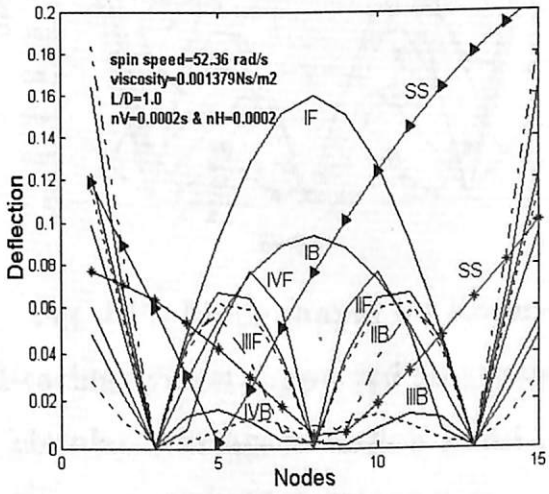

Fig. 4.15: Mode shapes for Rotor-Bearing System supported on grooved circular bearings at station 3 and 13 without cross-coupled stiffness

4.3.3.5 Effect of damping coefficients

To demonstrate the effect of bearing damping coefficients, natural whirl frequencies and mode shapes at operating speed 52.36 rad/s for first four modes for the rotor-bearing system supported on grooved circular bearing without considering damping are shown in Fig. 4.16 and Fig. 4.17. From these figures it is clear that, for lower order modes, natural whirl frequencies in the absence of bearing damping coefficients are not much different from those with damping. However the most importantly the evidence of sub-synchronous whirling is missing from the presented result. It is very much clear now that sub- synchronous whirling is due to bearing damping coefficients.

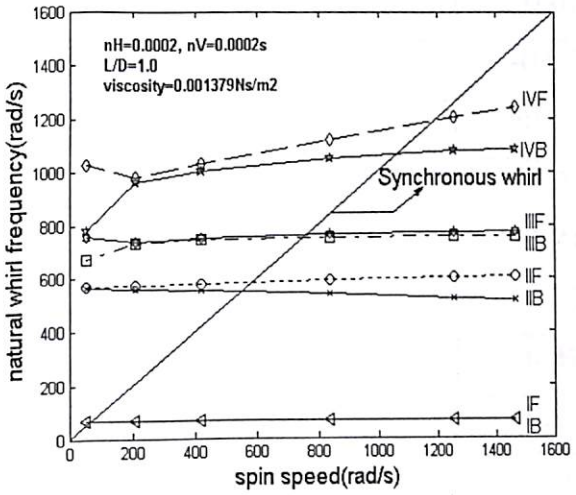

Fig. 4.16: Campbell Diagram for Rotor-Bearing System supported on grooved circular bearings without damping

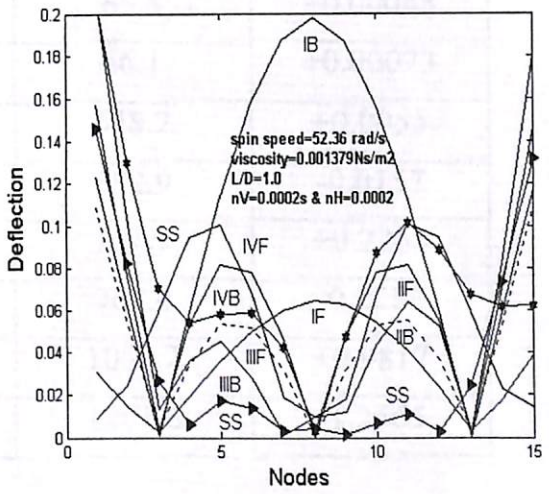

Fig. 4.17: Mode shapes for Rotor-Bearing System supported on grooved circular bearings at station 3 and 13 without damping

Further, the values of logarithmic decrements for first four modes of synchronous whirling are shown in Table 4.7. While compared with Table 4.6, it is found that the sense (positive or negative) is not different though the magnitudes are different when cross-coupled stiffness coefficients are ignored. However, when damping coefficients are ignored, both the sense (positive or negative) and magnitudes are different for all the forward modes. For example, logarithmic decrements corresponding to 1F, 2F, 3F, 4F are found to be +0.00073, -0.0157, -0.2288, -1.2565 (Table 4.7: without damping

coefficients) and -0.0047, +0.0045, +0.2167 and +0.8611 (Table 4.7: without cross-coupled stiffness coefficients).

Table 4.7: Comparison of synchronous frequency and logarithmic decrements of a Rotor-Bearing System supported on grooved circular bearing

Mode	Without cross-coupled stiffness		Without damping	
	Synchronous frequencies (rad/s)	Logarithmic decrements	Synchronous frequencies (rad/s)	Logarithmic decrements
1B	65.9	+0.0298	65.5	+0.00048
1F	66.0	-0.0047	66.1	+0.00073
2B	548.3	+0.0038	548.2	+0.0055
2F	583.1	+0.0045	582.9	-0.0157
3B	758.8	+0.2158	751.9	+0.2265
3F	767.0	+0.2167	761.4	-0.2288
4B	1213.3	+0.5903	1080.2	+0.9817
4F	1223.6	+0.8611	1201.6	-1.2565

4.3.4 Overhung rotor

The overhung rotor-bearing system as shown in Fig. 3.3 using Timoshenko beam is analysed using the present finite element model (Fig. 3.4). Initially higher element e.g., the fourteen-element model as shown in Fig. 3.5, was considered and tested for convergence. It was observed that seven-element discretisation is good enough as the results are not much different when higher element models are used. In view of this the analysis is carried out using seven-element model.

The code is already validated for Timoshenko beam in Chapter 3. Dynamic coefficients of finite bearing are used in the FEM model to estimate natural whirl frequencies. Samples of those are given in Table 2.1and Table 2.2 in Chapter 2.

4.3.4.1 Synchronous whirl frequencies

Results are presented in form of Campbell diagrams and mode shapes in Fig. 4.18 through Fig. 4.20. Natural whirl frequencies for first four modes are shown in Fig. 4.18. Mode shapes for different operating speeds are plotted and sample results for two operating speeds are shown in Fig. 4.19 and Fig. 4.20.

First four synchronous whirling frequencies in backward and forward directions and logarithmic decrements are shown in Table 4.8. The rotor has the maximum frequency (934.1 rad/s and 996.0 rad/s for backward and forward modes) at the fourth mode.

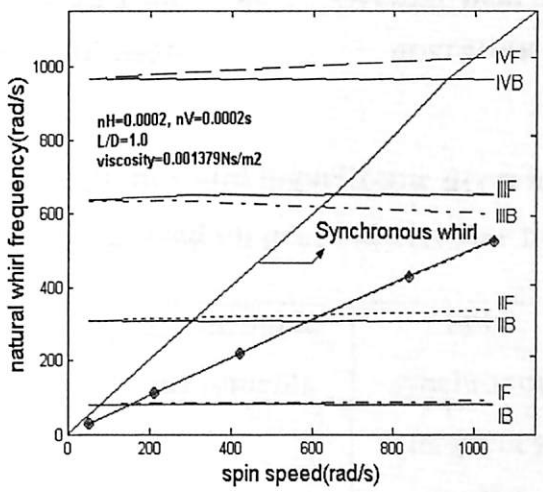

Fig. 4.18: Campbell Diagram for Rotor-Bearing System supported on grooved circular bearings

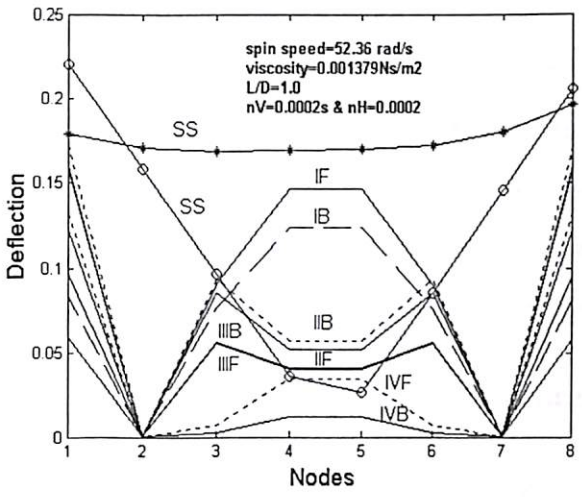

Fig. 4.19: Mode shapes for Rotor-Bearing System supported on grooved circular bearings at station 2 and 7 at operating speed 52.36 rad/s

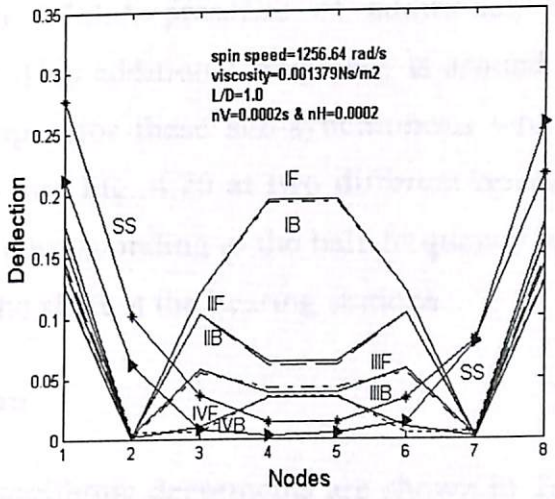

Fig. 4.20: Mode shapes for Rotor-Bearing System supported on grooved circular bearings at station 2 and 7 at operating speed 1256.64 rad/s

Table 4.8: Synchronous frequency and logarithmic decrements of a Rotor-Bearing System supported on grooved circular bearing

Mode	Synchronous frequency (rad/s)	Logarithmic decrements	Sub-synchronous frequency (rad/s)	Logarithmic decrements
1B	80.1	+0.0123	41.7	+4.2409
1F	80.5	+0.0272	41.9	+4.2568
2B	303.2	+0.0124	153.5	+1.6860
2F	312.2	+0.0263	153.7	+1.6264
3B	619.7	+0.0036	311.1	+0.7796
3F	653.6	-0.0023	323.7	+0.7769
4B	934.1	+0.0356	499.4	+1.3779
4F	996.0	+0.1500	501.3	+1.4026

4.3.4.2 Sub-synchronous whirl frequencies

Similar to observation made on the section 4.3.3.2, presence of additional whirl frequencies has been found on this model also. This additional frequency is around half the spin speed. The corresponding mode shapes for these sub-synchronous whirling frequencies are also demonstrated in Fig. 4.19 and Fig. 4.20 at two different operating speeds. It has been seen from the mode shapes corresponding to the half-frequency whirl speeds considered that there are deflections of the shaft at the bearing stations.

4.3.4.3 Stability of the rotor-bearing system

As mentioned above the estimated values of logarithmic decrements are shown in Table 4.8. From the estimated results it can be observed that the rotor-bearing system considered in this work is unstable only at the spin speed equal to the third forward synchronous whirl frequency. Logarithmic decrements are found to be positive at all other spin speeds due to either synchronous or sub-synchronous whirling.

4.3.4.4 Effect of viscosity

The same model (Model 2) is also studied for different viscosity of lubricating oil of the bearing. Natural whirl frequencies for first four modes are shown in the form of Campbell diagram in Fig. 4.9. Mode shapes are also plotted for two different spin speeds at Fig. 4.21 and Fig. 4.22. From the figures (Fig. 4.9, Fig. 4.21 and Fig. 4.22), it is observed that with change of viscosity not much variation is observed in natural whirl frequencies and mode shapes.

The estimated values of logarithmic decrements are shown in Table 4.9. From the estimated results it can be observed that the rotor-bearing system considered in this case is also unstable only at the spin speed equal to the third forward synchronous whirl frequency.

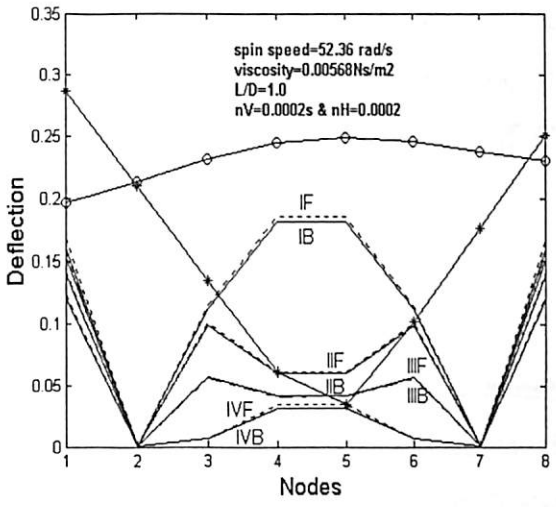

Fig. 4.21: Mode shapes for Rotor-Bearing System supported on grooved circular bearings at station 2 and 7 at operating speed 52.36 rad/s

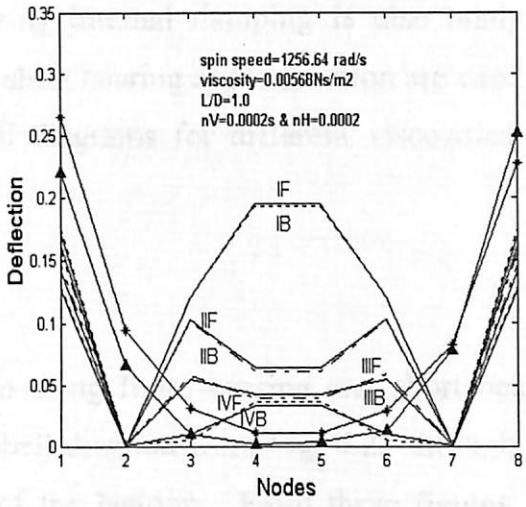

Fig. 4.22: Mode shapes for Rotor-Bearing System supported on grooved circular bearings at station 2 and 7 at operating speed 1256.64 rad/s

Table 4.9: Synchronous frequency and logarithmic decrements of a Rotor-Bearing System supported on grooved circular bearing

Mode	Synchronous frequency (rad/s)	Logarithmic decrements	Sub-synchronous frequency (rad/s)	Logarithmic decrements
1B	80.1	+0.0032	40.4	+2.2430
1F	80.7	+0.0206	40.5	+2.2327
2B	303.2	+0.0056	152.4	+0.6517
2F	312.5	+0.0084	156.9	+0.6050
3B	619.7	+0.0037	310.2	+0.2957
3F	653.6	-0.0023	330.2	+0.3146
4B	933.8	+0.0096	467.2	+0.1723
4F	997.5	+0.0210	496.8	+0.1713

4.4 Rotor-bearing system without internal damping

The same model (Model 2) without considering internal damping is also analysed. Dynamic coefficients of both finite bearing and short bearing approximation are used and results are presented in the form of Campbell diagrams for different viscosities and different aspect ratios.

4.4.1 Effect of viscosity

Natural whirl frequencies for the same system using finite bearing and short bearing approximation are shown in the form of Campbell diagram from Fig. 4.23 through Fig. 4.28 for different viscosity of lubricating oil of the bearing. From these figures it is observed that with change of viscosity, not much variation is observed in case of synchronous whirl frequencies. But sub-synchronous whirl frequency slightly decreases with increase of viscosity. This is true for both finite bearing and short bearing.

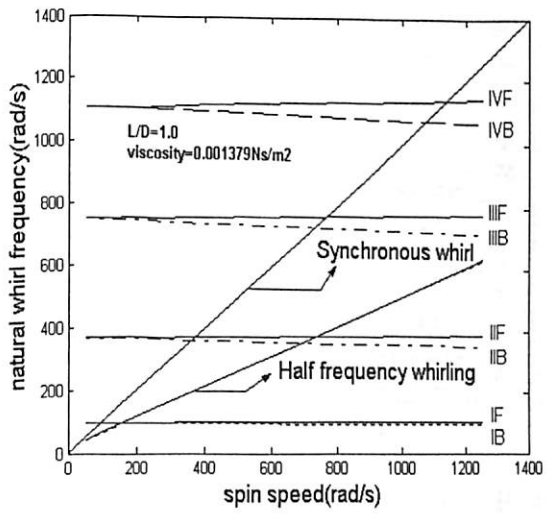

Fig. 4.23: Campbell Diagram for Rotor-Bearing System (finite bearing)

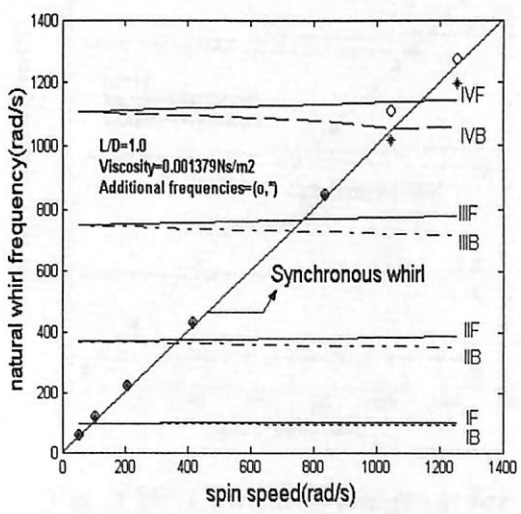

Fig. 4.24: Campbell Diagram for Rotor-Bearing System (short bearing)

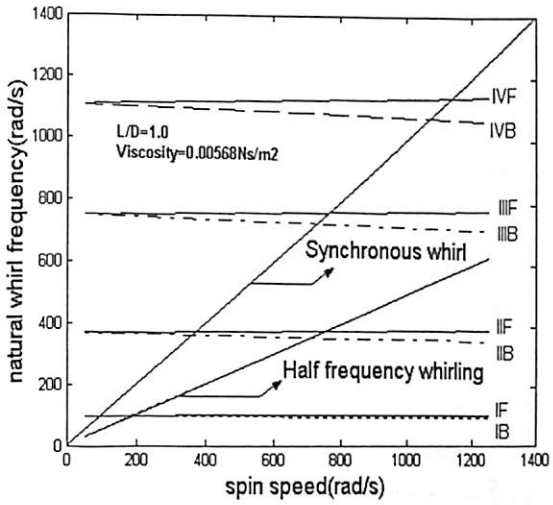

Fig. 4.25: Campbell Diagram for Rotor-Bearing System (finite bearing)

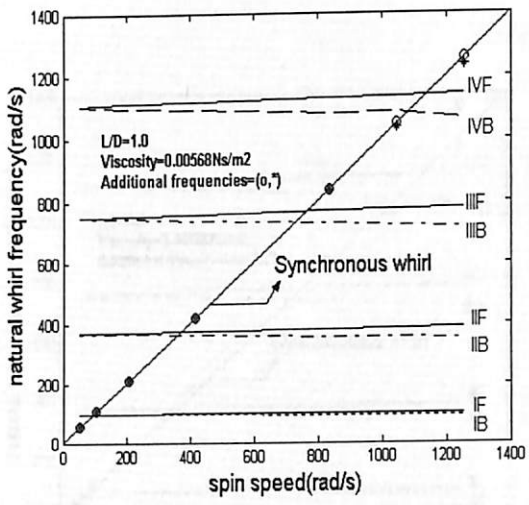

Fig. 4.26: Campbell Diagram for Rotor-Bearing System (short bearing)

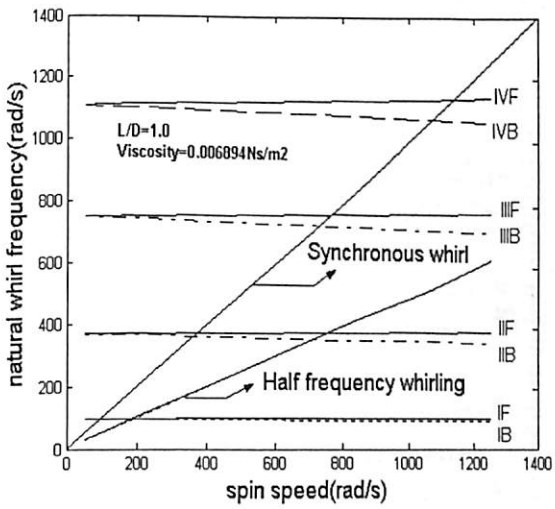

Fig. 4.27: Campbell Diagram for Rotor-Bearing System (finite bearing)

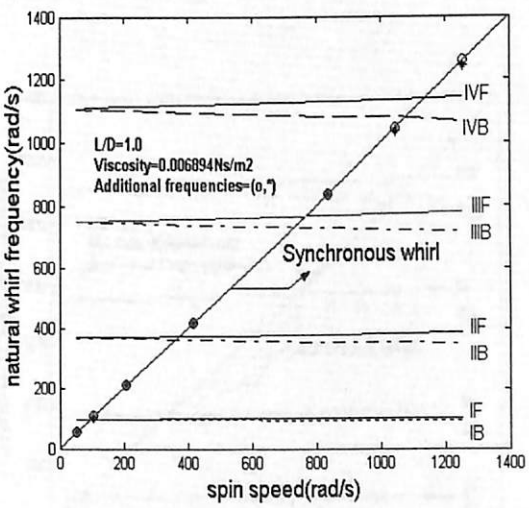

Fig. 4.28: Campbell Diagram for Rotor-Bearing System (short bearing)

4.4.2 Effect of aspect ratio

To find out the effect of bearing geometry, natural whirl frequencies for *L/D=0.5* and *1.5* with viscosity=$0.00568Ns/m^2$ are also plotted from Fig. 4.29 through Fig. 4.32. Comparing these figures also with Fig. 4.25 and Fig. 4.26 (*L/D=1.0*), it is observed that there is not much change on the natural whirl frequencies with change in *L/D* ratio for

both finite and short bearing. But sub-synchronous whirl frequency decreases with increase of *L/D* ratio.

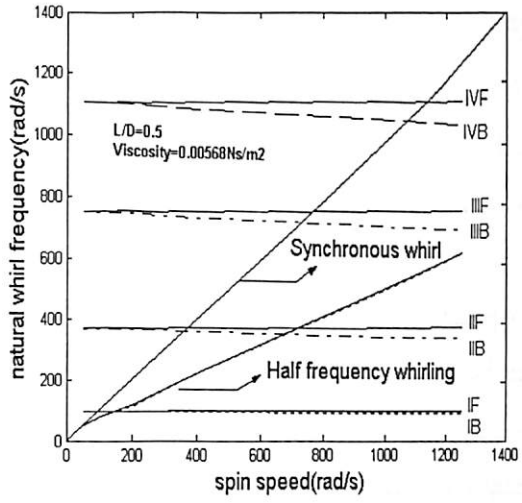

Fig. 4.29: Campbell Diagram for Rotor-Bearing System (finite bearing)

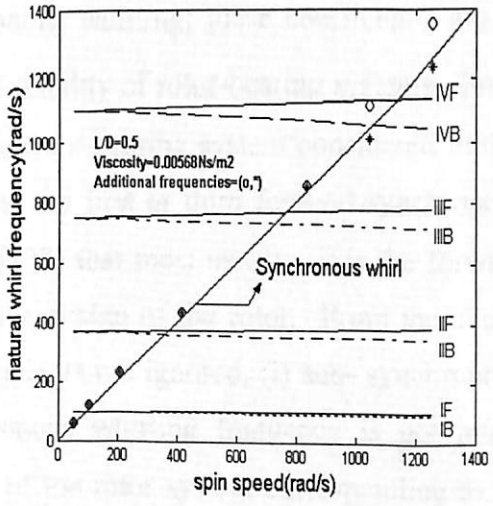

Fig. 4.30: Campbell Diagram for Rotor-Bearing System (short bearing)

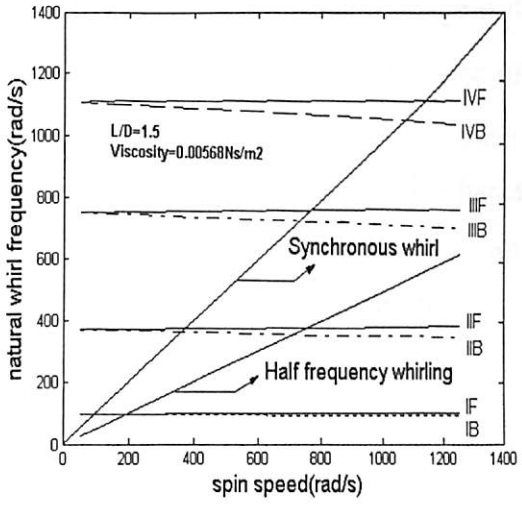

Fig. 4.31: Campbell Diagram for Rotor-Bearing System (finite bearing)

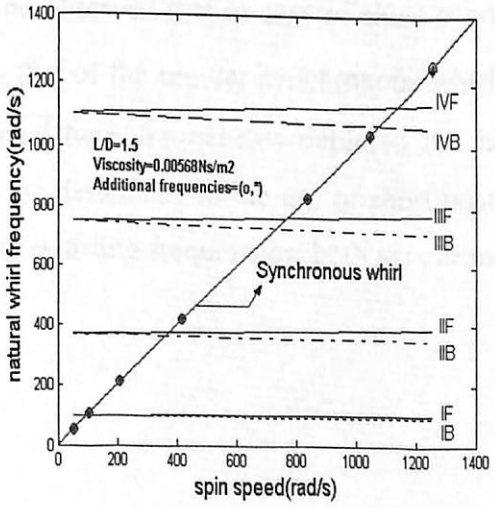

Fig. 4.32: Campbell Diagram for Rotor-Bearing System (short bearing)

From the presented results it can be concluded that oil viscosity and bearing geometry vis-à-vis length to diameter ratio does not have much influence on natural whirl frequency.

4.5 Conclusions

It has been established in this work that the bearing dynamic coefficients are not only important parameters for study of sub-synchronous whirling; these coefficients are of paramount interest so as to correctly predict the stability of rotor-bearing systems. From the estimated results it can be observed that the rotor-bearing system considered in this work is unstable only at the spin speed equal to the first or third forward synchronous whirl frequency. It has been reported by Rao [132] that most usually, it is the forward synchronous whirl speeds that is important in the design of the rotor. From the above study results it is evident that if damping coefficients are ignored, (i) sub- synchronous whirling frequency is suppressed, (ii) synchronous whirling frequency is not much effected and (iii) a wrong notion of instability of the rotor system corresponding to all forwarding modes (synchronous whirling) is created. Therefore, use of hypothetical bearing does not give the actual picture of the stability of rotor-bearing system and more significantly bearing damping is a very important parameter in studying the characteristics of such systems. Again it may be observed that in case of short bearing, additional frequencies are of the same order as that of the regular synchronous whirling frequencies. But in the case of finite bearings these frequencies depicted the half-frequency whirling condition. This has shown the deficiency in the use of short bearing approximation in studies relating to estimation of whirling frequencies, both synchronous and half-frequency whirl conditions.

Chapter 5

Whirling of rotors supported on multi lobe bearings

5.1 Introduction

In the previous chapter, whirl analysis was carried out for different types of beam models mounted on fluid film bearings. Plain circular bearings were used in rotating machineries. However, the problem of instability of such systems in high-speed machines and precision machine tools, plain bearing is mostly replaced by non-circular bearings, such as, multi-lobe bearings. In the present chapter an investigation is made to find out the behaviour of rotor-bearing system supported on multi-lobe bearings. Three different bearings, namely, two-lobe, three-lobe and four-lobe bearings are considered in the present study.

5.2 Models used

The code used in the analysis is already validated for grooved circular bearing in the section 4.3.1 of Chapter 4 by using Lund's steel shaft. Therefore only two types of models (Model 2 and Model 3) are used in this analysis. Physical properties of these models are given in Table 4.2 and Table 4.3 of Chapter 4.

5.3 Results and discussion

5.3.1 Jeffcott rotor

In order to evaluate the natural whirl frequencies and mode shapes, a typical fourteen-element Jeffcott model (Model 3) is considered. Two bearings are located at stations three and thirteen as shown in Fig 4.2. Dynamic coefficients of two lobe, three lobe and four lobe bearings [156,160] are first evaluated for use in the FEM model. A few sample

dynamic coefficients evaluated and used for rotor-bearing analysis are provided in Table 2.1 and Table 2.2 of Chapter 2.

5.3.1.1 Synchronous whirl frequencies

The bearing dynamic coefficients are incorporated in the FEM model, and then eigen value solution of the set of equation is obtained. Whirling frequencies are plotted against spin speed. Synchronous whirl frequencies of different modes are found from Campbell diagrams. Results are presented in form of Campbell diagrams and mode shapes for two-lobe bearing (with lobes separated by 20^0 oil grooves), three-lobe (with lobes separated by 20^0 oil grooves) and four-lobe bearing (with lobes separated by 10^0 oil grooves) in Fig. 5.1 through Fig. 5.9. Natural whirl frequencies for first four modes are shown in Fig.5.1, Fig. 5.4 and Fig. 5.7. Mode shapes for two different operating speeds (52.36 rad/s and 1256.64rad/s) are shown in Fig. 5.2 and Fig. 5.3 for two-lobe bearings, Fig. 5.5 and Fig. 5.6 for three-lobe bearings and Fig. 5.8 and Fig. 5.9 for four-lobe bearings.

5.3.1.2 Sub-synchronous whirl frequencies

From the present study it is clear that the natural whirl frequencies for the rotors mounted on four different types of bearings are not much different at lower order modes. However there is generally an upward trend when numbers of lobes are increased at higher order modes. Similar to observation made in Chapter 4, it has been found that there appears an additional whirl frequency as can be seen in Figs. 5.1, 5.4 and 5.7. This particular frequency is around half the spin speed. From the mode shapes corresponding to the half-frequency whirl for all types of bearings considered it is clear that there are deflections of the shaft at the bearing locations.

5.3.1.3 Stability of the Jeffcott rotor-bearing system

The estimated values of logarithmic decrements are shown in Table 5.1 through 5.3. It has been observed that except for the first forward synchronous frequency, logarithmic decrements are found to be positive in all other cases for all types of bearing considered in this work. From the estimated results it can be observed that the rotor-bearing system

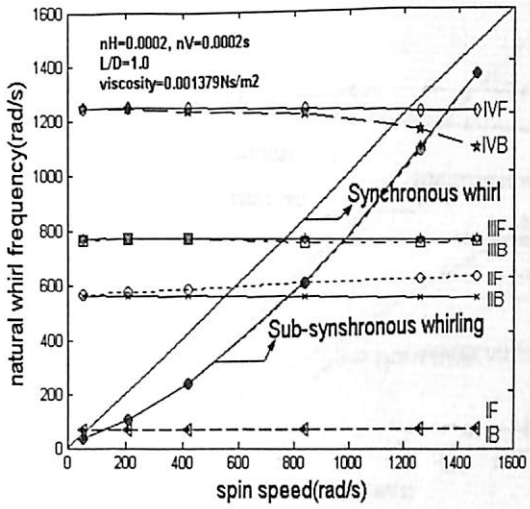

Fig. 5.1: Campbell Diagram for Rotor-Bearing System supported on two-lobe bearings

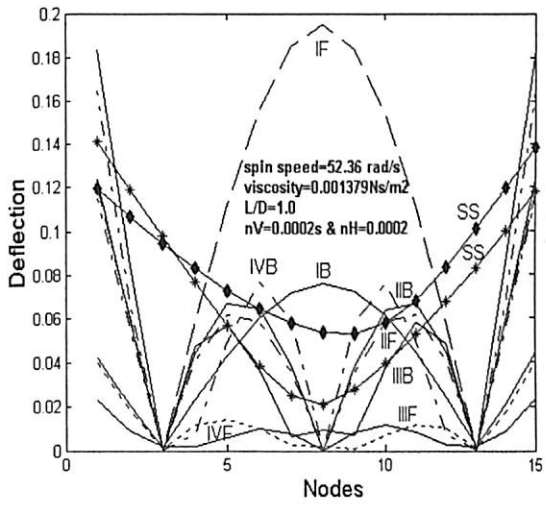

Fig. 5.2: Mode shapes for Rotor-Bearing System supported on two-lobe bearings at station 3 and 13 at operating speed 52.36 rad/s

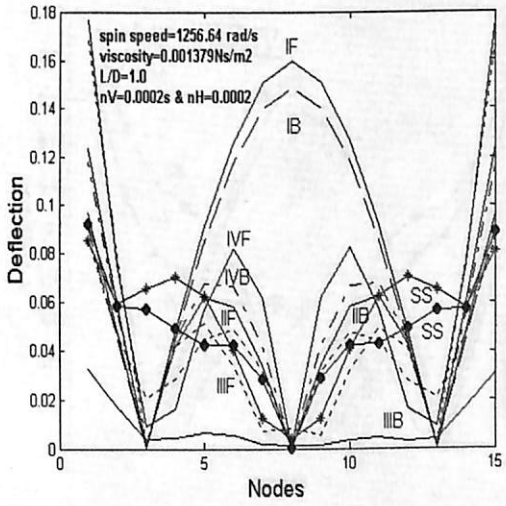

Fig. 5.3: Mode shapes for Rotor-Bearing System supported on two-lobe bearings at station 3 and 13 at operating speed 1256.64 rad/s

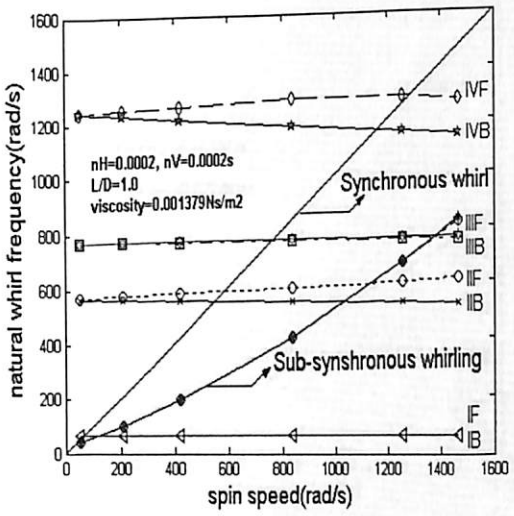

Fig. 5.4: Campbell Diagram for Rotor-Bearing System supported on three-lobe bearings

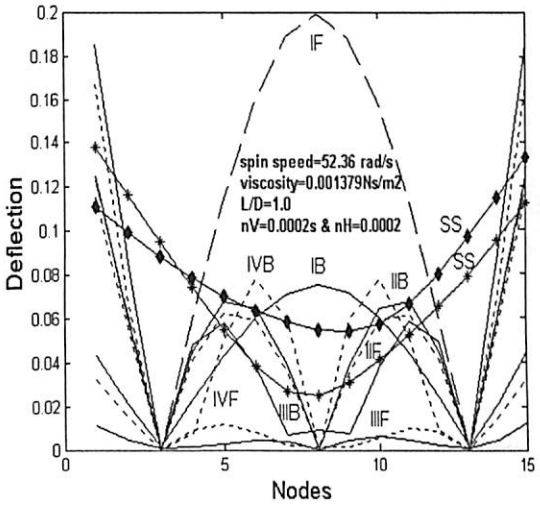

Fig. 5.5: Mode shapes for Rotor-Bearing System supported on three-lobe bearings at station 3 and 13 at operating speed 52.36 rad/s

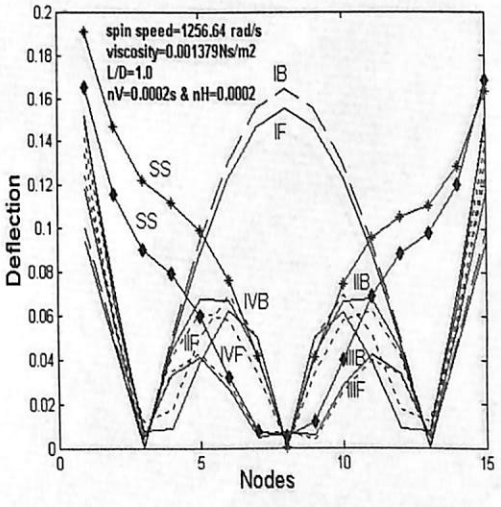

Fig. 5.6: Mode shapes for Rotor-Bearing System supported on three-lobe bearings at station 3 and 13 at operating speed 1256.64 rad/s

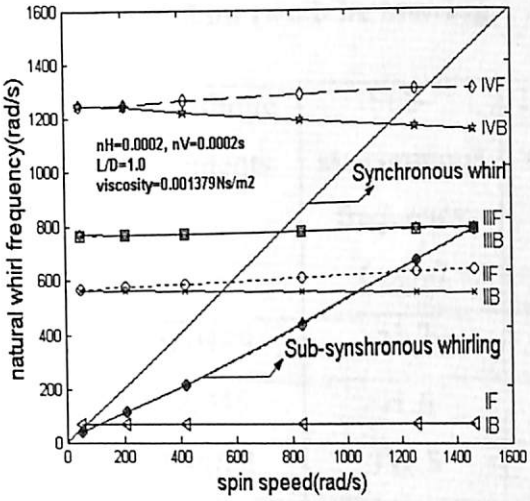

Fig. 5.7: Campbell Diagram for Rotor-Bearing System supported on four-lobe bearings

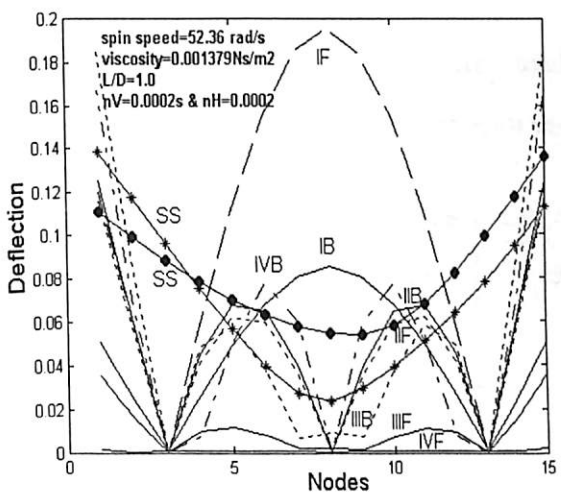

Fig. 5.8: Mode shapes for Rotor-Bearing System supported on four-lobe bearings at station 3 and 13 at operating speed 52.36 rad/s

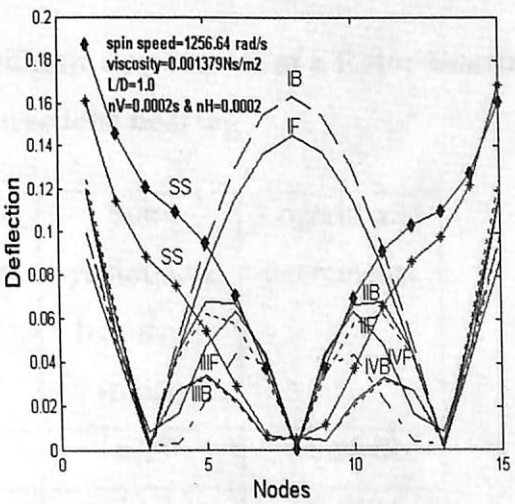

Fig. 5.9: Mode shapes for Rotor-Bearing System supported on four-lobe bearings at station 3 and 13 at operating speed 1256.64 rad/s

Table 5.1: Synchronous frequency and logarithmic decrements of a Rotor-Bearing System supported on two lobe bearing

Mode	Synchronous frequency (rad/s)	Logarithmic decrements	Sub-synchronous frequency (rad/s)	Logarithmic decrements
1B	65.6	+0.0499	41.2	+8.7526
1F	66.1	-0.0045	41.6	+8.7607
2B	548.3	+0.0028	332.8	+4.3072
2F	583.0	+0.0037	363.4	+4.2727
3B	754.6	+0.1664	524.9	+3.7814
3F	765.1	+0.0175	526.5	+3.8682
4B	1086.7	+0.9367	873.6	+3.3904
4F	1207.4	+0.1427	1081.2	+3.2435

Table 5.2: Synchronous frequency and logarithmic decrements of a Rotor-Bearing System supported on three lobe bearing

Mode	Synchronous frequency (rad/s)	Logarithmic decrements	Sub-synchronous frequency (rad/s)	Logarithmic decrements
1B	65.8	+0.0229	63.8	+6.0848
1F	66.1	-0.0074	64.2	+6.1204
2B	548.3	+0.0025	260.4	+4.2340
2F	583.2	+0.0014	278.7	+4.1312
3B	763.5	+0.0361	374.5	+3.7189
3F	767.0	+0.0629	375.3	+3.7396
4B	1163.7	+0.1310	609.7	+3.1019
4F	1284.2	+0.3938	695.1	+3.0118

Table 5.3: Synchronous frequency and logarithmic decrements of a Rotor-Bearing System supported on four lobe bearing

Mode	Synchronous frequency (rad/s)	Logarithmic decrements	Sub-synchronous frequency (rad/s)	Logarithmic decrements
1B	65.8	+0.0439	39.1	+9.3376
1F	66.1	-0.0077	39.4	+9.3199
2B	548.3	+0.0024	276.5	+4.5256
2F	583.2	+0.0009	294.0	+4.4145
3B	763.1	+0.0347	385.3	+3.9134
3F	767.3	+0.0515	385.9	+3.9336
4B	1161.6	+0.1020	592.7	+3.3098
4F	1296.8	+0.2865	666.8	+3.2382

considered in this work is unstable only at the spin speed equal to the first forward synchronous whirl frequency. However, even for the same spin speed equal to the unstable forward synchronous whirl frequency there is no instability caused due to synchronous whirling. This observation is true for all the bearings considered in the study.

5.3.2 Overhung rotor

An overhung rotor bearing system as shown in Figure 3.3 is also analyzed using different types of multi-lobe bearings. The analysis is conducted with seven-element model (Model 2) as shown in Figure 3.4. Dynamic coefficients for finite bearings [156,160] of the bearings are used in the FEM model to estimate natural whirl frequencies.

5.3.2.1 Synchronous whirl frequencies

Results are presented in form of Campbell diagrams and mode shapes for two-lobe bearing (with lobes separated by 20^0 oil grooves), three-lobe (with lobes separated by 20^0

oil grooves) and four-lobe bearing (with lobes separated by 10^0 oil grooves) in Fig. 5.10 through Fig. 5.18. Natural whirl frequencies for first four modes are shown in Fig.5.10, Fig. 5.13 and Fig. 5.16. Mode shapes for two different operating speeds (52.36 rad/s and 1256.64 rad/s) are shown in Fig. 5.11 and Fig. 5.12 for two-lobe bearings, Fig. 5.14 and Fig. 5.15 for three-lobe bearings and Fig. 5.17 and Fig. 5.18 for four-lobe bearings.

5.3.2.2 Sub-synchronous whirl frequencies

Similar to the observations made in Chapter 4, the present study also leads to the observation that when the natural whirl frequencies for the rotors mounted on four different types of bearings are not much different, there appears an additional whirl frequency as can be seen in Fig. 5.10, Fig. 5.13 and Fig. 5.16. This particular frequency is more than half the spin speed for two-lobe bearing and around half the spin speed for three and four lobe bearings. The corresponding mode shapes for these sub-synchronous whirling frequencies are also demonstrated in Fig. 5.11 and Fig. 5.12 for two-lobe bearings, Fig. 5.14 and Fig. 5.15 for three-lobe bearings and Fig. 5.17 and Fig. 5.18 for four-lobe bearings. It is seen from the mode shapes corresponding to the half-frequency whirl for all types of bearings considered that there are deflections of the shaft at the bearing stations.

5.3.2.3 Stability of the rotor-bearing system

The estimated values of logarithmic decrements are shown in Table 5.4 through Table 5.6 for two-lobe, three-lobe and four-lobe bearings. Similar to observation made in Chapter 4, it can be observed from these estimated results that the rotor-bearing system considered in this work is unstable only at the spin speed equal to the third forward synchronous whirl frequency. Logarithmic decrements are found to be positive at all other spin speeds due to either synchronous or sub-synchronous whirling. Therefore, like previous observations made in Chapter 4, for the same spin speed equal to the unstable synchronous whirl frequency there is no instability caused due to sub-synchronous whirling.

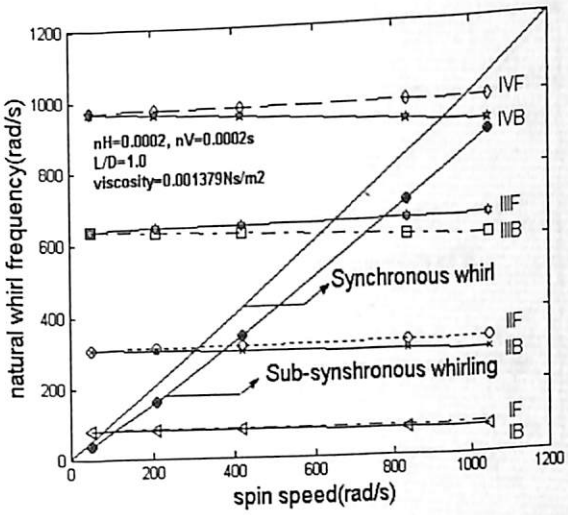

Fig. 5.10: Campbell Diagram for Rotor-Bearing System supported on two-lobe bearings

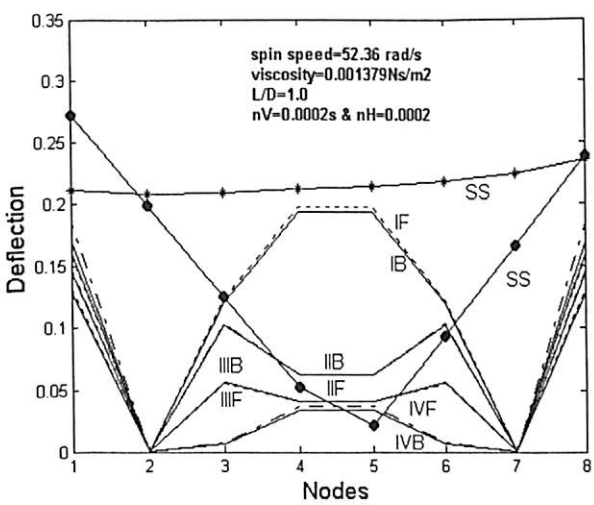

Fig. 5.11: Mode shapes for Rotor-Bearing System supported on two-lobe bearings at station 2 and 7 at operating speed 52.36 rad/s

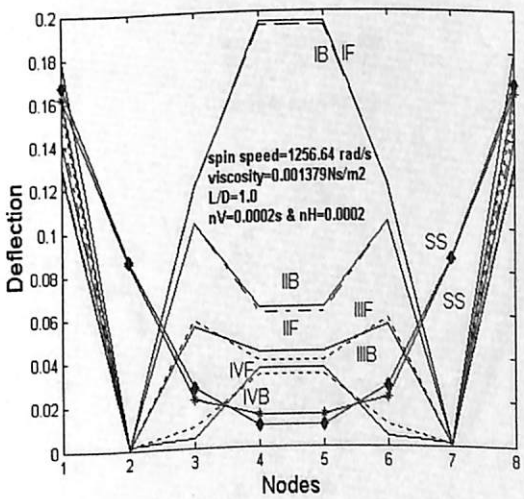

Fig. 5.12: Mode shapes for Rotor-Bearing System supported on two-lobe bearings at station 2 and 7 at operating speed 1256.64 rad/s

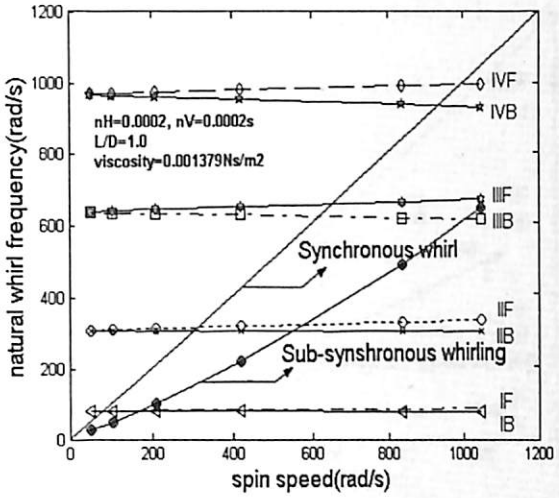

Fig. 5.13: Campbell Diagram for Rotor-Bearing System supported on three-lobe bearings

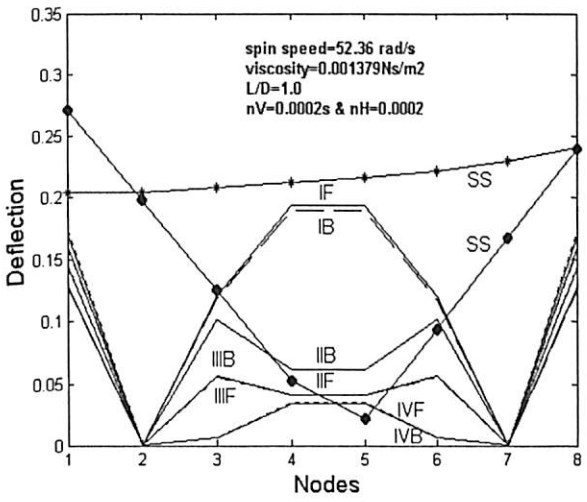

Fig. 5.14: Mode shapes for Rotor-Bearing System supported on three-lobe bearings at station 2 and 7 at operating speed 52.36 rad/s

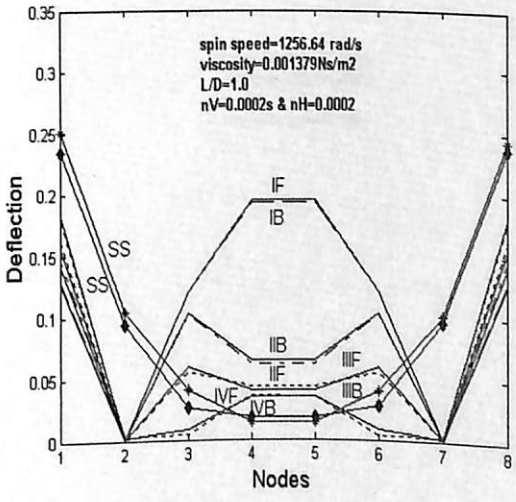

Fig. 5.15: Mode shapes for Rotor-Bearing System supported on three-lobe bearings at station 2 and 7 at operating speed 1256.64 rad/s

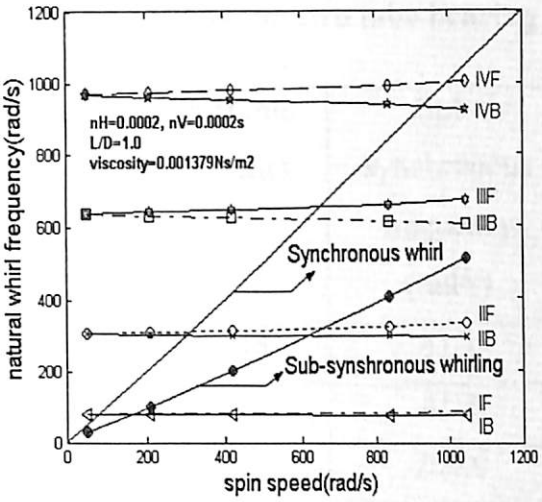

Fig. 5.16: Campbell Diagram for Rotor-Bearing System supported on four-lobe bearings

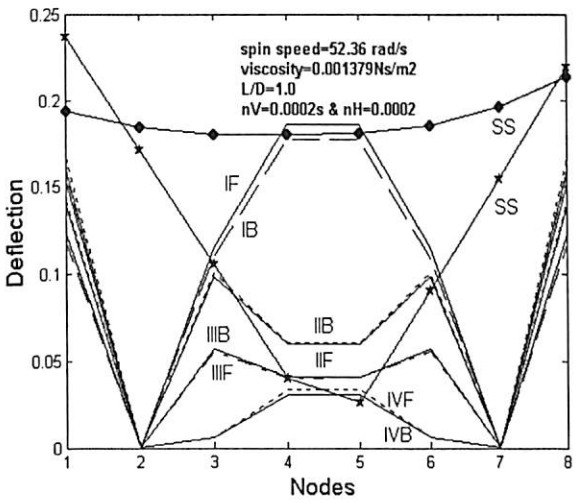

Fig. 5.17: Mode shapes for Rotor-Bearing System supported on four-lobe bearings at station 2 and 7 at operating speed 52.36 rad/s

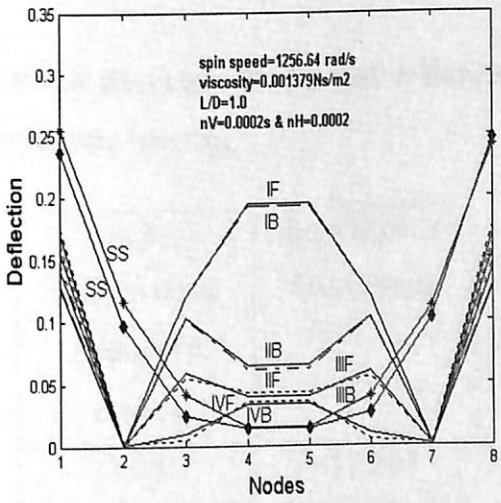

Fig. 5.18: Mode shapes for Rotor-Bearing System supported on four-lobe bearings at station 2 and 7 at operating speed 1256.64 rad/s

Table 5.4: Synchronous frequency and logarithmic decrements of a Rotor-Bearing System supported on two lobe bearing

Mode	Synchronous frequency (rad/s)	Logarithmic decrements	Sub-synchronous frequency (rad/s)	Logarithmic decrements
1B	80.1	+0.0046	41.1	+5.3312
1F	80.6	+0.0157	41.2	+5.3231
2B	303.1	+0.0093	200.8	+4.3291
2F	311.8	+0.0094	201.4	+4.3034
3B	619.7	+0.0038	440.1	+4.1933
3F	653.6	-0.0023	440.5	+4.2008
4B	932.6	+0.0173	684.7	+4.1807
4F	990.7	+0.0285	685.3	+4.1672

Table 5.5: Synchronous frequency and logarithmic decrements of a Rotor-Bearing System supported on three lobe bearing

Mode	Synchronous frequency (rad/s)	Logarithmic decrements	Sub-synchronous frequency (rad/s)	Logarithmic decrements
1B	80.0	+0.0036	39.5	+12.593
1F	80.5	+0.0223	39.8	+12.353
2B	303.1	+0.0218	144.2	+10.284
2F	311.8	+0.0293	148.5	+10.354
3B	619.7	+0.0037	304.5	+6.1844
3F	653.6	-0.0023	314.3	+6.2008
4B	932.5	+0.0194	464.7	+2.1207
4F	994.0	+0.0354	485.3	+2.3672

Table 5.6: Synchronous frequency and logarithmic decrements of a Rotor-Bearing System supported on four-lobe bearing

Mode	Synchronous frequency (rad/s)	Logarithmic decrements	Sub-synchronous frequency (rad/s)	Logarithmic decrements
1B	79.6	+0.0941	41.8	+5.8154
1F	80.1	+0.0273	42.5	+5.7726
2B	303.0	+0.0319	151.3	+3.5715
2F	310.9	+0.0699	152.1	+3.4225
3B	619.6	+0.0045	318.9	+3.0294
3F	653.6	-0.0022	323.7	+2.9988
4B	933.2	+0.0537	498.5	+2.7541
4F	990.6	+0.2234	501.7	+2.7768

5.3.2.4 Effect of viscosity

Natural whirl frequencies for the same system using different bearings are shown in the form of Campbell diagram from Fig. 5.19 through Fig. 5.27 for different viscosity (viscosity=0.00568Ns/m^2) of lubricating oil of the bearing. Results are presented in form of Campbell diagrams and mode shapes for two-lobe bearing (with lobes separated by 20^0 oil grooves), three-lobe (with lobes separated by 20^0 oil grooves) and four-lobe bearing (with lobes separated by 10^0 oil grooves) in Fig. 5.19 through Fig. 5.27. Natural whirl frequencies for first four modes are shown in Fig.5.19, Fig. 5.22 and Fig. 5.25. Mode shapes for two different operating speeds (52.36 rad/s and 1256.64 rad/s) are shown in Fig. 5.20and Fig. 5.21 for two-lobe bearings, Fig. 5.23 and Fig. 5.24 for three-lobe bearings and Fig. 5.26 and Fig. 5.27 for four-lobe bearings.

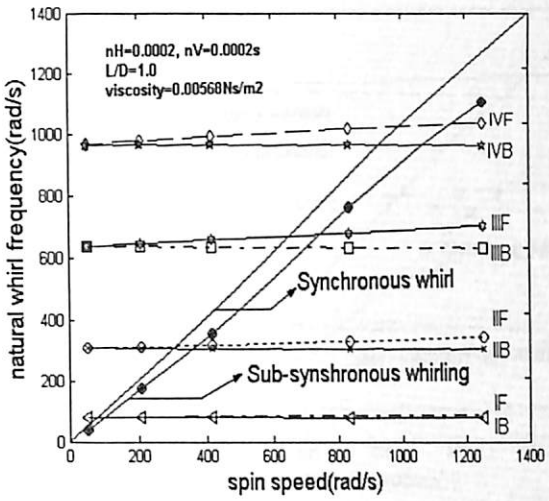

Fig. 5.19: Campbell Diagram for Rotor-Bearing System supported on two-lobe bearings

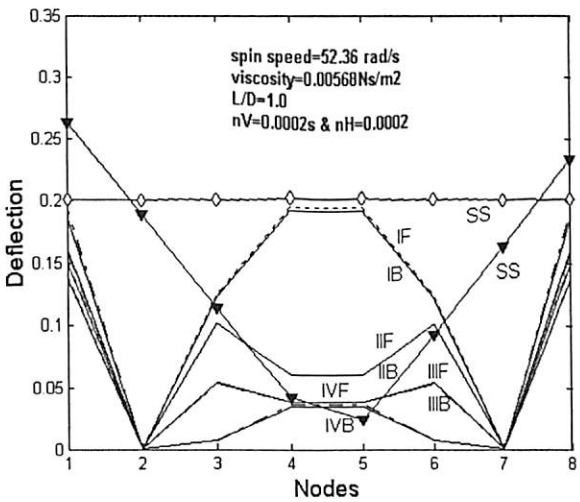

Fig. 5.20: Mode shapes for Rotor-Bearing System supported on two-lobe bearings at station 2 and 7 at operating speed 52.36 rad/s

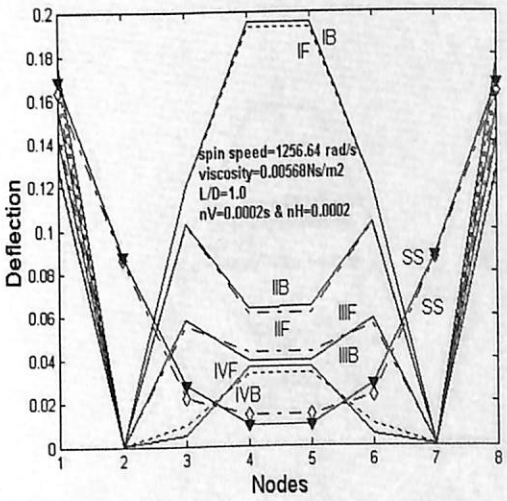

Fig. 5.21: Mode shapes for Rotor-Bearing System supported on two-lobe bearings at station 2 and 7 at operating speed 1256.64 rad/s

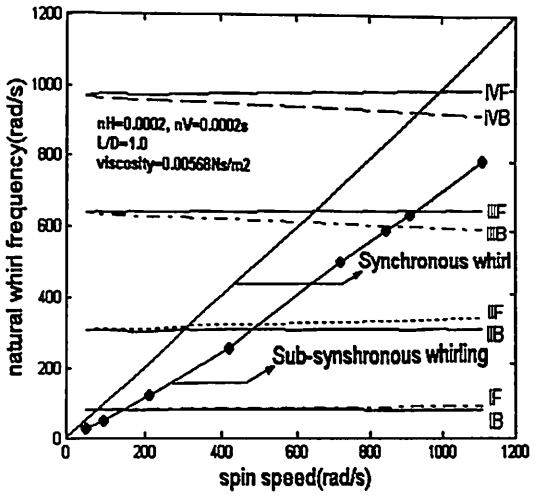

Fig. 5.22: Campbell Diagram for Rotor-Bearing System supported on three-lobe bearings

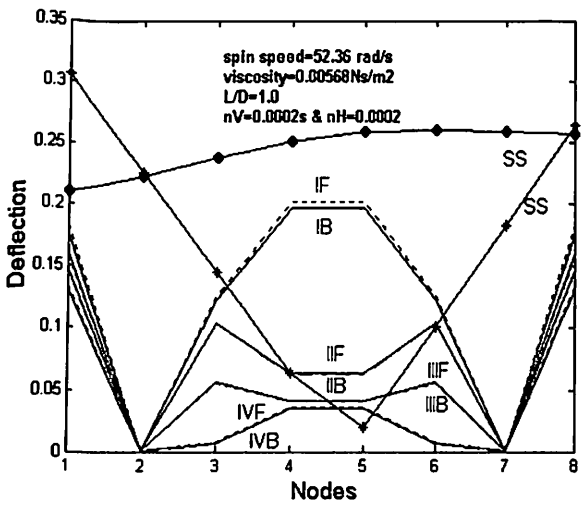

Fig. 5.23: Mode shapes for Rotor-Bearing System supported on three-lobe bearings at station 2 and 7 at operating speed 52.36 rad/s

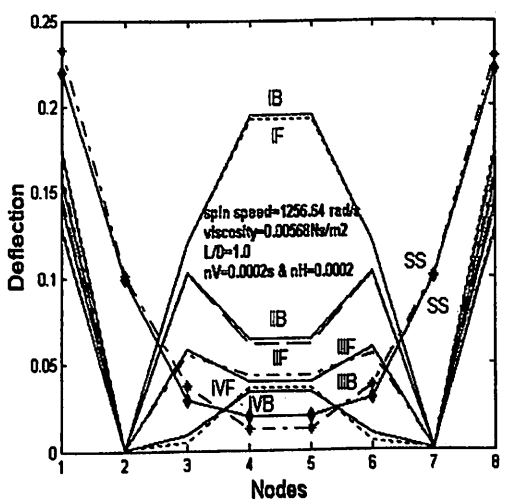

Fig. 5.24: Mode shapes for Rotor-Bearing System supported on three-lobe bearings at station 2 and 7 at operating speed 1256.64 rad/s

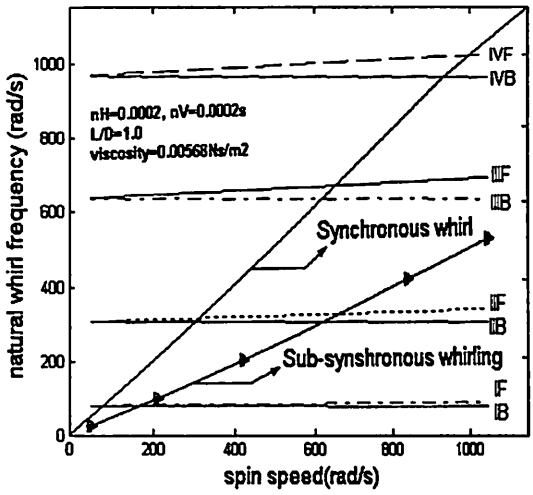

Fig. 5.25: Campbell Diagram for Rotor-Bearing System supported on four-lobe bearings

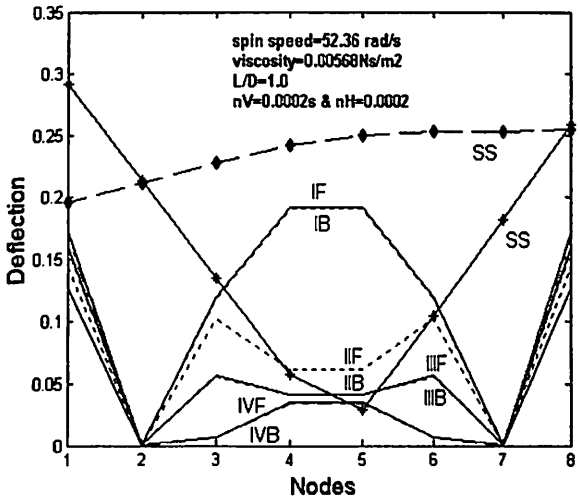

Fig. 5.26: Mode shapes for Rotor-Bearing System supported on four-lobe bearings at station 2 and 7 at operating speed 52.36 rad/s

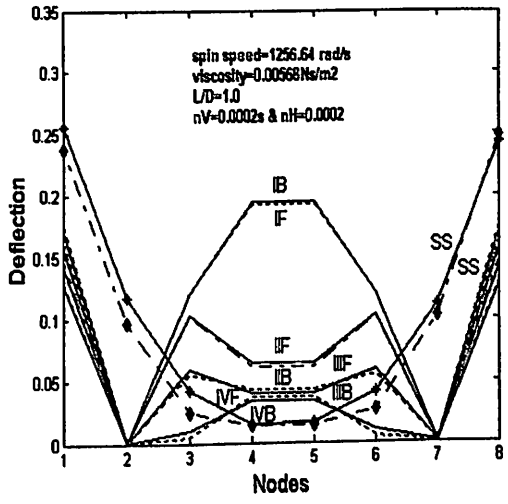

Fig. 5.27: Mode shapes for Rotor-Bearing System supported on four-lobe bearings at station 2 and 7 at operating speed 1256.64 rad/s

From these figures it is observed that there is not much variation in the natural whirl frequencies of all three types of bearings considered here. However, in case of two-lobe bearing, like the results of the previous section (viscosity=*0.001379*Ns/m^2), sub-synchronous frequency whirl takes place at more than half the spin speed.

5.4 Conclusions

From the above analysis it is clear that the natural frequencies of different types of bearings are not much different. But there appears an additional sub-synchronous frequency in all types of bearings. Different types of rotor bearing systems considered are unstable only at one forward mode. However, even for the same spin speed equal to the unstable forward synchronous whirl frequency there is no instability caused due to sub-synchronous whirling and that is true for all the bearings considered in the study.

Chapter 6

Stability analysis of rigid and flexible rotors

6.1 Introduction

In previous two chapters natural synchronous and sub-synchronous whirl frequencies were estimated using a FEM model. Stability study was carried out using the evaluated logarithmic decrement associated with these frequencies. However, it is difficult to ascertain the critical sub-synchronous frequencies by logarithmic decrements. In view of this, it has been proposed to find the critical frequencies following methods used by others [85,132] and then to compare these with the present results.

In the present chapter both Linearized stability analysis and Non-linear time transient analysis are adopted for stability analysis of rigid rotor supported on different types of fluid film bearings, namely two-groove bearings, two-lobe bearings, three-lobe bearings and four-lobe bearings. Results from two analyses are compared. Further, the linear analysis is extended to estimate the instability thresholds of flexible rotor systems supported on different types of bearing configurations. Simplified models of rigid and flexible rotors are used here.

6.2 Formulation of the problem

6.2.1 Stability analysis

When a rotor supported by fluid film bearing operates at high speeds, there is possibility of whirl instability. This limits the operating speed of the journal and therefore it is important to know the speed above which the system will be unstable. The stability analysis can be done in any one of the following ways:

1. Linearized Stability Analysis.
2. Non-linear Transient Analysis.

In Linearized stability analysis, the determination of stiffness and damping coefficients is important. These can be used to represent the forces developed in the bearing due to small amplitude motion of journal about its equilibrium position and to calculate the stability behaviours of rotors. Non-dimensional parameters of these bearings are analyzed based on these dynamic coefficients.

Linearized analysis is suitable for predicting the bearing behaviour for small amplitude motions about equilibrium position, but it fails to accurately provide information for large amplitudes of journal orbits above the threshold speed. Therefore, non-linear time transient analysis is performed to obtain the trajectories of the journal centre.

6.2.2 Rigid Rotor analysis

6.2.2.1 Linear stability analysis

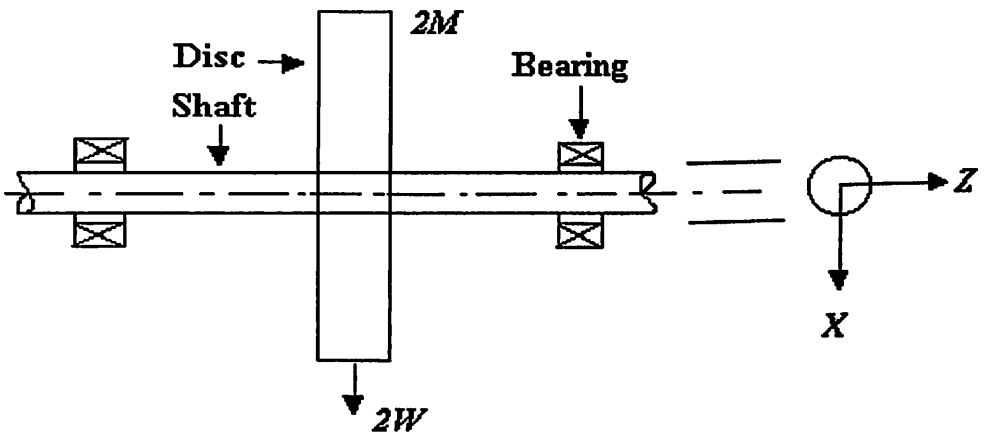

Fig. 6.1: Rotor-bearing configuration

The frequency of oil whirl or self-excited vibration due to fluid film force of the rotor is the half of the rotational speed of the rotor. For a rotor of mass *2M* supported by two identical fluid film bearings, the non-dimensional linearized equations of journal motion can be written as follows (*X*-*Z* coordinate system as shown in Fig. 6.1):

$$M\ddot{X} + k_{XX}X + k_{XZ}Z + c_{XX}\dot{X} + c_{XZ}\dot{Z} = 0$$
$$M\ddot{Z} + k_{ZZ}Z + k_{ZX}X + c_{ZZ}\dot{Z} + c_{ZX}\dot{X} = 0 \qquad (6.1)$$

For a small disturbance from the equilibrium position of the journal

$$X = X_0 \exp \nu t$$
$$Z = Z_0 \exp \nu t \qquad (6.2)$$

where ν is a complex number

$$\nu = \alpha + i\omega . \qquad (6.3)$$

If α is positive, the solution is unstable and if it is negative, the whirl orbit reverts to a steady position in the bearing circle. The threshold condition is therefore

$$X = X_0 \exp(i\omega t)$$
$$Z = Z_0 \exp(i\omega t) \qquad (6.4)$$

Substituting the equation (6.4) in the equation (6.1), we get the following equation

$$\begin{bmatrix} (k_{XX} - M\omega^2 + i\omega c_{XX}) & (k_{XZ} + i\omega c_{XZ}) \\ (k_{ZX} + i\omega c_{ZX}) & (k_{ZZ} - M\omega^2 + i\omega c_{ZZ}) \end{bmatrix} \begin{Bmatrix} X \\ Z \end{Bmatrix} = 0 \qquad (6.5)$$

For nontrivial values of X and Z, we have,

$$\begin{aligned} &(k_{XX} - M\omega^2)(k_{ZZ} - M\omega^2) - \omega^2 c_{XX}c_{ZZ} - k_{ZX}k_{XZ} + \\ &\omega^2 c_{XZ}c_{ZX} + i\omega[c_{XX}(k_{ZZ} - M\omega^2) + \\ &c_{ZZ}(k_{XX} - M\omega^2)] - i\omega(c_{ZX}k_{XZ} + k_{ZX}c_{XZ}) = 0 \end{aligned} \qquad (6.6)$$

Separating real and imaginary parts and simplifying we obtain non-dimensional relationship,

$$\frac{\left(\overline{K}_{XX} - \frac{M\omega^2 C}{W}\right)\left(\overline{K}_{ZZ} - \frac{M\omega^2 C}{W}\right) - \overline{K}_{ZX}\overline{K}_{XZ}}{\overline{C}_{XX}\overline{C}_{ZZ} - \overline{C}_{XZ}\overline{C}_{ZX}} = \frac{\omega^2}{\Omega^2} = \frac{1}{\lambda^2} \qquad (6.7)$$

$$\frac{\left(\overline{C}_{XX}\overline{K}_{ZZ} + \overline{C}_{ZZ}\overline{K}_{XX} - \overline{C}_{ZX}\overline{K}_{XZ} - \overline{C}_{XZ}\overline{K}_{ZX}\right)}{\overline{C}_{XX} + \overline{C}_{ZZ}} = \frac{M\omega^2 C}{W} \qquad (6.8)$$

For a given Sommerfeld number of the bearing, the equation (6.8) can be written as

$$K_0 = \frac{M\omega^2 C}{W} = \frac{\overline{M}}{\lambda^2} \tag{6.9}$$

where $\overline{M} = \frac{MC\Omega^2}{W}$ is the non-dimensional mass parameter.

Hence the equation (6.7) becomes

$$\frac{(\overline{K}_{XX} - K_0)(\overline{K}_{ZZ} - K_0) - \overline{K}_{ZX}\overline{K}_{XZ}}{\overline{C}_{XX}\overline{C}_{ZZ} - \overline{C}_{XZ}\overline{C}_{ZX}} = \frac{K_0}{\overline{M}} = \frac{1}{\lambda^2} \tag{6.10}$$

From the definition of Sommerfeld number and writing

$$\chi = \frac{\sqrt{CMW}}{\mu DL\left(\frac{R}{C}\right)^2} \tag{6.11}$$

the equation (6.10) can be written as

$$\chi = \frac{1}{2\pi S}\sqrt{\frac{K_0(\overline{C}_{XX}\overline{C}_{ZZ} - \overline{C}_{XZ}\overline{C}_{ZX})}{(\overline{K}_{XX} - K_0)(\overline{K}_{ZZ} - K_0) - \overline{K}_{ZX}\overline{K}_{XZ}}} = \frac{1}{2\pi S}\sqrt{\overline{M}} \tag{6.12}$$

The non-dimensional parameter χ for a rigid rotor can be determined for chosen values of S where the instability is expected. The dynamic coefficients for different fluid film bearings are used [160]. The relation between χ and S have been plotted and threshold instability speed can be determined from this plot.

For a certain bearing eccentricity ratio or Sommerfeld number, non-dimensional stiffness and damping coefficients are determined. These dynamic coefficients are then used for calculating the critical non-dimensional parameter χ_{crit} that can be calculated as follows:

$$\frac{(\overline{C}_{XX}\overline{K}_{ZZ} + \overline{C}_{ZZ}\overline{K}_{XX} - \overline{C}_{ZX}\overline{K}_{XZ} - \overline{C}_{XZ}\overline{K}_{ZX})}{\overline{C}_{XX} + \overline{C}_{ZZ}} = K_0 = \frac{\overline{M}_{crit}}{\lambda_{crit}^2} \tag{6.13}$$

K_0 is a constant and depends on the values of a particular set of coefficients.

Thereby,

$$\frac{1}{\lambda_{crit}^{\ 2}} = \frac{(\overline{K}_{XX} - K_0)(\overline{K}_{ZZ} - K_0) - \overline{K}_{ZX}\overline{K}_{XZ}}{\overline{C}_{XX}\overline{C}_{ZZ} - \overline{C}_{XZ}\overline{C}_{ZX}} \tag{6.14}$$

$$\chi_{crit} = \frac{1}{2\pi S}\sqrt{\frac{K_0(\overline{C}_{XX}\overline{C}_{ZZ} - \overline{C}_{XZ}\overline{C}_{ZX})}{(\overline{K}_{XX} - K_0)(\overline{K}_{ZZ} - K_0) - \overline{K}_{ZX}\overline{K}_{XZ}}} = \frac{1}{2\pi S}\sqrt{\overline{M}_{crit}} \tag{6.15}$$

6.2.2.2 Non-linear stability analysis

This system may be fully described for non-linear transient simulation by the rotating co-ordinate system as shown in the Fig. 6.1 and Fig. 6.2 where $\varepsilon\,(t)$ and $\phi\,(t)$ are the co-ordinates of the rotor mass centre, and F_ε, F_ϕ are the fluid film bearing reaction forces.

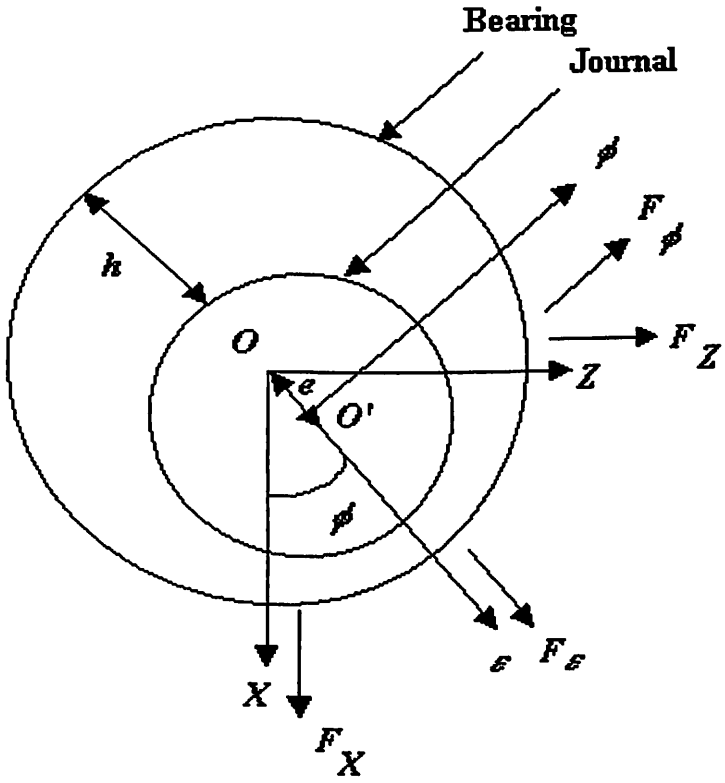

Fig. 6.2: Plain circular journal bearing

The equations of motion of the non-dimensional form in rotating frame of reference [161] are,

$$\begin{aligned} \overline{MW}[\ddot{\varepsilon} - \varepsilon(\dot{\phi})^2 &= \overline{F}_\varepsilon + \overline{W}\cos\phi \\ \overline{MW}[\varepsilon\ddot{\phi} + 2\varepsilon\dot{\phi}] &= \overline{F}_\phi - \overline{W}\sin\phi \end{aligned} \tag{6.16}$$

The fourth-order Runge-Kutta method is used for solving these equations of motion to compute new set of eccentricity ratio, attitude angle and their time derivatives (ε, ϕ, $\dot{\varepsilon}$ and $\dot{\phi}$) at every time step. Fluid film forces are calculated at every time step by solving unsteady Reynolds equation for updated ε, ϕ, $\dot{\varepsilon}$ and $\dot{\phi}$. The motion trajectories are obtained by plotting eccentricity ratio and attitude angle at every time step showing position of journal centre. One can find out whether the system is stable, unstable or at critical condition by observing these trajectories. Critical mass parameter of particular eccentricity ratio is found when the trajectory of journal centre ends in a limit cycle or it changes its trend from stable to unstable.

6.2.3 Flexible Rotor Instability: Linear Analysis

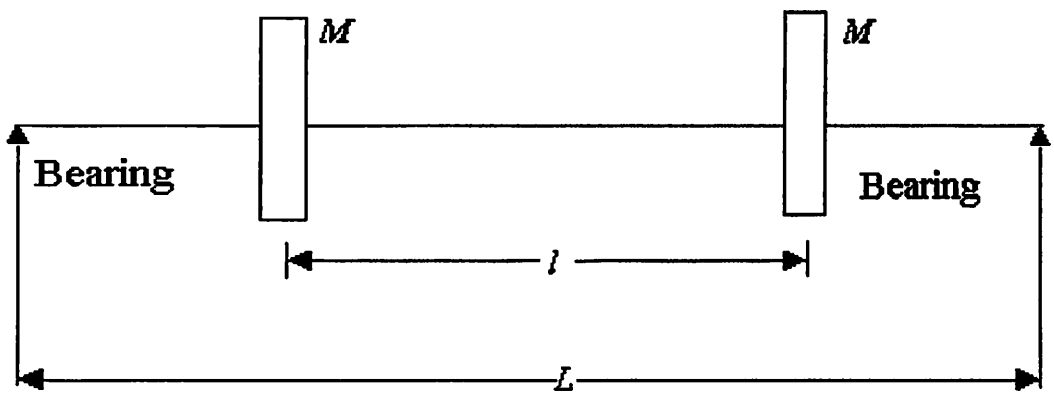

Fig. 6.3: Flexible rotor on fluid film bearing

For a flexible rotor, it is convenient to use an equivalent rotor as given by Rao [132]. The shaft carries two disks of mass M each and separated by a distance l symmetrically with centre as shown in Fig.6.3.

For flexible rotor non-dimensional parameter of the bearing can be written as

$$\chi_f = \frac{1}{2\pi S}\sqrt{\frac{K_0\sigma}{(K_0+\sigma)}\frac{\left(\overline{C}_{xx}\overline{C}_{zz}-\overline{C}_{xz}\overline{C}_{zx}\right)}{(\overline{K}_{xx}-K_0)(\overline{K}_{zz}-K_0)-\overline{K}_{zx}\overline{K}_{xz}}} = \chi\sqrt{\frac{\sigma}{(K_0+\sigma)}} \qquad (6.17)$$

where

$$\sigma = \frac{C}{W\alpha}.$$

α can be evaluated by calculating rigid bearing critical speed of the rotor that is described as

$$\omega_n{}^2 = \frac{1}{\alpha M}$$

Initially for a rigid rotor the non-dimensional parameter χ can be determined for chosen values of S where the instability is expected. The relation between χ and S have been plotted and threshold instability speed can be determined from this plot. Flexible rotor threshold speed can be determined by plotting χ_f and S.

6.2.4 Finite Element Formulation of Rotor bearing system

Finite element formulation is carried out for Timoshenko beam incorporating translational inertia, rotary inertia, bending deformation; shear deformation, gyroscopic effect in Chapter 3 and the resultant system equation of motion is also given in the same chapter.

A Campbell type of diagram is drawn which shows the system resonant frequency as a function of rotor speed. The first critical speed is evaluated where the rotational speed is equal to the system natural frequency. Half frequency whirl line and additional frequency line have been drawn. The instability threshold, which is known as oil whip, is the speed where the system frequency and half frequency whirl line meet.

6.3 Results and Discussion

6.3.1 Validation

For validation, the parameter χ is determined for rigid rotor supported on plain journal bearing with $L/D=1.0$ and the relation between χ and S are plotted as shown in the Fig.6.4. This plot is found identical to the plot provided by Rao [132], which validates the present model.

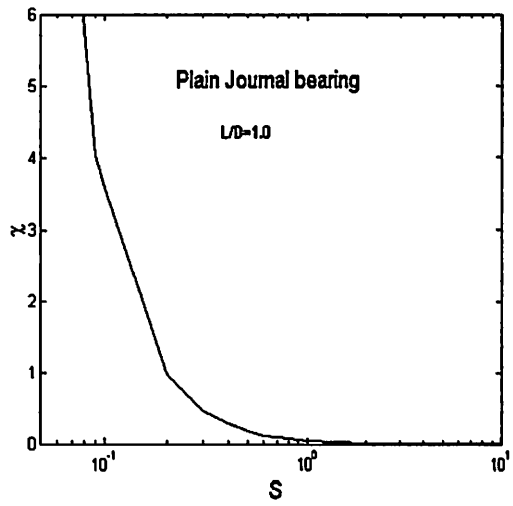

Fig. 6.4: Stability of a rigid rotor supported on plain journal bearing

6.3.2 Rigid rotor analysis

6.3.2.1 Stability analysis: Linear analysis Vs Non-linear analysis

For rigid rotor, non-dimensional parameters (χ) at the stability threshold using both linear and non-linear analysis against Sommerfeld number are plotted in Fig. 6.5 through Fig. 6.8. It has been observed that results using linear analysis are least stable than results using non-linear analysis for all speeds in case of two-groove and two-lobe bearing. But for three-lobe and four-lobe bearing, at moderate and high-speed operation, linear analysis results are more stable than non-linear results.

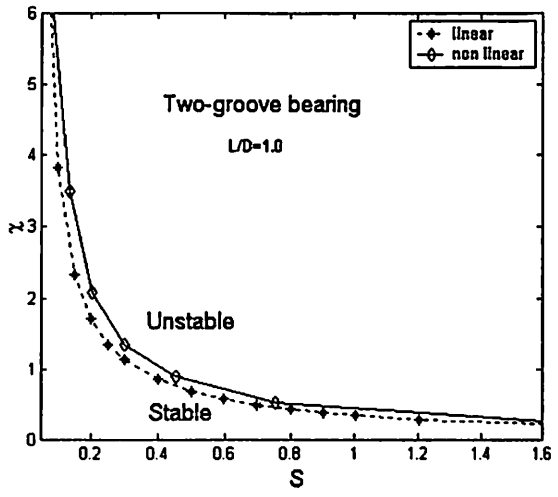

Fig. 6.5: Comparison of stability analysis of grooved circular bearings

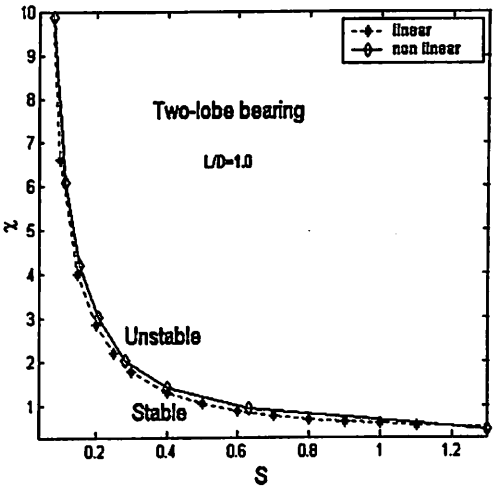

Fig. 6.6: Comparison of stability analysis of two-lobe bearings

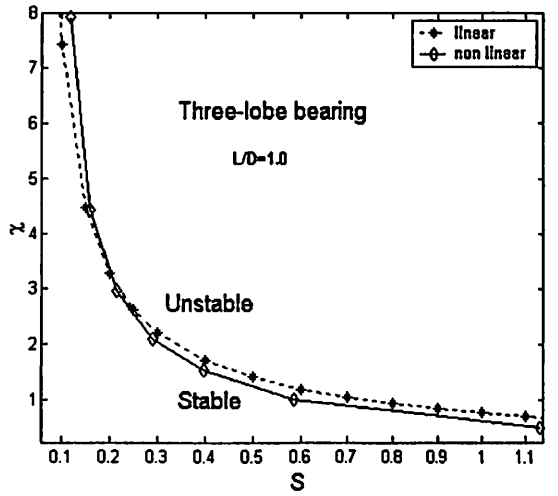

Fig. 6.7: Comparison of stability analysis of three-lobe bearings

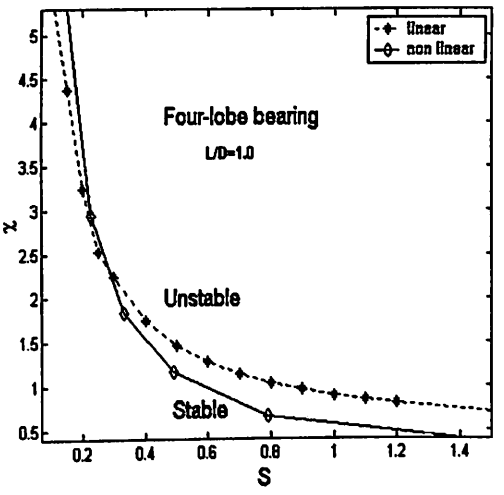

Fig. 6.8: Comparison of stability analysis of four-lobe bearings

Stability curves for all four types of bearings using both linear and non-linear analysis are plotted together for comparison of non-dimensional parameter over Sommerfeld number in Fig. 6.9 and Fig. 6.10. From both analyses, it is clear that two-lobe bearing is least suitable non-circular bearing, which is just ahead of grooved circular bearing. From Non-linear analysis, it has been observed that three-lobe bearing is most stable in high

speed and low load condition (higher value of Sommerfeld number). At moderate and heavy load conditions; three-lobe is the second best, only after four-lobe bearing. Grooved circular bearing is least desirable from stability point of view for all operating conditions.

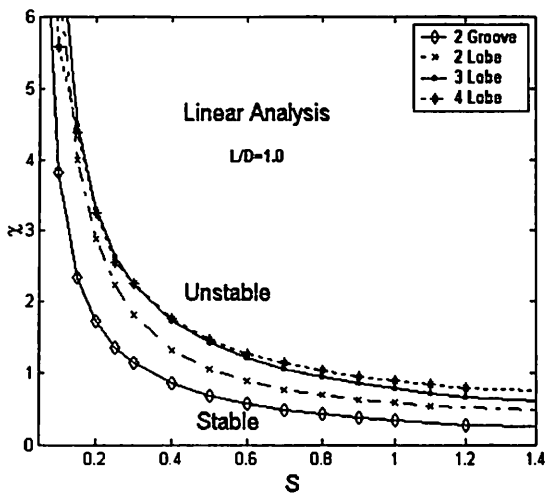

Fig. 6.9: Stability analysis of different bearings using linear analysis

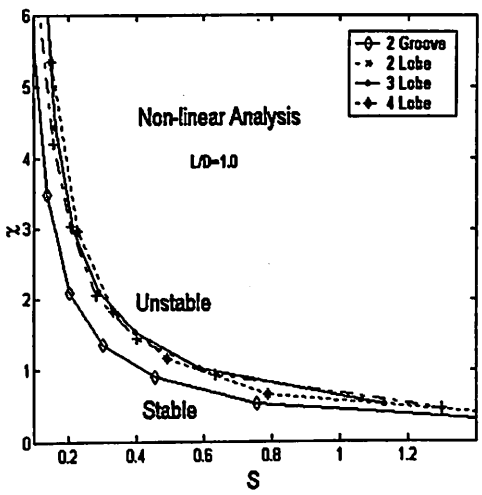

Fig. 6.10: Stability analysis of different bearings using non-linear analysis

6.3.3 Flexible rotor analysis

6.3.3.1 Stability Analysis: Rigid Vs Flexible Rotor

The first critical speed for the rotor model with the same configuration as discussed in the section 3.2.1.1 of Chapter 3 (Fig. 3.1), having slenderness ratio 0.0064, with rigid supports is estimated to evaluate the rotor stiffness and that is equal to 889.32 rpm. Non-dimensional parameter of the bearing for rigid rotor (χ) as well as flexible rotor (χ_f) supported on grooved circular bearing is calculated as 0.5091. The value of σ is evaluated as 0.04495. Different values of χ are plotted (Fig.6.11) against different values of Sommerfeld number (S) where the instability is expected. From these plots the rigid rotor threshold speed is evaluated which is given by S=0.66 and that corresponds to 8859 rpm. Again different values of χ_f and S are plotted (Fig.6.11) from which the flexible rotor threshold speed is given by S=0.1359 which corresponds to 1824 rpm. Threshold

speed for the rotor model used here (sr=0.0064) is quite low as compared to rigid rotor. It is evident from these results that the assumption of rigid rotor does not provide the threshold speed for rotors of low slenderness ratio. To demonstrate the fact it has been proposed to estimate the threshold speed of different rotor models with different slenderness ratio mounted on identical bearings.

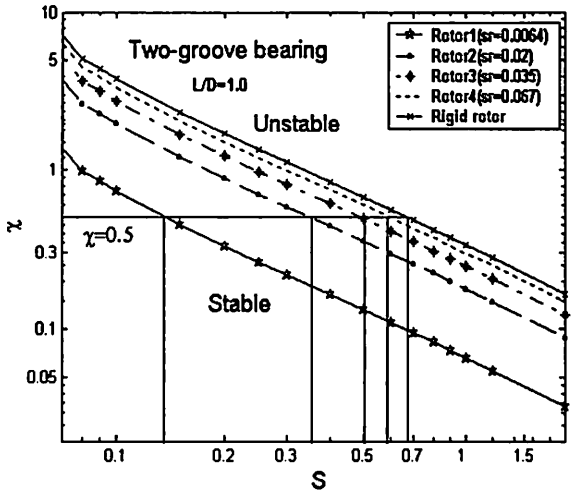

Fig. 6.11: Instability threshold speed of rigid and flexible rotor supported on grooved circular bearing

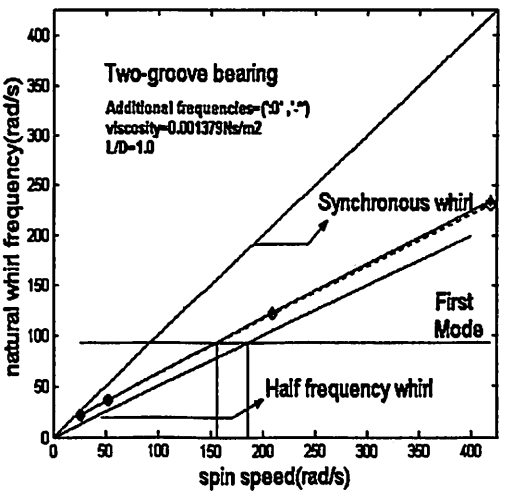

Fig. 6.12: Instability threshold speed of Rotor supported on grooved circular bearing using FEM model

As stated above, different rotor models of different slenderness ratios (sr=0.02, 0.035 and 0.067) with first natural frequencies being 2747.8 rpm, 4735.5 rpm and 8594.2 rpm respectively are considered and the values of χ_f for different rotors are plotted in the same figure (Fig.6.11) against different values of Sommerfeld number. Threshold speeds for different rotors (sr=0.02, 0.035 and 0.067) are found to be 4856 rpm, 6711 rpm and 8053 rpm respectively. From this observation it is clear that with the increase in the slenderness ratio, there is increase in the threshold speed of the rotor-bearing system.

Threshold speed approaches to rigid rotor threshold speed at slenderness ratio higher than 0.067. The results presented clearly indicate that assumption of a rigid rotor is valid only when the slenderness ratio of the rotor is relatively high and thereby its first natural frequency is also quite high.

6.3.4 Stability analysis using FEM model

A rotor system mounted on two identical fluid film bearings located at two ends as shown Fig.3.2 is analysed. The physical properties of the shaft and bearing geometry are provided in the Table 4.3.

A Campbell type of diagram only for first mode is drawn (Fig.6.12), which shows the system natural whirl frequency as a function of rotor speed. The first critical speed is evaluated as 883 rpm. The half frequency whirl line is drawn. The instability threshold for half frequency whirling can be found at the point where the system frequency and half frequency whirl line meet and that equals to 1763 rpm (Fig.6.12). Another line is also drawn from the different values of additional frequencies and instability threshold is evaluated. In this case the threshold speed is found to be *to 1420 rpm.* Considering the same rotor system, the analysis is also carried out for non-circular bearings and results are given in from Fig. 6.13 through Fig. 6.18. Threshold speeds are given in Table 6.1.

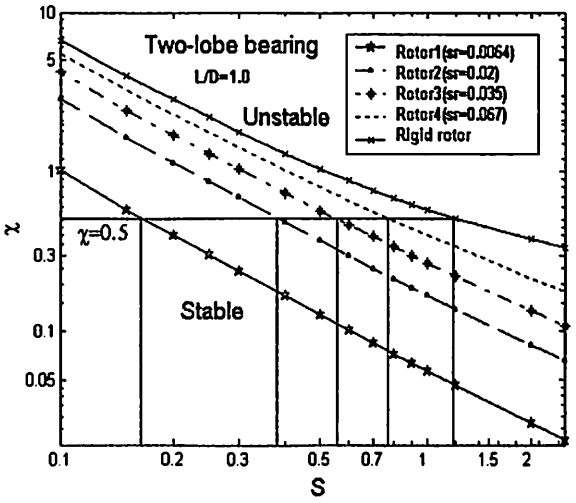

Fig. 6.13: Instability threshold speed of rigid and flexible rotor supported on two-lobe bearing

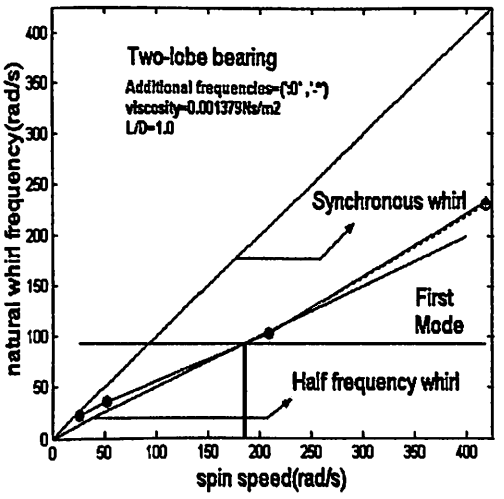

Fig. 6.14 Instability threshold speed of Rotor supported on two-lobe bearing using FEM model

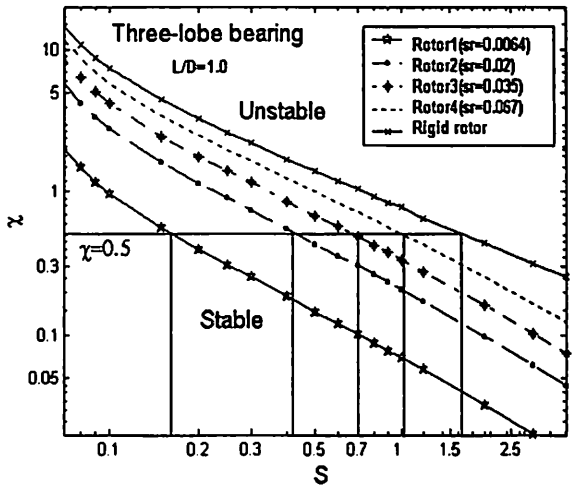

Fig. 6.15 Instability threshold speed of rigid and flexible rotor supported on three-lobe bearing

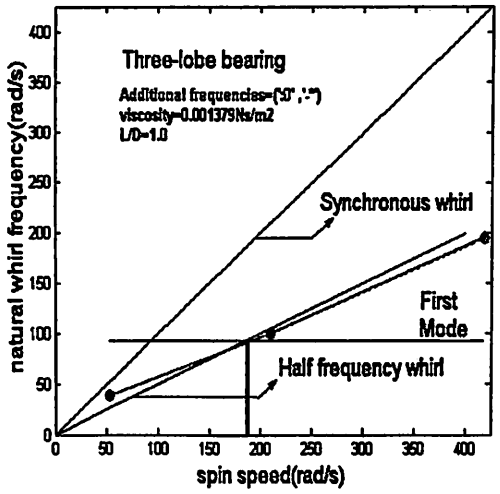

Fig. 6.16 Instability threshold speed of Rotor supported on three-lobe bearing using FEM model

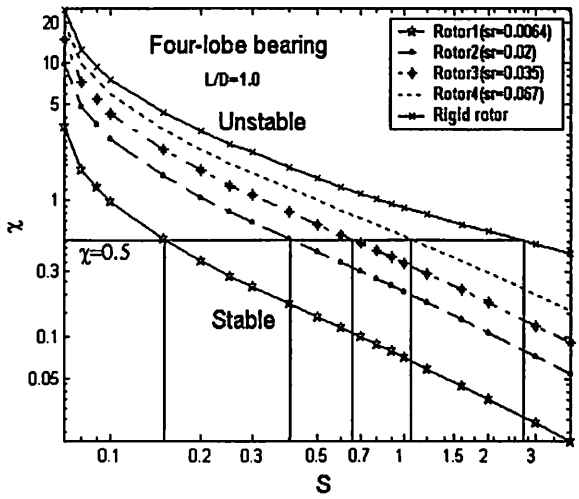

Fig. 6.17 Instability threshold speed of rigid and flexible rotor supported on four-lobe bearing

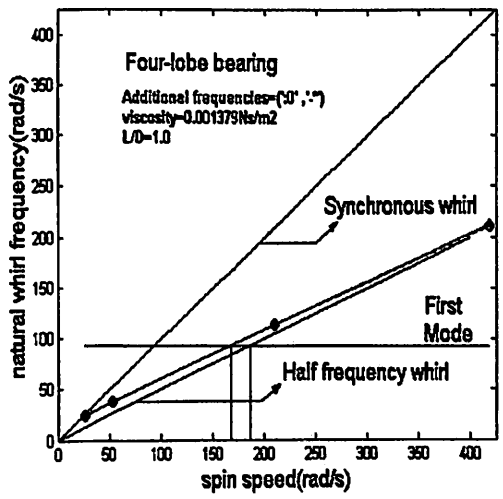

Fig. 6.18: Instability threshold speed of Rotor supported on four-lobe bearing using FEM model

Table 6.1: Threshold speeds for rotors supported on different bearings

Bearing type	Half frequency threshold speeds (rpm)			
	Rigid rotor	Flexible rotor	From half frequency whirl line	From additional frequency line
Two-groove	8859	1824	1763	1420
Two-lobe	13691	2296	1781	1763
Three-lobe	22550	2147	1776	1795
Four-lobe	33750	2181	1776	1598

6.4 Conclusions

From this study one can observe that the threshold sub-synchronous whirling frequency of bearing considering rigid rotor is quite high compared that of flexible rotor model used in this work. If slenderness ratio is increased threshold speed increases. Therefore the assumption of rigid rotor does not provide the threshold speed for rotors of low slenderness ratio. The rotor model used in this study is too flexible and rigid rotor approximation leads to erroneous results in this type of rotor. Further, using FEM model, threshold frequencies are estimated from both half-frequency whirl line and estimated sub-synchronous frequency line for all the types of bearings considered here. It is evident from these results that, except for three lobe bearings, threshold speeds estimated from sub-synchronous frequency line are different from threshold speeds estimated from other methods. For three-lobe bearing, threshold speed estimated from sub-synchronous frequency line is slightly higher than the value estimated from half frequency line. However this value is quite lower than the estimated value from Rao's flexible rotor analysis. From the above observations it is clear that results estimated from the method used in this study are better than the results using other methods discussed here.

Chapter 7

Concluding remarks

7.1 Importance of present study

With the increase in performance requirements of high-speed rotating machinery in various fields the resulting instability problems of the system has become aggravated. In view of this there are many studies carried out to study the characteristics of high speed rotating machinery. In such studies, critical whirling speeds are estimated. The critical speeds of a rotor are frequently computed assuming the bearings to act as rigid supports. But in actual practice bearings have flexibility, which inherently lower the critical speed.

In high-speed applications, rotor stability is an important factor to be considered in the rotor design. Such instabilities may originate from fluid film bearings. Again most of the study on bearing stability is limited to the assumption of rigid rotors. Stability analyses of high-speed machinery based on rigid rotor model are found to be inadequate for stability predictions. Calculations of natural whirl frequencies (the eigen values) of a flexible rotor supported on fluid film bearings establish the critical speeds of the rotor that are more realistic than the conventional critical speeds. However, in most of the cases of fluid film bearings, simplified (short-bearing approximation) bearing models are used. Therefore sub-synchronous whirling is not reported in such analyses as pointed out in Chapter 1.

Again now a days new bearing designs are sought to meet the new requirements and these bearings are usually characterized by their noncircular cross sections. Generally plain circular bearing does not suit the stability requirements of high-speed machines and precision machine tools and almost any noncircular bearing geometry enhances shaft stability.

In view of this it has been proposed to study the characteristics of rotors mounted on finite hydrodynamic bearings. Therefore, the inherent deficiency of earlier study as described above is eliminated in the present study. It is because in the present study neither the rotor is considered as rigid nor the supports are considered as rigid. Further, dynamic coefficients of the bearings are estimated using finite bearing numerical solution scheme. Major contributions of the present work can be summarized as follows.

- An investigation is made to find out the behaviour including stability of rotor-bearing system supported on circular as well as non-circular, i.e., multi-lobe hydrodynamic bearings.
- Finite bearing dynamic coefficients are used instead of approximate solution like short bearing theory.
- Timoshenko beam is used as it provides a more complete model than either the Euler-Bernoulli or Rayleigh beams.
- Finite element formulation is carried out for Timoshenko beam by incorporating translational inertia, rotary inertia, bending deformation, shear deformation, gyroscopic effect and internal damping.
- Synchronous and sub-synchronous whirling speeds are plotted in Campbell diagrams and critical frequencies are estimated for different bearings; namely, two grooved circular, two-lobe, three lobe and four-lobe bearings.
- Mode shapes for first four modes and mode shapes corresponding to half frequency whirling are also plotted.
- Stability characteristics at different spin speeds are studied by estimating the logarithmic decrements.
- To ascertain the importance of the present study simplified models like bearings supporting rigid rotor and flexible rotors are also studied for different bearing configuration. The stability margins are estimated for these bearings.

- It has been observed that as slenderness ratio vis-à-vis first critical frequency increases threshold speed of flexible rotor also increases. Therefore rotors with different slenderness ratios are considered and threshold speeds are estimated.

7.2 Important results

The important results of the present study are summarized as follows.

- In addition to the synchronous natural whirl frequencies of rotors mounted on finite bearings, for every spin speed another whirling frequency appears in the solution which is identified as the half-frequency whirling.
- When short bearing theory is used to estimate dynamic characteristics, these additional frequencies are of the same order as that of the regular synchronous whirling frequencies. This has shown the deficiency in the use of short bearing approximation in studies relating to estimation of whirling frequencies.
- From the present study it is clear that the natural whirl frequencies for the rotors mounted on four different types of bearings are not much different.
- It has been seen from the mode shapes corresponding to the half-frequency whirl for all types of bearings considered that there are deflections of the shaft at the bearing stations.
- It is observed from the estimated results that except for the few forward synchronous frequency, logarithmic decrements are found to be positive in all other cases for all types of bearing considered in this work, which indicates stability in all those cases.
- However, even for the same spin speed equal to the unstable forward synchronous whirl frequency there is no instability due to sub-synchronous whirling.
- It is very important to note that when rotor instability is studied by estimating only synchronous whirling and ignoring sub-synchronous whirling, it would lead to an erroneous analysis.

- If damping coefficients are ignored, wrong notions of instability to all forwarding modes are created. Therefore, use of hypothetical bearing does not give the actual picture of the stability of the rotor-bearing system and more significantly bearing damping is a very important parameter in studying the characteristics of rotor bearing systems.
- It has been demonstrated that the assumption of rigid rotor and simplified rotor model do not provide actual estimate of threshold speed.
- As slenderness ratio increases threshold speed of flexible rotor also increases and at a particular value, threshold speed of flexible rotor approaches to rigid rotor threshold speed.
- Therefore, it is recommended that the estimation of threshold speed for rotors with relatively low first critical frequency should be made by using FEM model and plotting Campbell diagram as has been done in the present study.

7.3 Scope for future work

- In the present work bearings are considered to be isothermal, i.e., there is no provision of expansion or contraction of the bearing due to change of temperature. Therefore the present study can be extended to incorporate those types of bearings in which expansion or contraction due to temperature change is considered.
- Due to temperature change viscosity of bearing lubricant may change. Therefore the present study can be extended to consider viscosity variation due to temperature change.
- At high-pressure application also, viscosity of lubricant may change. The present study can be extended to consider those changes also.
- Time transient analysis of flexible rotors mounted on fluid film bearings can be done by extending the present work. This analysis can be done at various speeds and the instability phenomenon, which occurs due to fluid film forces, can be observed.

References

[1] Brancati, R., Rocca, E., Russo, M., and Russo, R., "Journal orbits and their stability for rigid unbalanced rotors," *ASME Transaction: Journal of Tribology*, Vol. 117, pp.709-716, 1995.

[2] Lund, J.W., and Nielsen, H.B., "Instability threshold of an unbalanced rigid rotor in short journal bearings", *Second International Conference on Vibration in Rotating Machinery*, Cambridge, 1980.

[3] Russo, M., and Russo, R, "Parametric excitation instability of a rigid unbalanced rotor in short turbulent journal bearings", *Proceedings of the Institution of Mechanical Engineers*, Part c, Vol. 207, pp. 149-160, 1993.

[4] Newkirk, B.L., and Taylor, H.D., "Shaft Whipping due to oil action in Journal bearings," *General Electrical Review*, Vol. 28, August, pp.559-568, 1925.

[5] Stadola, A., "Kritische Wellenstorung infolge Nachgiebigkeit des Oelposters in Lager," *Schweiz. Bauz.*, pp. 267, 1925.

[6] Hummel, C., "Kritische Drehzahlen als Folge der Nachgiebigkeit des Schmiernmittelsin lager," *VDI Forschungsh*, pp.287, 1926.

[7] Newkirk, B.L., "Whirling balanced shafts," *Third International Congress, Applied Mechanics*, Sweden, 1930.

[8] Hagg, A.C., "The influence of oil-film journal bearings on the stability of rotating machines", *ASME Transaction: Journal of Applied Mechanics*, Vol. 68, pp.211-220, 1946.

[9] Ono, K., and Tamuri, A., "On the vibrations of horizontal shaft supported in oil-lubricated bearings," *Bulletin of JSME*, Vol.11, No.47, pp.813-824, 1968.

[10] Akers, A., Michaelson, S., and Cameron, A., "Stability contours for a whirling finite journal bearing," *ASME Transaction: Journal of Lubrication Technology*, Vol. 93, No. 1, pp.177-190, 1971.

[11] Lund, J.W., "Stability and damped critical speeds of a flexible rotor in fluid film bearings," *ASME Transaction: Journal of Engineering for Industry*, Series B, Vol. 96, No. 2, pp.509-517, 1974.

[12] Lund, J.W., "Modal response of a flexible rotor in fluid-film bearings," *ASME Transaction: Journal of Engineering for Industry*, Series B, Vol. 96, No.2, pp.525-533, 1974.

[13] Kirk, R.G., and Gunter, E.J., "Short bearing analysis applied to rotor bearing dynamics, Part1: Theory," *ASME transaction: Journal of Engineering of Lubrication Technology*, Vol. 98, pp.47-56, 1976.

[14] Kirk, R.G., and Gunter, E.J., "Short bearing analysis applied to rotor dynamics, Part2: Results of Journal bearing response," *ASME transaction: Journal of Engineering of Lubrication Technology*, Vol. 98, pp. 319-329, 1976.

[15] Muller- Karger, C.M., and Granados, A.L., "Deviation of hydrodynamic bearing coefficients using minimum square method," *ASME Transaction: Journal of Tribology*, Vol. 119, pp. 802-807, 1977.

[16] Rao, J.S., Bhat, R.B., and Sankar, T.S., "Effect of damping on the synchronous whirl of a rotor on hydrodynamic bearings," *Trans. Canadian Society of Mechanical Engineers*, Vol. 6, No.3, pp.155, 1981.

[17] Bhat, R.B., Rao, J.S., and Sankar T.S., "Optimum journal bearing parameters for minimum rotor unbalance response in synchronous whirl," *ASME Transaction: Journal of Mechanical Design*, Vol. 104, pp.339, 1982.

[18] Rao, J.S., "Synchronous whirl of a flexible rotor in hydrodynamic bearings," *Mechanism and Machine Theory*, Vol.17, No.2, pp.143, 1982.

[19] Rao, J.S., Sarma, K.V.B., "Simulation of Multishaft rotors mounted on fluid film bearings to determine unbalance response," *Proceeding of International Conference Power Plant Simulation*, Mexico, pp.85, 1984.

[20] Subbiah, R., Bhat, R.B., Sankar, T.S., and Rao, J.S., "Backward whirl in a simple rotor supported on hydrodynamic bearings, Instability in rotating machinery," *NASA Conference Publication 2409*, pp.145, 1985.

[21] Ken, I., and Mori, H., "Effects of cavity fluctuation on the dynamic coefficients of journal bearing", *Proceedings 13th Leeds-Lyon Synopsis on Tribology*, pp.481-485, 1986.

[22] Rajalingham, C., Ganesan, N., and Prabhu, B., "The effect of modified inlet boundary conditions on the stiffness and damping characteristics of finite hydrodynamic journal bearings," *Wear*, Vol. 108, pp.203-211, 1986.

[23] Rao, T.V.V.L.N., Hirani, H., Biswas, S., and Athere, K., "An analytical approach to evaluate dynamic coefficients and nonlinear transient analysis of a hydrodynamic journal bearing," *STLE Tribology Transactions*, Vol. 43, No. 1, pp.109-115, 2000.

[24] Raghunandana, K., Majumdar, B.C., and Maiti, R., "Stability of flexibly supported oil journal bearings using non-Newtonian Lubricants: Linear Perturbation Analysis," *ASME Transaction: Journal of Tribology*, Vol. 123, No.3, pp.651–654, 2001.

[25] Cheng-Chi Wang, Cheng-Ying Lo and Cha'o-Kuang Chen, "Non-linear dynamic analysis of a flexible rotor supported by externally pressurized porous gas journal bearings," *ASME Transaction: Journal of Tribology*, Vol. 124, No.3, pp.553-561, 2002.

[26] Zhu, Q., and Zhang, W. J., "A preliminary nonlinear analysis of the axial transient response of the sector-shaped hydrodynamic thrust bearing-rotor system," *ASME Transaction: Journal of Tribology*, Vol. 125, No.4, pp. 854–858, 2003.

[27] Matsuda, K., Kanemitsu, Y. and Kijimoto, S., "Optimal clearance configuration of fluid-Film journal bearings for stability improvement," *ASME Transaction: Journal of Tribology*, Vol. 126, No.1, pp. 125–131, 2004.

[28] Newkirk, B.L., and Grobel, L.P., "Oil-film whirl-a non whirling bearing", *ASME Transaction: Journal of Applied Mechanics*, Vol. 56, pp. A-607-A-615, 1934.

[29] Pinkus, O., "Analysis of elliptical bearings" *Transaction of ASME*, Vol. 78, pp.965-973, 1956.

[30] Pinkus, O., "Power losses in elliptical and three-lobe bearing," *Transaction of ASME*, Vol. 78, pp.899-904, 1956.

[31] Pinkus, O., "Experimental investigation of resonant whip," *Transaction of ASME*, Vol. 78, pp.975-983, 1956.[32] Pinkus, O., "Analysis and characteristics of the three-lobe bearing," *ASME Transaction: Journal of Basic Engineering*, Vol. 81, pp.49-55, 1959.

[33] Glienicke, J., "Experimental investigation of the stiffness and damping coefficients of turbine bearings and their application to instability predictions", Paper No. 13, *Proceedings of the Institution of Mechanical Engineers*, London, Vol.181, No. 38, pp.116-129, 1966.

[34] Glienicke, J., Han, D.C., and Leonhard, M., "Practical determination and use of bearing dynamics coefficients," *Tribology International*, pp.297-309, 1980.

[35] Falkenhagen, G.L., Gunter, E.J., and Schuller, "Stability and transient motion of a vertical three-lobe bearing system," *Journal of Engineering for Industry*, pp.665-677, F.T, 1972.

[36] Schuller, F.T., ""Experiments on the stability of various water-lubricated fixed geometry hydrodynamic journal bearings at zero load," *Journal of Lubrication Technology*, Vol. 95, No. 4, pp.434-446, 1973.

[37] Schuller, F.T., "Stability experiments with hydrodynamic journal bearings of various numbers of lobes and length to diameter ratios," *ASLE Transactions*, Vol. 20, No. 4, pp.271-281, 1977.

[38] Holmes, A.G., Ettles, C.M., and Mayes, I.W., "The dynamics of flexible rotor systems supported on oil film bearings," *ASME Transaction: Journal of Mechanical Design*, Vol. 100, No.1, pp.156-164, 1977.

[39] Lund, J.W., and Thomsen, K.K., "A calculation method and data for the dynamic coefficients of oil-lubricated journal bearings," Topics in fluid film-bearings and rotor bearing systems design and optimization, *ASME Design Engineering Conference and Shows*, III, Chicago, New York, pp. 1-28, 1978.

[40] Akkok, M., and Ettles, C.M., "The onset of whirl instability in journal bearings of various bore shapes and groove sizes," *ASME Transaction: Journal of Lubrication Technology*, Vol. 105, No.3, pp.342-352, 1983.

[41] Leader, M.E., Flack, R.D., and Allaire, "Experimental study of three journal bearings with a flexible rotor," *ASLE Transactions*, Vol. 23, No.4, pp.363-369, P.E., 1979.

[42] Flack, R.D., Leader, M.E., and Allaire, P.E., "An experimental and theoretical investigation of pressures in four-lobe bearings," *Wear*, Vol. 61, No.2, pp.233-242, 1980.

[43] Leader, M.E., Flack, R.D., and Lewis, D.W., "An experimental determination of the instability of a flexible rotor in four-lobe bearings," *Wear*, Vol. 58, No.1, pp.35-47, 1980.

[44] Kumar, A., Sinhasan, R., and Singh, D.V., "Performance characteristics of two-lobe hydrodynamic journal bearings," *Journal of Lubrication Technology*, Vol. 102, pp.425-429, 1980.

[45] Li, D.F., Choy, K.C., and Allaire, P.E., "Stability and transient characteristics of four multi-lobe journal bearing configurations," *Journal of Lubrication Technology*, Vol. 102, No.3, pp. 291-299, 1980.

[46] Sinhasan, R., Malik, M., and Chandra, M., "Analysis of two-lobe porous hydrodynamic journal bearings," *Wear*, Vol. 64, No.2, pp.339-353, 1980.

[47] Malik, M., Sinhasan, R., and Chandra, M., "On performance characteristics of three-lobe porous hydrodynamic journal bearings," *ASLE Transactions*, Vol. 24, No.3, pp.354-361, 1981.

[48] Soni, S.C., Sinhasan, R., and Singh, D.V., "Performance characteristics of noncircular bearings in laminar and turbulent flow regimes," *ASLE Transactions*, Vol. 24, No.1, pp.29-41, 1981.

[49] Ng, C.W., and Pan, C.H.T., "A linearized turbulent lubrication theory," *ASME Transaction: Journal of Basic Eng.*, Vol. 87, pp.675-688, 1965.

[50] Malik, M., Sinhasan, R., and Chandra, M, "Design data for three-lobe bearings," *ASLE Transactions*, Vol. 24, No.3, pp.345-353, 1981.

[51] Flack, R.D., and Allaire, P.E., "An experimental and Theoretical determination of the static characteristics of three lobe bearing," *ASLE Transaction*, Vol. 25, No.1, pp.88-94, 1982.

[52] Malik, M., "A comparative study of some two-lobed journal bearing configurations," *ASLE Transactions*, Vol. 26, No.I, pp.118-124, 1983.

[53] Taylor, D.V., Kostrzewsky, G.J., Flack, R.D., and Barret, L.E., "Measured performance of a highly preloaded three-lobe journal bearing-Part I: Static characteristics," *STLE Tribology Transactions*, Vol. 38, No.3, pp.507-516, 1995.

[54] Taylor, D.V., Kostrzewsky, G.J., Barret, L.E., and Flack, R.D., "Measured performance of a highly preloaded three-lobe journal bearing-Part II: Dynamic characteristics," *STLE Tribology Transactions*, Vol. 38, No.3, pp. 707-713, 1994.

[55] Kostrezewsky, G.J., Flack, R.D., and Barrett, L.E., "Comparison between measured and predicted performance of a two-axial groove journal bearings," *STLE Tribology Transactions*, Vol. 39, No.3, pp.571-578, 1996.

[56] Muller-Karger, C.M., Barrett, L.E., and Flack, R.D., "Influence of fluid non linearity on the experimental determination of dynamic stiffness and damping coefficients for

three-lobe journal bearings," *STLE Tribology Transactions*, Vol. 40, No.1, pp.49-56, 1997.

[57] Rao, T.V.V.L.N., Biswas, S., and Athere, K., "A methodology for dynamic coefficients and non linear response of multi-lobe journal bearings," *STLE Tribology Transactions*, Vol. 44, No.1, pp. 111-117, 2001.

[58] Rankine, W.A., "On the centrifugal forces of rotating force," *Engineer*, London, Vol. 27, pp.249-256, 1869.

[59] Jeffcott, H.H., "The lateral vibration of loaded shafts in the neighbourhood of a whirling speed- the effect of want of balance," *Philos. Mag.*, Series 6, Vol. 37, pp.304-314, 1919.

[60] Newkirk, B.L., "Shaft whipping", *General Electric review*, Vol. 27, pp.169, 1924.

[61] Kimball, A.L., "Internal friction as a cause of shaft whirling", *Phil. Mag.*, Vol. 49, pp.724-727, 1925.

[62] Smith, D.M., "The motion of a rotor carried by a flexible shaft in flexible bearings", *Proc. Roy. Soc.*, (A), Vol. 142, pp.92, 1933.

[63] Prohl, M.A., "A general method for calculating critical speeds of flexible rotor," *ASME Transaction: Journal of Applied Mechanics*, Vol. 67, pp. A 142-A148, 1945.

[64] Poritsky, H., "Contribution to the theory of oil whip," *Transaction of ASME*, Vol. 75, pp. 1153-1161, 1953.

[65] Hagg, A.C., and Warner, P.C., "Oil whip of flexible rotors," *Transaction of ASME*, Paper No.52-A-162, Vol. 75, pp.1339-1344, 1953.

[66] Newkirk, B.L., and Lewis, J.F., "Oil-film whirl-An investigation of disturbances due to oil films in journal bearings," *Transaction of ASME*, Vol. 78, pp.21-27, 1956.

[67] Boekar, G.F., and Sternlicht, B., "Investigation of translatory fluid whirl in vertical machines," *Transaction of ASME*, Vol. 78, pp.13-19, 1956.

[68] Hori, Y., "A theory of oil whip," *ASME Transaction: Journal of Applied Mechanics*, Vol. 81, pp.189-198, 1959.

[69] Dimentberg, F.M., "Flexural vibrations of rotating shafts," *Butterworth's Publishing House*, London, 1961.

[70] Tondl, A., "Some problems of rotor dynamics," *Chapman and Hall*, Publishing House of Czechoslovakian Academy of Science, London, Prague, 1965.

[71] Lund, J.W., "The stability of an elastic rotor in journal bearings with flexible damped supports," *ASME Transaction: Journal of Applied Mechanics*, Series E, Vol. 87, No.4, pp. 911-920, 1965.

[72] Gunter, E.J., "The influence of internal friction on the stability of high speed rotors," *ASME Transaction: Journal of Engineering for industry*, Series B, Vol. 89, No.4, pp.683-688, 1966.

[73] Lund, J.W., and Sternlicht, B., "Rotor-bearing dynamics with emphasis on attenuation," *ASME Transaction: Journal of Basic Engineering*, Series D, Vol. 84, No.4, pp.491-502, 1962.

[74] Reddi, M.M., and Trumpler, P.R., "Stability of high-speed journal bearings under steady load-1: The compressible film," *ASME Transaction: Journal of Engineering for Industry*, Vol. 84, pp. 351-358, 1962.

[75] Sternlicht, B., "Stability and dynamics of rotors supported on fluid film bearings," *ASME Paper*, No.62-WA-190, 1962.

[76] Alford, J.S., "Protecting turbo machinery from self-excited rotor whirl," *ASME Transaction: Journal of Engineering for Power*, Series A, Vol. 87, No. 4, pp.333-344, 1965.

[77] Gunter, E.J., Jr, "Dynamics stability of rotor bearing systems," *NASA SP-113*, Office of Technology Utilization, U.S. Government Printing Office, 1966.

[78] Kirk, R.G., "Transient journal bearing analysis," *Master's Thesis*, Department of Mechanical Engineering, University of Virginia, June, 1969.

[79] De Choudhary, P., and Gunter, E.J., Jr., "Dynamic stability of flexible rotor bearing systems," *Report No. ME-4040-104-70U*, Research Laboratory For Engineering. Science, Vol. 10, University of Virginia, Charlottesville, December, pp.252, 1970.

[80] Kirk, R.G., and Gunter, E.J., "The effect of support flexibility and damping on the synchronous response of a single mass flexible rotor," *ASME transaction: Journal of Engineering for Industry*, Vol. 98, pp.221-232, 1972.

[81] Kirk, R.G., "Non-linear transient analysis of multi mass flexible rotors," *Ph.D. Thesis*, University of Virginia, Charlottesville, VA, 1972.

[82] Bansal, P.N. and Kirk, R.G., "Stability and damped critical speeds of a flexible rotor in fluid film bearings," *ASME transaction: Journal of Engineering for Industry*, Series B, Vol. 97, No.4, pp. 1325-1332, 1975.

[83] Allaire, P., "Design of journal bearings for high speed rotating machinery," *Fundamentals of the Design of Fluid Film Bearings, ASME*, pp.45-83, 1979.

[84] Barret, L., Allaire, P., and Gunter, E.J., "A finite length bearing correction factor for short bearing theory," *ASME transaction: Journal of Engineering of Lubrication Technology*, Vol. 102, pp.283-290, 1980.

[85] Majumdar, B., Brewe, D., and Khonsari, M., "Stability of a rigid rotor supported on flexible oil journal bearings," *ASME transaction: Journal of Tribology*, Vol.110, No.1, pp.181-187, 1988.

[86] Ramesh, K., and Kirk, R.G., "Stability and response of rotors supported on active magnetic bearings," *Proceedings of the 14th ASME Vibrations and Noise Conference*, DE-60, Vibrations of Rotating Systems, pp.289-296, 1993.

[87] Elrod, H.G., and Vijayaraghavan, D., "A stability analysis for liquid lubricated bearings incorporating the effects of cavity flow, Part I: Classical one-dimensional journal bearing," *ASME Transaction: Journal of Tribology*, Vol. 116, pp. 330-336, 1994.

[88] Elrod, H.G., and Vijayaraghavan, D., "A stability analysis for liquid lubricated bearings incorporating the effects of cavity flow, Part II: Classical one-dimensional journal bearing," *ASME Transaction: Journal of Tribology*, Vol. 117, pp. 365-367, 1995.

[89] Tieu, A., and Qiu, Z., "Stability of finite journal bearings-from linear and non-linear bearing forces," *STLE Tribology Transactions*, Vol. 38, No.3, pp. 627-635, 1995.

[90] Ramesh, J., Majumdar, B.C., and Rao, N.S., "Non-linear transient analysis of submerged oil journal bearings considering surface roughness and thermal effects," *Journal of Engineering Tribology, Proc. of Inst. of Engineers*, London, Part J, Vol. 209, pp.53-61, 1995.

[91] Crandall, S.H., "The instability mechanism responsible for oil whirl and oil whip," *Proceedings 4th Greek National Congress on Mechanics*, Democritus university of Thrace, Xanthi, pp. 659-672, 1995.

[92] Crandall, S.H., "Velocity linearization of the dynamic response of fluid film bearings," *Proceedings EUROMECH-2nd European Nonlinear Oscillation Conference*, Prague, September 9-13, 1996.

[93] Horattas, G.A., Adams, M.L., and Abdel Magied, M.F., "Experimental investigation of dynamic nonlinearities in rotating machinery," *Proceedings ASME DETC'97*, Sacramento, California, September 14-17, 1997.

[94] Guo, Z.L., "Study on external elastic damping support for bearing-rotor system," *Ph.D. Thesis*, Xi'an Jiaotong University, Xi'an, China, 1997.

[95] Ramesh, J., Majumdar, B.C., and Rao, N.S., "Stability characteristics of rough submerged oil elliptical bearings under dynamic load," *Tribology International*, Vol. 30, No.12, pp. 857-863, 1998.

[96] Jang, G.H., and Yoon, J.W., "Nonlinear dynamic analysis of a hydrodynamic journal bearing considering the effect of a rotating or stationary herringbone groove," *ASME Transaction: Journal of Tribology*, Vol. 124, pp. 97-304, 2002.

[97] Jang, G.H., and Yoon, J.W., "Stability analysis of a hydrodynamic journal bearing with rotating herringbone grooves," *ASME Transaction: Journal of Tribology*, Vol. 125, No.2, pp.291-300, 2003.

[98] Guo, Z., and Kirk, R.G., "Instability boundary for rotor-hydrodynamic bearing systems, Part 1: Jeffcott rotor with external damping," *ASME Transaction: Journal of Vibration and Acoustics*, Vol. 125, pp.417-422, 2003.

[99] Guo, Z., and Kirk, R.G., "Instability boundary for rotor-hydrodynamic bearing systems, Part 2: Rotor with external flexible damped support," *ASME Transaction: Journal of Vibration and Acoustics*, Vol. 125, pp.423-426, 2003.

[100] Ghosh, M.K., and Satish, M.R., "Rotordynamic characteristics of multilobe hybrid bearings with short sills-Part I," *Tribology International*, Vol. 36, pp. 625-632, 2003.

[101] Ghosh, M.K., and Satish, M.R., "Stability of multilobe hybrid bearings with short sills-Part II, *Tribology International*, Vol. 36, pp. 633-636, 2003.

[102] Rao, T. V. V. L. N., and Sawicki, J.T., "Stability characteristics of herringbone grooved journal bearings incorporating cavitation effects," *ASME Transaction:Journal of Tribology*, Vol. 126, No. 2, pp. 281–287, 2004.

[103] Rao, T. V. V. L. N., and Sawicki, J.T., "Stability analysis of a rough journal bearing considering cavitation effects," *ASME Transaction:Journal of Tribology*, Vol. 127, No. 1, pp. 112–119, January 2005.

[104] Lund, J.W., and Orcutt, F.K., "Calculation and experiments on the unbalance response of a flexible rotor," *ASME Transaction: Journal of Engineering for Industry*, Series B, Vol. 89, No.4, pp.785-796, 1967.

[105] Ruhl, R., "Dynamics of distributed parameter rotor systems: transfer matrix and finite element techniques," *Ph. D. Thesis*, Cornell University, Ithaca, New York, 1970.

[106] Uhrig, R., "The transfer matrix method seen as one method of structural analysis among others," *Journal of Sound and Vibration*, Vol.4, No.2, pp.136-148, 1966.

[107] Archer, J.S., "Consistent mass matrix of distributed mass systems," *Proceedings of the American Society of Civil Engineers*," Vol.89, pp.161-178, 1963.

[108] Ruhl, R.L., and Booker, J.F., "A finite element model for distributed parameter turbo rotor systems," *ASME Transaction: Journal of Engineering for Industry*, Series B, Vol. 94, No.1, pp.128-132, 1972.

[109] Thorkildsen, T., "Solution of a distributed mass and unbalanced rotor system using a consistent mass matrix approach," *MSE Engineering Report,* Arizona State University, 1972.

[110] Polk, S.R., "Finite element formulation and solution of flexible rotor-rigid disk systems for natural frequencies and critical whirl speeds," *MSE Engineering Report*, Arizona State University, 1974.

[111] Diana, G., Massa, E., and Pizzigoni, "A finite element method for computing oil whirl instability of a rotating shaft supported by elastic bearing," *Journal of Mechanical Engineers*, pp.659-663, 1975.

[112] Dimaragonas, A.D., "A general method for stability analysis of rotating shafts," *Ingenieur-Archive*, Vol. 44, H.1, pp.9-20, 1975.

[113] Gasch, R., "Vibration of large turbo-rotors in fluid film bearings on elastic foundation," *Journal of Sound and Vibration*, Vol.47, No.1, pp.53-73, 1976.

[114] Nelson, H.D., and McVaugh, J.M., "The dynamics of rotor-bearing systems using finite elements," *ASME transaction: Journal of Engineering for Industry*, Vol. 98, No.2, pp.593-600, 1976.

[115] Guyan, R.J., "Reduction of stiffness and mass matrices," *American Institute of Aeronautics and Astronautics Journal*, Vol. 3, No.2, pp.380, 1965.

[116] Gunter, E.J., "Rotor bearing stability," *Proceedings of the First Turbomachinery Symposium*, pp.119-141, 1966.

[117] Bolotin, V.V., "Non conservative problems of the theory of elastic stability," Pergamon Press, New York, 1963.

[118] Vance, J.M., and Lee, J., "Stability of high speed rotors with internal friction," *ASME transaction: Journal of Engineering for Industry*, Series B, August, 1974.

[119] Zorzi, E.S., and Nelson, H.D., "Finite element simulation of rotor-bearing systems with internal damping", *ASME transaction: Journal of Engineering for Power*, Series A, No.1 Vol. 99, pp.71-76, 1977.

[120] Rouch, K.E., and Kao, J.S., "Dynamic reduction in rotor dynamics by the finite element method," *ASME transaction: Journal of Mechanical Design*, Vol. 102, pp.360-368, 1980.

[121] Nelson, H.D., "A finite rotating shaft element using Timoshenko beam theory," *ASME transaction: Journal of Mechanical Design*, Vol. 102, pp.793-803, 1980.

[122] Ozguven, H.N., and Ozkan, Z.L., "Whirl speeds and unbalance response of multibearing rotors using finite elements," *ASME transaction: Journal of Vibration, Acoustics, Stress and Reliability in Design*, Vol.106, pp.72-79, 1984.

[123] Edney, S.L., Fox, C.H.J., and Williams, E.J., "Tapered Timoshenko finite elements for rotor dynamics analysis," *Journal of Sound and Vibration*, Vol. 137, pp.463-481, 1990.

[124] Rouch, K.E., and Kao, J.S., "A tapered beam finite element of rotor dynamics analysis," *Journal of Sound and Vibration*, Vol. 66, pp.119-140, 1979.

[125] Greenhill, L.M., Bickford, W.B., and Nelson, H.D., "A conical beam finite element for rotor dynamicS analysis," *ASME transaction: Journal of Vibration, Acoustics, Stress and Reliability in Design*, Vol. 107, pp.421-430, 1985.

[126] Kim, Y.D. and Lee, C.W., "Finite element analysis of rotor bearing systems using a modal transformation matrix," *Journal of Sound and Vibration*, Vol. 111, No.3, pp.441-456, 1986.

[127] Leung, A.Y.T. and Fung, T.C., "Spinning finite elements," *Journal of Sound and Vibration*, Vol. 125, pp.523-537, 1988.

[128] Sauer, G., and Wolf, M., "Finite element analysis of gyroscopic effects," *Finite Elements in Analysis and Design 5*, pp.131-140, 1989.

[129] Gmur, T.C. and Rodrigues, J.D., "shaft finite elements for rotor dynamics analysis," *ASME transaction: Journal of Vibration and Acoustics*, Vol. 113, pp.482-493, 1991.

[130] Chen, L.W. and Ku, D.M., "Finite element analysis of natural whirl speeds of rotating shafts," *Computers and Structures*, Vol. 40, No. 3, pp.741-747, 1991.

[131] Ku, D.M., "Finite element analysis of natural whirl speeds for rotor-bearing systems with internal damping," *Mechanical Systems and Signal Processing*, Vol. 12, No.5, pp.599-610, 1998.

[132] Rao, J.S., "Rotor Dynamics," *New Age International Publishers*, Third Edition, pp.152, pp. 258-266, pp.316-318, pp.319-323, 1996.

[133] Lord Rayleigh, "Theory of Sound," *Macmillan Company*, Second edition, New York, N.Y., pp.293-294, 1877.

[134] Timoshenko, S., "On the correction for shear of the differential equation for transverse vibrations of prismatic bars," *Philosophical Magazine*, Series 6, Vol. 41, pp.744-746, 1921.

[135] Timoshenko, S., "On the transverse vibrations of bars of uniform cross-sections," *Philosophical Magazine*, Series 6, Vol. 43, pp.125-131, 1922.

[136] Huang, T.C., "The effect of rotary inertia and shear deformation on the frequency and normal mode equations of uniform bars with simple end conditions," *ASME transaction: Journal of Applied Mechanics*," Vol. 28, pp.579-584, 1961.

[137] Huang, T.C., "Eigen values and modifying quotients of vibration of beams," *Report No.25, Engineering Experiment Station*, University of Wisconsin, Madison, WI, 1964.

[138] Wang, F.Y., and Guan, G., "Influences of rotatory inertia, shear and loading on vibrations of flexible manipulators," *Journal of Sound and Vibration*, Vol. 171, No.4, pp.433-452, 1994.

[139] Stafford, R.O., and Giurgiurtiu, V., "Semi-analytic methods for rotating Timoshenko beams," *International Journal of Mechanical Science*, Vol. 17, pp.719-727, 1975.

[140] Abbas, B.A.H., "Dynamic stability of a rotating Timoshenko beam with a flexible root," *Journal of Sound and Vibration*, Vol. 108, No.1, pp.25-32, 1986.

[141] Datta, P.K., and Ganguli, R., "Vibration characteristics of a rotating blade with localized damage including the effects of shear deformation and rotary inertia," *Computers and Structures*, Vol. 36, No.6, pp.734-739, 1990.

[142] Zu, J.W.Z., and Han, R.P.S., "Natural frequencies and normal modes of a spinning Timoshenko beam with general boundary conditions," *ASME transaction: Journal of Applied Mechanics*," Vol. 59, pp.s197-s204, 1992.

[143] Rossi, R.E., Laura, P.A.A., and Gutierrez, R.H., "A note on transverse vibrations of a Timoshenko beam of non-uniform thickness clamped at one end and carrying a concentrated mass at the other," *Journal of Sound and Vibration*, Vol. 143, pp.491-503, 1990.

[144] Gutierrez, R.H., Laura, P.A.A., and Rossi, R.E., "Fundamental frequency of vibration of a Timoshenko beam of non-uniform thickness," *Journal of Sound and Vibration*, Vol. 145, pp.341-344, 1991.

[145] Lee, S.Y., and Lin, S.M., "Exact vibration solutions for non-uniform Timoshenko beam with attachments," *American Institute of Aeronautics and Astronautics Journal*, Vol. 30, pp.2930-2934, 1992.

[146] Cleghorn, W.L., and Tabarrok, B., "Finite element formulation of a tapered Timoshenko beam for free lateral vibration analysis," *Journal of Sound and Vibration*, Vol. 152, pp.461-470, 1992.

[147] White, M.W.D., and Heppler, G.R., "Dynamics of Timoshenko beams with attached rigid bodies," *Proceedings of the Second International Conference on the Dynamics and Control of Space Structures*, Cranfield University, Cranfield, England, pp.209-244, 1993a.

[148] White, M.W.D., and Heppler, G.R., "Timoshenko beam theory with modeling applications," *ConStruct TR-93-001*, University of Waterloo, Waterloo, Ontario, Canada, 1993b.

[149] White, M.W.D., and Heppler, G.R., "Vibration of a rotating Timoshenko beam," *ConStruct TR-93-002*, University of Waterloo, Waterloo, Ontario, Canada, 1993c.

[150] White, M.W.D., and Heppler, G.R., "Vibration modes and frequencies of Timoshenko beams with attached rigid bodies," *ASME transaction: Journal of Applied Mechanics*," Vol. 62, No.1, pp.193-199, 1995.

[151] Du, H., Lim, M.K., and Liew, K.M., "A power series solution for vibration of a rotating Timoshenko beam," *Journal of Sound and Vibration*, Vol. 175, No.4, pp.505-523, 1994.

[152] Tong, X., Tabarrrok, B., and Yeh, K.Y., "Vibration analysis of Timoshenko beams with non-homogeneity and varying cross-section," *Journal of Sound and Vibration*, Vol. 186, No.5, pp.821-835, 1995.

[153] White, M.W.D., and Heppler, G.R., "Vibration of a rotating Timoshenko beam," *ASME transaction: Journal of Vibration and Acoustics*, Vol. 118, pp.606-613, 1996.

[154] Ziegler, H., "Principles of Structural Stability," *Blaisdell Publishing Co.*, 1968.

[155] Satyanarayna, N., "Finite element formulation of rotor-bearing systems with higher effects", *M.Tech Thesis*, Department of Mechanical Engineering, IITG, Guwahati, 2000.

[156] Lund, J.W., 1979, "Rotor-Bearing Dynamics," *Lecture notes*, Technical University of Denmark, ISBN 83-04-00267-1.

[157] Den Hartog, J.P., "Mechanical Vibration," Dover Publications, Inc., pp.262-263, 1985.

[158] Shames, I.H. and Dymes, C.L., "Energy and finite element methods in structural mechanics," *New Age International Publisher Limited*, pp. 259-275, 1985.

[159] Eshleman, R.L., and Eubanks, R.A., "On the critical speeds of a continuous rotor," *ASME transaction: Journal of Engineering for Industry*," Series B, Vol. 91, No.4, pp.1180-1188, 1969.

[160] Patra, K., "Estimation of dynamic coefficients and stability analysis of multi lobe bearing," *M.Tech Thesis*, Department of Mechanical Engineering, IITG, Guwahati, 2003.

[161] Thivagar, T., "Non-linear time transient stability analysis of multi lobe bearings," *M.Tech Thesis*, Department of Mechanical Engineering, IITG, Guwahati, 2004.

Appendices

Shaft element matrices for Euler-Bernoulli beam model:

$$\text{Stiffness matrix } [K]^e = \frac{EI}{l^3}\begin{bmatrix} 12 & 6l & -12 & 6l \\ & 4l^2 & -6l & 2l^2 \\ & & 12 & -6l \\ sym & & & 4l^2 \end{bmatrix}$$

$$\text{Consistent mass matrix } [M]^e = \frac{1}{420}\rho Al\begin{bmatrix} 156 & 22l & 54 & -13l \\ & 4l^2 & -13l & -3l^2 \\ & & 156 & -22l \\ sym & & & 4l^2 \end{bmatrix}$$

Elemental matrices for Timoshenko beam model

Rigid disk element matrices:

$$\text{Mass matrix } [M^d] = \begin{bmatrix} m_d & 0 & 0 & 0 \\ 0 & m_d & 0 & 0 \\ 0 & 0 & I_d & 0 \\ 0 & 0 & 0 & I_d \end{bmatrix}$$

$$\text{Gyroscopic matrix } [G^d] = \begin{bmatrix} 0 & 0 & 0 & 0 \\ 0 & 0 & 0 & 0 \\ 0 & 0 & 0 & -I_p \\ 0 & 0 & I_p & 0 \end{bmatrix}$$

Shaft element matrices:

Translational mass matrix $[M_T]=[M_T]_0+\Phi[M_T]_1+\Phi^2[M_T]_2$

$$[M_T]_0=\frac{\rho Al}{420(1+\Phi)^2}\begin{bmatrix}
156 & & & & & & & sym\\
0 & 156 & & & & & & \\
0 & -22l & 4l^2 & & & & & \\
22l & 0 & 0 & 4l^2 & & & & \\
54 & 0 & 0 & 13l & 156 & & & \\
0 & 54 & -13l & 0 & 0 & 156 & & \\
0 & 13l & -3l^2 & 0 & 0 & 22l & 4l^2 & \\
-13l & 0 & 0 & -3l^2 & -22l & 0 & 0 & 4l^2
\end{bmatrix}$$

$$[M_T]_1=\frac{\rho Al}{420(1+\Phi)^2}\begin{bmatrix}
294 & & & & & & & sym\\
0 & 294 & & & & & & \\
0 & -38.5l & 7l^2 & & & & & \\
38.5l & 0 & 0 & 7l^2 & & & & \\
124 & 0 & 0 & 31.5l & 294 & & & \\
0 & 126 & -31.5l & 0 & 0 & 294 & & \\
0 & 31.5l & -7l^2 & 0 & 0 & 38.5l & 7l^2 & \\
-31.5l & 0 & 0 & -7l^2 & -38.5l & 0 & 0 & 7l^2
\end{bmatrix}$$

$$[M_T]_2=\frac{\rho Al}{420(1+\Phi)^2}\begin{bmatrix}
140 & & & & & & & sym\\
0 & 140 & & & & & & \\
0 & -17.5l & 3.5l^2 & & & & & \\
17.5l & 0 & 0 & 3.5l^2 & & & & \\
70 & 0 & 0 & 17.5l & 140 & & & \\
0 & 70 & -17.5l & 0 & 0 & 140 & & \\
0 & 17.5l & -3.5l^2 & 0 & 0 & 17.5l & 3.5l^2 & \\
-17.5l & 0 & 0 & -3.5l^2 & -17.5l & 0 & 0 & 3.5l^2
\end{bmatrix}$$

Rotational mass matrix $[M_R]=[M_R]_0+\Phi[M_R]_1+\Phi^2[M_R]_2$

$$[M_R]_0=\frac{\rho\,\pi r^4}{120l(1+\Phi)^2}\begin{bmatrix}
36 & & & & & & & \\
0 & 36 & & & & & & \\
0 & -3l & 4l^2 & & & & & \\
3l & 0 & 0 & 4l^2 & & & & \\
-36 & 0 & 0 & -3l & 36 & & & \\
0 & -36 & 3l & 0 & 0 & 36 & & \\
0 & -3l & -l^2 & 0 & 0 & 3l & 4l^2 & \\
3l & 0 & 0 & -l^2 & -3l & 0 & 0 & 4l^2
\end{bmatrix}$$

$$[M_R]_1=\frac{\rho\,\pi r^4}{120l(1+\Phi)^2}\begin{bmatrix}
0 & & & & & & & sym \\
0 & 0 & & & & & & \\
0 & 15l & 5l^2 & & & & & \\
-15l & 0 & 0 & 5l^2 & & & & \\
0 & 0 & 0 & 15l & 0 & & & \\
0 & 0 & -15l & 0 & 0 & 0 & & \\
0 & 15l & -5l^2 & 0 & 0 & 15l & 5l^2 & \\
-15l & 0 & 0 & -5l^2 & 15l & 0 & 0 & 5l^2
\end{bmatrix}$$

$$[M_R]_2=\frac{\rho\,\pi r^4}{120l(1+\Phi)^2}\begin{bmatrix}
0 & & & & & & & sym \\
0 & 0 & & & & & & \\
0 & 0 & 10l^2 & & & & & \\
0 & 0 & 0 & 10l^2 & & & & \\
0 & 0 & 0 & 0 & 0 & & & \\
0 & 0 & 0 & 0 & 0 & 0 & & \\
0 & 0 & 5l^2 & 0 & 0 & 0 & 10l^2 & \\
0 & 0 & 0 & 5l^2 & 0 & 0 & 0 & 10l^2
\end{bmatrix}$$

Gyroscopic matrix $[G]=[G]_0+\Phi[G]_1+\Phi^2[G]_2$

$$[G]_0=\frac{\rho\pi r^4}{60l(1+\Phi)^2}\begin{bmatrix} 0 & & & & & & & \text{skew sym} \\ -36 & 0 & & & & & & \\ 3l & 0 & 0 & & & & & \\ 0 & 3l & -4l^2 & 0 & & & & \\ 0 & -36 & 3l & 0 & 0 & & & \\ 36 & 0 & 0 & 3l & -36 & 0 & & \\ 3l & 0 & 0 & -l^2 & -3l & 0 & 0 & \\ 0 & 3l & l^2 & 0 & 0 & -3l & -4l^2 & 0 \end{bmatrix}$$

$$[G]_1=\frac{\rho\pi r^4}{60l(1+\Phi)^2}\begin{bmatrix} 0 & & & & & & & \text{skew sym} \\ 0 & 0 & & & & & & \\ -15l & 0 & 0 & & & & & \\ 0 & -15l & -5l^2 & 0 & & & & \\ 0 & 0 & -15l & 0 & 0 & & & \\ 0 & 0 & 0 & -15l & 0 & 0 & & \\ -15l & 0 & 0 & -5l^2 & 15l & 0 & 0 & \\ 0 & -15l & 5l^2 & 0 & 0 & 15l & -5l^2 & 0 \end{bmatrix}$$

$$[G]_2=\frac{\rho\pi r^4}{60l(1+\Phi)^2}\begin{bmatrix} 0 & & & & & & & \text{skew sym} \\ 0 & 0 & & & & & & \\ 0 & 0 & 0 & & & & & \\ 0 & 0 & -10l^2 & 0 & & & & \\ 0 & 0 & 0 & 0 & 0 & & & \\ 0 & 0 & 0 & 0 & 0 & 0 & & \\ 0 & 0 & 0 & 5l^2 & 0 & 0 & 0 & \\ 0 & 0 & -5l^2 & 0 & 0 & 0 & -10l^2 & 0 \end{bmatrix}$$

Stiffness matrix $[K]=[K]_0+\Phi[K]_1$

$$[K]_0=\frac{EI}{(1+\Phi)l^3}\begin{bmatrix} 12 & & & & & & & sym \\ 0 & 12 & & & & & & \\ 0 & -6l & 4l^2 & & & & & \\ 6l & 0 & 0 & 4l^2 & & & & \\ -12 & 0 & 0 & -6l & 12 & & & \\ 0 & -12 & 6l & 0 & 0 & 12l & & \\ 0 & -6l & 2l^2 & 0 & 0 & 6l & 4l^2 & \\ 6l & 0 & 0 & 2l^2 & -6l & 0 & 0 & 4l^2 \end{bmatrix}$$

$$[K]_1=\frac{EI}{(1+\Phi)l^3}\begin{bmatrix} 0 & & & & & & & sym \\ 0 & 0 & & & & & & \\ 0 & 0 & l^2 & & & & & \\ 0 & 0 & 0 & l^2 & & & & \\ 0 & 0 & 0 & 0 & 0 & & & \\ 0 & 0 & 0 & 0 & 0 & 0 & & \\ 0 & 0 & -l^2 & 0 & 0 & 0 & l^2 & \\ 0 & 0 & 0 & -l^2 & 0 & 0 & 0 & l^2 \end{bmatrix}$$

where

$$\Phi=\frac{12EI}{\kappa GAl^2}$$

Circulation matrix

$$[K_C]^e=\frac{EI}{(1+\Phi)l^3}\begin{bmatrix} 0 & 12 & -6l & 0 & 0 & -12 & -6l & 0 \\ -12 & 0 & 0 & -6l & 12 & 0 & 0 & -6l \\ 6l & 0 & 0 & 4l^2 & -6l & 0 & 0 & 2l^2 \\ 0 & 6l & -4l^2 & 0 & 0 & -6l & 2l^2 & 0 \\ 0 & -12 & 6l & 0 & 0 & 12 & 6l & 0 \\ 12 & 0 & 0 & 6l & -12 & 0 & 0 & -6l \\ 6l & 0 & 0 & -2l^2 & -6l & 0 & 0 & 4l^2 \\ 0 & 6l & -2l^2 & 0 & 0 & 6l & -4l^2 & 0 \end{bmatrix}$$

List of publications

Journals

- **Kalita, M.**, and Kakoty, S.K., "Analysis of Whirl Speeds for Rotor-Bearing Systems Supported on Fluid Film Bearings," *Mechanical Systems and Signal Processing*, Vol. 18, pp.1369-1380, 2004.

- **Kalita, M.**, and Kakoty, S.K., "Synchronous And Sub-Synchronous Whirling Of Rotor-Bearing System Mounted On Circular And Non-Circular Fluid Film Bearings," *STLE Transactions* (communicated), 2005.

- **Kalita, M.**, and Kakoty, S.K., "Regarding Stability study of circular and non-circular bearings supporting rigid and flexible rotors," *Advance Vibration Engineering* (communicated), 2005.

Conferences

- Kakoty, S.K. and **Kalita, M.**, "Stability Of Rotors Supported on Fluid Film Bearings," *Proceedings of Second International Conference on Vibration Engineering and Technology of Machinery (VETOMAC-2)*, Mumbai, India, December 2002.
- **Kalita, M.**, and Kakoty, S.K., 2003, "Analysis of Synchronous and Sub-synchronous Whirl of Rotor with Timoshenko Beam Element Mounted on Circular or Non-circular Fluid-film Bearings," *Proceedings of National Symposium of Rotor Dynamics (NSRD-2003)*, Guwahati, India, December 2003.
- Kakoty, S.K., **Kalita, M.**, and Thivagar, T., "Nonlinear Time Transient Stability Analysis of Multilobe Bearings," *Abstract accepted for World Tribology Conference,* September 2005.

Vitae

Born and brought up at Assam, Ms. Madhumita Kalita was the youngest of three daughters of Late Soneswar Kalita and Mrs. Bichitra Kalita. After doing schooling at Nagaon and Guwahati, she passed pre-university (P.U.) from Cotton College and took her Bachelor of Engineering (B.E.) degree in Mechanical Engineering from Gauhati University as a student of Assam Engineering College, Guwahati in 1987. She worked for a short duration as Lecturer in Bongaigaon Polytechnic and finally joined in Assam Engineering Institute. She went for Master of Technology (M.Tech) in Machine Design to Institute of Technology (B.H.U.) and received the degree in 1997. She went to Melbourne, Australia for two months to attend a training programme on Multimedia under World Bank Project in 1998.

Ms. Kalita, as a part time research scholar, joined Mechanical Engineering of Indian Institute of Technology Guwahati and worked under supervision of Dr. S.K. Kakoty.